Static performance of a hybrid stepping motor with ring coils

STATIC PERFORMANCE OF A HYBRID STEPPING MOTOR WITH RING COILS

B. H. A. GODDIJN

STATIC PERFORMANCE OF A HYBRID STEPPING MOTOR WITH RING COILS

B. H. A. GODDIJN

STATIC PERFORMANCE OF A HYBRID STEPPING MOTOR WITH RING COILS

PROEFSCHRIFT

TER VERKRIJGING VAN DE GRAAD VAN DOCTOR IN DE TECHNISCHE WETENSCHAPPEN AAN DE TECHNISCHE HOGESCHOOL EINDHOVEN, OP GEZAG VAN DE RECTOR MAGNIFICUS, PROF. IR. J. ERKELENS, VOOR EEN COMMISSIE AANGEWEZEN DOOR HET COLLEGE VAN DEKANEN, IN HET OPENBAAR TE VERDEDIGEN OP DINSDAG 9 SEPTEMBER 1980 TE 16.00 UUR.

DOOR

BEN. H. A. GODDIJN

GEBOREN TE AMSTERDAM

DIT PROEFSCHRIFT IS GOEDGEKEURD DOOR
DE PROMOTOREN

PROF. DR. IR. J.G. NIESTEN
EN
PROF. P.J. LAWRENSON,
D.Sc., A.F.I.M.A., Sen. Mem. I.E.E.E., C. Eng., M.I.E.E.

Aan

mijn ouders,
Aukje,
Maaike,
Pieter,
Sanja

CONTENTS

LIST OF SYMBOLS

A	surface area
A_{pm}	surface area of the permanent magnet
A_{sh}	cross-sectional area of the shaft
A_z	z-component of the vector potential
B	magnetic induction
B_r	remanent magnetic induction
B_{sat}	saturation value of the magnetic induction
E	induced voltage
F_c	m.m.f. of the excitation coil
F_{1c}	m.m.f. of the excitation coil of stator part 1
F_{2c}	m.m.f. of the excitation coil of stator part 2
F_{pm}	m.m.f. of the permanent magnet
g	air gap length
H	magnetic field intensity
H_c	coercitive field
H_{pm}	magnetic field intensity in the permanent magnet
I	excitation current
$i_1, i_2, .., i_q$	phase currents
J	moment of inertia
K	disk height ratio
l	length
l_{pm}	length of the permanent magnet
l_{sh}	length of the shaft
L	phase self inductance
L'	normalized self inductance
n	number of teeth per disk
N	number of turns
p	number of pole pairs
P	amplitude of the variable part of the permeance P_i
P_o	constant part of the permeance P_i
P_i	permeance of disk i
P_a	permeance of the unslotted airgap
P_b	permeance of the butt joints
P_{b1}	permeance of the butt joints of stator part 1
P_{b2}	permeance of the butt joints of stator part 2
P_{in}	permeance of the disk in the in line position
P_{out}	permeance of the disk in the out of line position
P_m	measured permeance
P_s	permeance of the permanent magnet
P_{sh}	permeance of the shaft
P_t	total permeance
P_{tm}	total permeance of the measuring model

P_{tz}	permeance of the tooth zone
P_y	permeance of the iron circuit
P_λ	permeance of one tooth pitch
P_{12s}	series permeance of P_s and P_1' parallel with P_2.
P_{34s}	series permeance of P_s and P_4' parallel with P_3.
P_{pm}	series permeance of P_s and P_{sh}
P_{by1}	series permeance of P_{b1} and P_y
P_{by2}	series permeance of P_{b2} and P_y
P_1'	series permeance of P_1 and P_b
P_4'	series permeance of P_4 and P_b
q_i	quality factor
R	phase resistance
R'	normalized phase resistance
S	surface
T	torque
T_i	torque produced by disk i
T_D	detent torque
T_H	hybird torque
T_{Hi}	hybird torque produced by disk i
T_R	reluctance torque
T_{Ri}	reluctance torque produced by disk i
T_{Rex}	extra reluctance torque
T_λ	torque produced by one tooth pitch
t_{h1}	disk height of disk 1
t_{h2}	disk height of disk 2
t	time
U_{c1}	magnetic potential difference across the air gap of disk 1 due to the coil excitation
U_{c2}	magnetic potential difference across the air gap of disk 2 due to the coil excitation
$U_{ci\alpha}$	magnetic potential difference across the air gap of disk i due to the coil excitation of stator part 1
$U_{ci\beta}$	magnetic potential difference across the air gap of disk i due to the coil excitation of stator part 2
U_g	magnetic potential difference across the air gap
U_i	magnetic potential difference across the air gap of disk i
U_{max}	maximum magnetic potential difference across the air gap
U_{pm}	magnetic potential difference outside the permanent magnet
U_{pm1}	magnetic potential difference across stator part 1 due to the permanent magnet
U_{pm2}	magnetic potential difference across stator part 2 due to the permanent magnet
U_{pmsh}	magnetic potential difference across the shaft due to the permanent magnet

U_y	magnetic potential difference across the iron circuit
V	volume
W_m	magnetic energy
W'_m	magnetic coenergy
$\alpha, \alpha_1, \alpha_2$	dimensionless constants accounting for design variables
γ	ratio between the mimum and maximum holding torque
θ	rotor angle
θ_0	stepping angle
μ_0	permeability of air
μ_y	permeability of iron
τ	time constant
Φ	flux
Φ_i	flux through disk i
Φ_λ	flux of one tooth pitch
Φ_{sh}	flux through the shaft

INTRODUCTION

In recent years there has been a substantial growth in the demand for stepping motors, which is due mainly to a growing application of digital electronics to which the stepping motor as digital actuator is very well suited. In this area the need for a stepping motor having a small and accurate stepping angle is the most urgent one.

A small stepping angle can be obtained in motors with double salient air gap where the torque is produced by reluctance forces. Depending on the type of excitation, a distinction is made between variable reluctance motors and hybrid motors. In the variable reluctance motor the excitation is brought about solely by means of a coil. In hybrid motors the excitation is effected using a permanent magnet in conjunction with a coil. In the present thesis a hybrid stepping motor will be described.

The principle of the hybrid motor is shown in fig. 1. The permanent magnet passes a flux through the two poles to the rotor. The direction of the flux is the same for both poles. Seen from the permanent magnet the two poles are arranged in parallel.

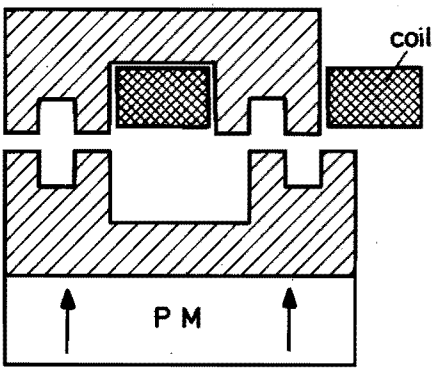

Fig. 1 – Principle of hybrid motor operation

During the excitation of the coil a flux will flow from one pole via the rotor to the other, where the flux directions in the two poles are opposite. Seen from the coil, the two poles are connected in series. The effect of coil excitation is an increase of the resulting flux in one pole and a decrease of it in the other. Both the rotor and the two poles are provided with teeth. When the teeth under one pole are aligned, they are out of line under the other. If the rotor can move freely in the tangential direction, then on exciting the coil the rotor teeth will be aligned under that pole in which the flux is the largest. Depending on the direction of the excitation current, the rotor teeth will be aligned either under one or under the other pole.

A well known version of a hybrid motor has been described by Snowdon and Madsen (ref. 1), Bakhuizen (ref. 2). Its design requires the use of two pole pairs per phase, the stator coils being situated in the axial direction. The motor dealt with in the present thesis has only a single pole pair per phase which is fitted with ring coils giving a high torque to stator-volume ratio as compared with existing types. As a consequence the magnetic circuit is asymmetric, which depending on the current direction gives rise to an asymmetry in the holding torque and to stepping angles errors that are inherent in this design (ref. 3, 4). It is particularly these inherent errors and the methods of compensating for these errors that necessitate a thorough study of the motor's static behaviour.

The use of only a single pole pair, which is made possible by the application of ring coils, leads to a novel design for the hybrid motor, which can be manufactured by a highly automated method and which has an extremely large torque-to-volume ratio (ref. 5).

1. THE EFFECT OF THE NUMBER OF POLE PAIRS AND PERMANENT MAGNET EXCITATION ON THE PERFORMANCE OF A HYBRID STEPPING MOTOR

The principle of the hybrid motor has been described in the introduction. The torque produced by the motor can be calculated by means of the energy method as described by Woodson and Melcher (ref. 9). The torque follows from the well known relation

$$T = \frac{\partial W_m'(u_1, u_2, \ldots u_q; \theta)}{\partial \theta} = \frac{\partial \sum_{i=1}^{q} \int_0^{u_i} P_{mi}\, u_i\, du_i}{\partial \theta} \qquad (1.1)$$

where W_m' is the magnetic coenergy
θ the rotor position
u_i the magnetic potential difference across permeance P_{mi}.

The use of magnetic potential differences and permeances to express the magnetic coenergy is chosen because, as will be shown in chapter 2, the permeances in the motor are simple functions of θ.
To study the effect of the number of pole pairs and permanent magnet excitation it suffices to assume the iron being ideal which means that no magnetic energy is stored in the iron. To obtain more precise results the idealization of the iron will be abandoned in later calculations. In the hybrid motor the permeance of the permanent magnet is independent of the rotor position. The only permeances in the hybrid motor depending on the rotor position are the permeances of the air gaps between the rotor and the stator. The magnetic coenergy stored in the air gap over one tooth pitch can be expressed by

$$W_m' = \frac{1}{2} U_g^2 P_\lambda \qquad (1.2)$$

where U_g is the magnetic potential difference across the air gap and
P_λ the permeance of the air gap over one tooth pitch.

The torque produced by one tooth pitch can be found by substituting (1.2) into (1.1) (ref. 6, 7)

$$T_\lambda = \frac{1}{2} U_g^2 \frac{dP_\lambda}{d\theta} \qquad (1.3)$$

The magnetic potential difference across the air gap is formed by the sum of the contributions originating from the permanent magnet and the coil excitation. The magnetic potential difference across the gap is found from

$$U_g = \alpha_1 U_{pm} + \alpha_2 F_c \tag{1.4}$$

where U_{pm} is the magnetic potential difference of the permanent magnet outside the permanent magnet.
F_c is the m.m.f. of the excitation coil.
α_1, α_2 are dimensionless constants accounting for design variables.

Substitution of (1.4) in (1.3) gives

$$T_\lambda = \left(\frac{\alpha_1^2}{2} U_{pm}^2 + \alpha_1 \alpha_2 U_{pm} F_c + \frac{\alpha_2^2}{2} F_c^2\right) \frac{dP_\lambda}{d\theta} \tag{1.5}$$

The torque contains three terms, consecutively the detent torque, the hybrid torque and the reluctance torque. The total motor torque is found by summation of the torque produced by all tooth pitches in the motor. In practice the motor is designed in such a way that the hybrid torque is many times larger than the other torque contributions. We shall only be concerned here with the contribution of the hybrid torque. For the single phase excited motor the hybrid torque may be defined by the equation

$$T_H = \alpha F_c U_{pm} \frac{dP_\lambda}{d\theta} \tag{1.6}$$

where α is a dimensionless constant accounting for design variables of all tooth pitches together.

In this chapter we shall consider the hybrid torque T_H of the single phase excited motor only, denoted by the torque T. The expression applies exclusively to a non saturated motor.

To gain a fuller understanding of the motor performance we assume that the iron has an infinitely large permeability as long as the saturation value of the magnetic flux density has not yet been reached and that the magnetic flux density can not exceed the saturation value. The corresponding B.H. curve is shown in fig. 1.1.

The magnetic potential difference across the air gap is tied to a maximum by the iron saturation

$$U_{max} = \frac{B_{sat}\, g}{\mu_o} \tag{1.7}$$

where μ_o is the permeability of air,
g is the air gap length
B_{sat} is the saturation value of the magnetic flux density in the iron.

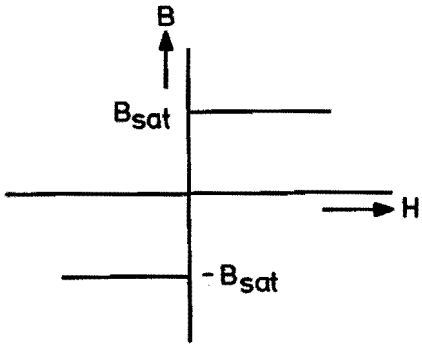

Fig. 1.1 – B.H. curve of the idealized iron

In the following we assume the motor to be excited to such an extent that it just fails to attain saturation. Therefore the sum of $\alpha_1 U_{pm}$ and $\alpha_2 F_c$ is tied to the maximum U_{max}.
The output torque of the motor is then at a maximum when the contributions of the magnetic potential difference across the air gap from the permanent magnet and that from the excitation coil are equal. This maximum torque is given by

$$T = \frac{\alpha}{4\,\alpha_1\,\alpha_2} U_{max}^2 \frac{dP_\lambda}{d\theta}. \tag{1.8}$$

1.1. Quality criteria

In order to investigate the effect of the number of pole pairs and the permanent magnet excitation on the static and the dynamic behaviour of the motor the following quality criteria are introduced.
The first is:

$$q_1 = \frac{T}{V}. \tag{1.9}$$

The ratio of the torque to the motor volume is the main criterion for the static

motor performance. Since the motor must not be thermally overloaded if it is to attain a large torque we introduce

$$q_2 = \frac{T}{I^2 R} \tag{1.10}$$

where I is the excitation current
R the phase resistance.

The criteria q_1 and q_2 are closely related. With increasing copper volume, q_1 decreases and q_2 increases. In practice the motor is excited up to the thermally permissible limit, so that q_1 is of much more interest for a comparison between various types of motors. For a comparison of various types of motors the torque of the two phase excited motor usually is taken (ref. 15).

The dynamic behaviour of the motor, which is understood to be the pull-out and pull-in curves and the single step response, is determined by electrical parameters (self-inductance, resistance and rotational e.m.f.) and mechanical parameters (moment of inertia and friction). In this thesis the dynamic behaviour of the motor will be dealt with only in very general terms. No attention will be paid to instabilities or resonances or whatsoever complicates the motor behaviour under running conditions.

The motor properties are independent of the cross-sectional area of the wire, whereas the self inductance and the motor resistance are functions of the number of turns and therefore depend on the cross-sectional area of the wire. We eliminate this by introducing the following normalizing equations.

$$L' = \frac{L}{N^2} \tag{1.11}$$

$$R' = \frac{R}{N^2} \tag{1.12}$$

where N is the number of turns.

The magnetic energy produced by the coil is independent of the wire cross-section and is uniquely determined by the magnetic circuit. The electric time constant is also independent of the wire cross-section:

$$\tau = \frac{L}{R} = \frac{L'}{R'}. \tag{1.13}$$

This time constant is only significant if R is the series resistance of the motor and the source of power. In practice often resistance is added to enhance the dynamic performance. The time constant of the motor is therefore less interesting. Because of practical limitations of the power source in the drive circuit it is however recommended to minimize the normalized self inductance of any motor. The magnetic energy produced by the coil excitation is obtained by conversion of electric energy supplied by the drive circuit. The lower this magnetic energy is the lower is the electric energy to be converted and the higher is the available electric energy to create the mechanical work. Therefore in creating the torque, the dynamic behaviour of the work is better the lower is the magnetic energy produced by the coils. This is expressed by the criterion:

$$q_3 = \frac{T}{I^2 L}. \tag{1.14}$$

The moment of inertia of the rotor is one of the main parameters governing the dynamic behaviour. Therefore we introduce

$$q_4 = \frac{T}{J}. \tag{1.15}$$

The motor friction hardly affects the performance and is therefore left out of account.

In assessing the effect of the number of pole pairs and the permanent magnet excitation, we assume that the rotor geometry remains unchanged.

1.2. Effect of the number of pole pairs

The output torque of the motor is at a maximum when the magnetic potential difference of the coil excitation α_2 F_c across the airgap is equal to α_1 F_{pm} of the permanent magnet. Each pole pair invariable needs the same number of ampere turns to obtain the desired magnetic potential across the airgap. Therefore the copper volume per pole pair decreases by a factor of 1/p when the copper volume in the motor remains constant, so that the current density increases by a factor p.

If the motor were designed in such a way that the copper length is as small as possible, then the copper length per pole pair decreases by $1/\sqrt{p}$ owing to the decrease of the pole surface by 1/p. Because the copper volume per pole pair decreases by a factor of 1/p and the copper length decreases by $1/\sqrt{p}$ the copper cross-section per pole pair decreases also by $1/\sqrt{p}$. The resistance per pole pair will

therefore be constant and consequently the total losses of the phase coil will rise by a factor p. If, as in the case of the current hybrid stepping motors (see fig. 1.2), with wound stator, the copper length is made up of coil sides and coil overhangs, the loss will rise even faster with increasing p. The number of coil sides and coil

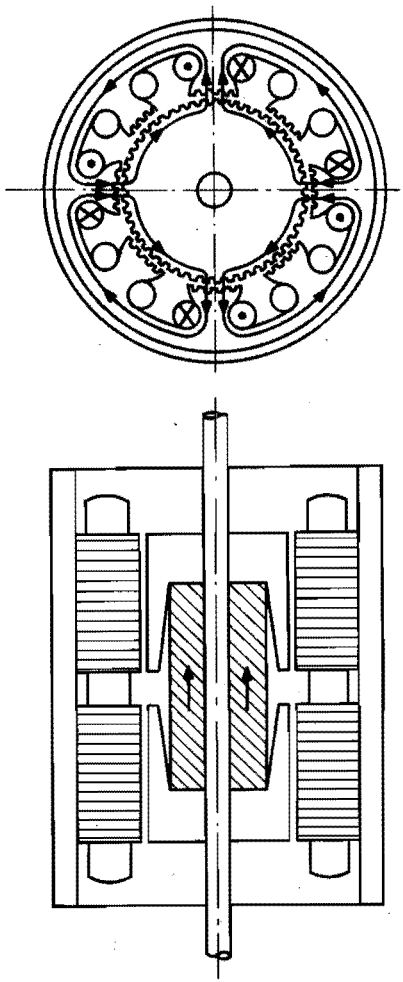

Fig. 1.2 – Hybrid stepping motor with wound stator

overhangs increases by a factor p, while only the coil overhangs become shorter. When the coil overhang is short in comparison with the coil side, the loss in the phase coil increases by a factor p^2. Hence the quality criterion q_2 depends very much on the number of pole pairs

$$q_2 \sim p^{-1} \text{ to } p^{-2} \tag{1.16}$$

By enlarging the copper volume and hence the motor volume we can increase q_2 again so that the motor will not be thermally overloaded.

The magnetic energy produced by the phase coil, the torque and the moment of inertia remain unaltered, so that q_3 and q_4 are independent of the number of pole pairs.

1.3. Effect of the permanent magnet excitation

The magnetic potential difference across the air gap is limited by the iron saturation. The magnetic potential difference originating from the permanent magnet and the coil is governed by

$$U_{max} = \alpha_2 \, F_c + \alpha_1 \, U_{pm} \, . \tag{1.17}$$

The torque expressed in terms of the coil m.m.f. is

$$T = \frac{\alpha}{\alpha_1} F_c \, (U_{max} - \alpha_2 \, F_c) \, \frac{dP_\lambda}{d\theta} . \tag{1.18}$$

The volume of the motor depends only slightly on that of the permanent magnet. If the permanent magnet is located in the rotor then, because the rotor geometry does not change, a change of the permanent magnet has no effect whatsoever on the motor volume. Therefore the quality factor q_1 is almost completely determined by the torque variation:

$$q_1 \sim F_c \, (U_{max} - \alpha_2 \, F_c) \, . \tag{1.19}$$

For a constant copper volume and air gap geometry, the dissipation losses can be written as

$$I^2 \, R \sim F_c^{\,2} \, . \tag{1.20}$$

The criterion q_2 varies with a varying ratio between the permanent magnet and coil excitation as

$$q_2 \sim \frac{F_c\,(U_{max} - \alpha_2\,F_c)}{F_c^2} \sim \frac{U_{max} - \alpha_2\,F_c}{F_c}. \tag{1.21}$$

The magnetic energy linked with the excitation winding is also proportional to F_c^2, so that it is true to say that

$$q_3 \sim \frac{U_{max} - \alpha_2\,F_c}{F_c}. \tag{1.22}$$

The moment of inertia of the rotor only changes if the permanent magnet is located in the rotor. The contribution of the permanent magnet to the moment of inertia is small because the permanent magnet is not located at the exterior of the rotor. The quality factor q_4 therefore has almost the same character as q_1.

Fig. 1.3 shows a plot of q_1, q_2 and q_3 versus the m.m.f. of the excitation coil on an arbitrary scale. The graph reveals clearly that a small deviation of q_1 from its optimum results in a much greater variation of q_2 and q_3.

It is possible to choose a different copper volume, which increases q_1 with decreasing q_2, and vice versa.

When the permanent magnet excitation is increased q_2 and q_3 will sharply rise while q_1 only slightly decreases. If in addition the copper volume is lowered, q_1 and q_2 remain practically unchanged whereas q_3 sharply rises.

1.4. The hybrid stepping motor with ring coils

From the foregoing it follows that a stepping motor with a single pole pair offers advantages over one with several pole pairs. In the frequently used type of motor with a "wound stator" at least two pole pairs are employed. An inadmissibly large radial force will act on the bearings, if only one pole pair per phase is used, which is avoided when a ring coil motor is employed (ref. 3).

Fig. 1.4 shows the motor, which is simply constructed by the use of ring coils. The stator consists of two parts which are connected with each other by a permanent magnet. Each stator part is made up from two magnetically conducting disks and a ring coil. The disks are coupled through a ferromagnetic conductor. The rotor consists of a shaft on which four disks are mounted. The rotor is entirely made from ferromagnetic material.

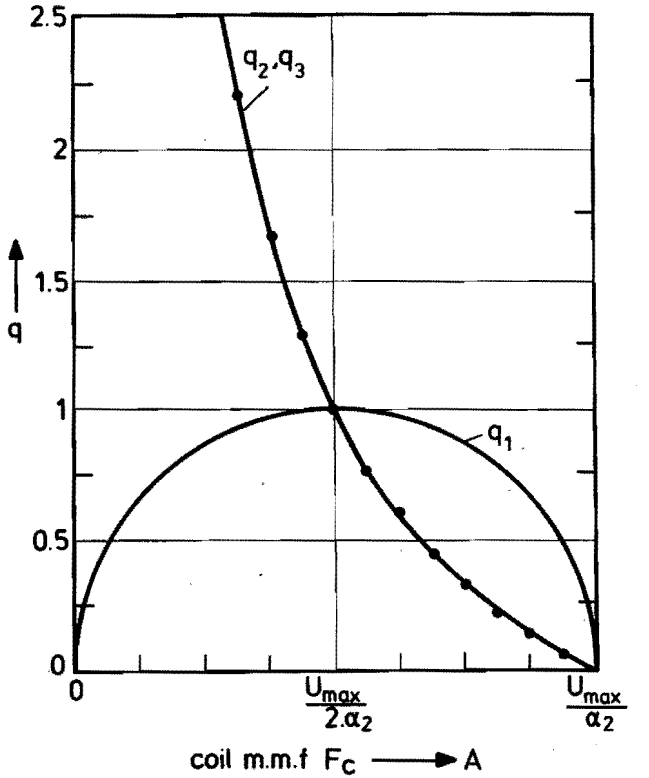

Fig. 1.3 – Quality criteria as a function of the applied coil excitation

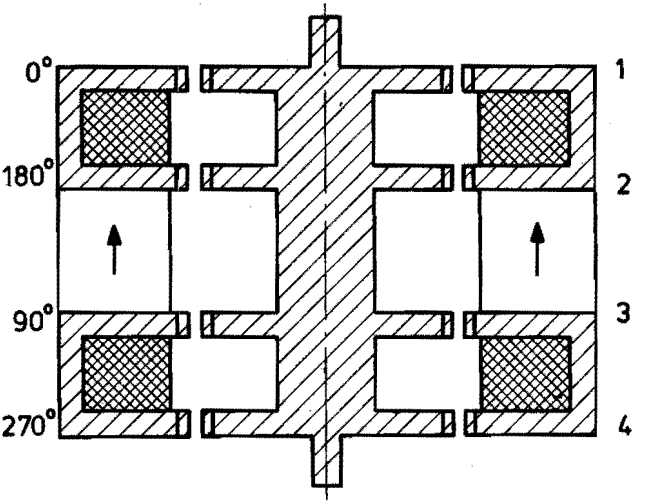

Fig. 1.4 – Diagram of the hybrid stepping motor with ring coils

Both the rotor and stator disks are provided with teeth on the air gap surface. The number of teeth is equal for the rotor and the stator and they are uniformly distributed around their circumferences. When the teeth of the first rotor disk are in line with those of the stator disk, then they are out of line for the second disk. The teeth of the third and the fourth disk are shifted by a quarter of a tooth pitch with respect to those of respectively the first and the second disk. In fig. 1.4 the teeth configuration is taken to be the same for all rotor disks and the stator teeth are shifted according to the indicated values in electrical degrees. We shall henceforth use the numbering of the disks as indicated in the drawing.

The stepping angle is expressed by

$$\theta_0 = \frac{360}{4n} \tag{1.23}$$

where θ_0 is the stepping angle in degrees and
n is the number of the teeth for each disk.

Because the number of teeth is the same for stator and rotor, the stepping angle can be much wider varied than in current hybrid stepping motors.
Unless otherwise specified, we henceforth take n=50 to obtain a stepping angle of 1.8 degree or 200 steps per revolution.

The permanent magnet passes a flux from one stator part to the other (see fig. 1.5). Depending on the rotor position the flux through the first disk will be larger than through the second, or vice versa. The sum of the fluxes through the two disks remains virtually constant. When a coil is excited a flux will flow from one disk to the other of the same stator part. The permanent magnet acts as a large air gap,

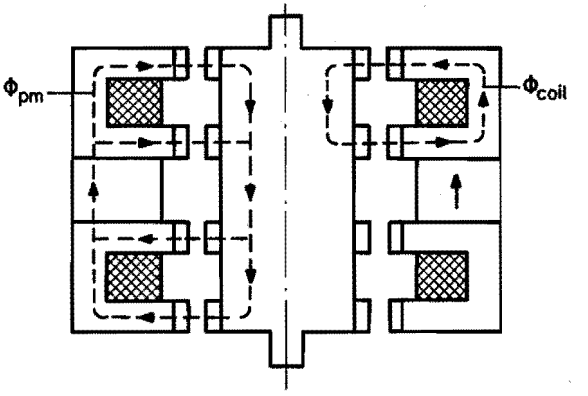

Fig. 1.5 – Magnetic paths of the permanent magnet flux and the coil flux

with the result that the two stator parts are almost magnetically disconnected. The coil excitation will intensify the flux from the permanent magnet in one disk and attenuate that in the other disk. The rotor will then be aligned with the teeth of the disk where the flux is intensified. By exciting the coils alternately in one of the two directions, the motor will assume its stepping character.

The motor design is from the electromechanical point of view not symmetrical in that the amplitude of the torque depends on the direction of the current. The difference in torque owing to the current direction is henceforth referred to as torque asymmetry.

The magnetic path of the flux from the permanent magnet is different from the first and the second disk. This leads to asymmetry in the permanent magnet excitation for the various disks. The asymmetric magnetic circuit gives rise to a stepping angle error which is inherent to the motor design.

2. TORQUE CALCULATIONS ON AN IDEALIZED HYBRID STEPPING MOTOR WITH RING COILS

In chapter 1 we have described a hybrid stepping motor with ring coils. The construction of the motor is asymmetric. This asymmetry is clearly see in fig. 2.1.

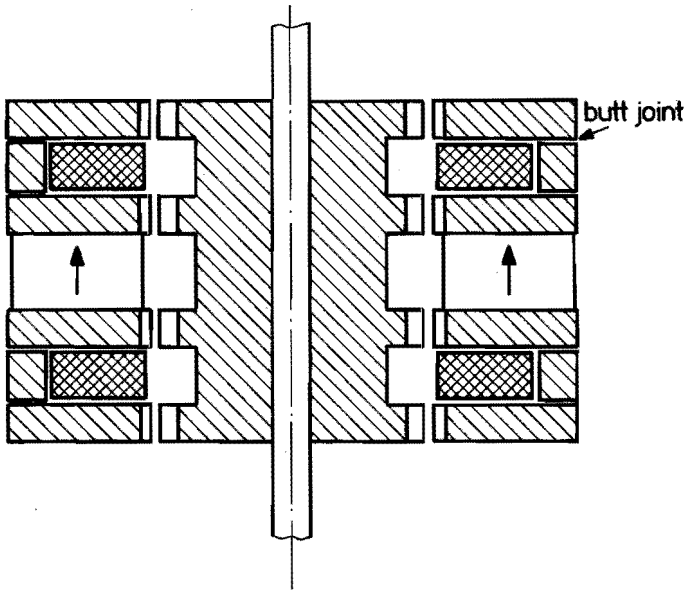

Fig. 2.1 – Butt joints in the motor construction

The magnetic path from the permanent magnet to the toothed poles is not equal for all poles. The outer poles are situated further away from the permanent magnet than the inner poles. As a consequence the permeance of the path of the flux flowing from the permanent magnet through disks 1 and 4 is different from that of the path of the flux flowing through disks 2 and 3.
Moreover while the whole flux generated by an excitation coil flows through the outer disk, a portion of this flux does not flow through the inner disk of the same part of the stator but will flow through the other stator part and the permanent magnet. This means that the flux from the excitation coil is not equal for the inner and outer disks. These asymmetries in the magnetic circuit will lead to asymmetries in the static torque production of the motor. To investigate the problems which will arise due to the asymmetric magnetic circuit we will first idealize the motor to such an extent that the motor becomes symmetric again. In later calculations the effects of the deviations from the ideal motor will be considered.
The assumptions for an ideal motor are:
1. The permeability of the iron is infinitely large.

2. The construction has no butt joints.
3. The flux generated by an excitation coil flows only from one disk to the other disk of the same stator part. No flux generated by an excitation coil flows through the other stator part and the permanent magnet. This means that, seen from the excitation coil, the permeance of the permanent magnet is considered to be zero.
4. The teeth of the rotor and stator are identical.
5. The air gap permeance can be described by a function consisting of a constant part and a sinusoidal variation as a function of the rotor position.
6. End effects are negligibly small.
7. Fringing fluxes flowing outside the air gaps are considered to be negligible.
8. During the calculations only the first stator will be excited. Excitation of the other stator part leads to identical results at only a different rotor position.

The permeance functions in the in-line and the out of line positions of the disks are known if use is made of Mukherji and Neville's results (ref. 8).
The permeance of the first disk is:

$$P_1 = P_0 + P\cos(n\theta) \tag{2.1}$$

and of the other disks

$$P_2 = P_0 - P\cos(n\theta) \tag{2.2}$$

$$P_3 = P_0 - P\sin(n\theta) \tag{2.3}$$

$$P_4 = P_0 + P\sin(n\theta) \tag{2.4}$$

Here P_0 is the constant and P is the amplitude of the variable part of the permeance. P_0 and P are found from

$$P_0 = \frac{P_{in} + P_{out}}{2} \tag{2.5}$$

$$P = \frac{P_{in} - P_{out}}{2}, \tag{2.6}$$

where P_{in} is the permeance of the disk when the rotor and stator teeth are in alignment and P_{out} when they are out of alignment.

The magnetic potential difference from the permanent magnet is equal across the first and the second disk because they are in parallel as seen from the permanent magnet. The parallel permeance of the first and second disks is

$$P_1 + P_2 = 2P_0. \tag{2.7}$$

The permeance of the second stator part is also equal to $2P_0$. The permeance of the magnetic circuit as seen from the permanent magnet is therefore independent of the rotor position.
The size of the permanent magnet, the type of magnetic material and the permeance P_0 determine the flux from the permanent magnet. If we call U_{pm} the magnetic potential difference from the permanent magnet outside the permanent magnet, then it is true to say

$$\Phi_{pm} = U_{pm} P_0, \tag{2.8}$$

where Φ_{pm} is the flux from the permanent magnet and P_0 the series permeance of the two stator parts.
The magnetic induction in the permanent magnet follows from the flux Φ_{pm} and the surface area A_{pm} of the permanent magnet:

$$B_{pm} = \frac{\Phi_{pm}}{A_{pm}} = \frac{U_{pm} P_0}{A_{pm}}. \tag{2.9}$$

The length of the permanent magnet l_{pm} and the magnetic potential difference U_{pm} outside the permanent magnet determine the magnetic field strength in the magnet:

$$H_{pm} = -\frac{U_{pm}}{l_{pm}}. \tag{2.10}$$

From (2.9) and (2.10) we arrive at the magnetic induction of the magnet

$$B_{pm} = -H_{pm} \frac{l_{pm}}{A_{pm}} P_0, \tag{2.11}$$

which yields the working line of the magnetic circuit.

In fig. 2.2 the working line and the magnetization curve of the magnet are drawn.

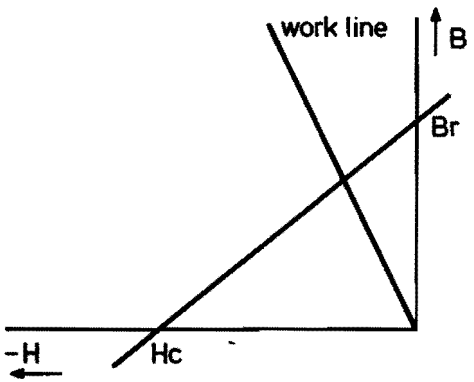

Fig. 2.2 – Magnetization curve of the permanent magnet

The intersection of the working line and the magnetization curve of the magnet is the working point. The magnetization curve can be approximated by

$$B = -B_r\left(\frac{H}{H_c} - 1\right). \tag{2.12}$$

Substitution of (2.11) in (2.12) results in the working point

$$-B_r\left(\frac{H_{pm}}{H_c} - 1\right) = -H_{pm}\,\frac{l_{pm}}{A_{pm}}P_0. \tag{2.13}$$

The magnetic field strength in the magnet is

$$H_{pm} = \frac{B_r}{\left(\frac{B_r}{H_c} - \frac{l_{pm}P_0}{A_{pm}}\right)}. \tag{2.14}$$

The magnetic potential difference from the permanent magnet outside the permanent magnet is

$$U_{pm} = -H_{pm}\,l_{pm} = -\frac{B_r\,l_{pm}}{\left(\frac{B_r}{H_c} - \frac{l_{pm}P_0}{A_{pm}}\right)}. \tag{2.15}$$

In the following we will calculate the magnetic potential difference distribution in the motor by using U_{pm}, the magnetic potential difference of the permanent magnet outside the permanent magnet.
Because the permeance of the magnetic circuit as seen from the permanent magnet is equal to P_0 and therefore independent of the rotor position, the magnetic potential difference U_{pm} is independent of the rotor position.
The magnetic potential difference due to the permanent magnet excitation across the air gap in each stator part is equal to $U_{pm}/2$.

To the m.m.f. from the coil it applies that

$$U_{c1}\,(P_0 + P\cos(n\theta)) = U_{c2}\,(P_0 - P\cos(n\theta)) \tag{2.16}$$

and

$$F_c = U_{c1} + U_{c2} \tag{2.17}$$

Here (see fig. 2.3)
F_c is the m.m.f. from the coil,
U_{c1} is the magnetic potential difference across the air gap at disk 1,
U_{c2} is the magnetic potential difference across the air gap at disk 2.

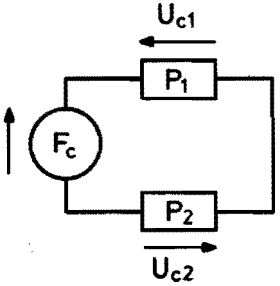

Fig. 2.3 – Distribution of the m.m.f. of the coil excitation

In the figures the positive values of the variables are indicated by the direction of the arrows.

For the magnetic potential difference across the air gaps we may write

$$U_{c1} = F_c \frac{(P_0 - P\cos(n\theta))}{2P_0} \tag{2.18}$$

$$U_{c2} = F_c \frac{(P_0 + P\cos(n\theta))}{2P_0}. \tag{2.19}$$

The total magnetic potential difference across the air gaps is formed by the m.m.f.s from the permanent magnet and the coil excitation:

$$U_1 = \frac{U_{pm}}{2} + U_{c1} \tag{2.20}$$

$$U_2 = \frac{U_{pm}}{2} - U_{c2}. \tag{2.21}$$

The magnetic potential difference across the air gap is accompanied by magnetic energy. In air the magnetic coenergy equals the magnetic energy. Differentiation of the magnetic coenergy with respect to the angular position at constant magnetic potential difference across the air gap yields the torque (ref. 9).
The torque on the first disk is

$$T_1 = \frac{U_1^2}{2}\frac{dP_1}{d\theta} = -\frac{U_1^2}{2} n P \sin(n\theta) \tag{2.22}$$

and on the second disk

$$T_2 = \frac{U_2^2}{2}\frac{dP_2}{d\theta} = \frac{U_2^2}{2} n P \sin(n\theta). \tag{2.23}$$

The torque on the two disks is the total torque delivered by the motor. The magnetic energy of disks 3 and 4 together remains unaltered during rotation. The total torque follows from the summation of T_1 and T_2 with equations (2.20, 21, 22, 23) and we may write

$$T = T_1 + T_2 = -\frac{n}{2} P \sin(n\theta) \left\{U_1^2 - U_2^2\right\}$$

$$T = -\frac{n}{2} P U_{pm} F_c \sin(n\theta) + \frac{n}{4}\frac{P^2}{P_0} F_c^2 \sin(2n\theta). \tag{2.24}$$

The torque consists of two terms. The first term, the hybrid torque, contains the product of the m.m.f.s from the permanent magnet and the excitation coil. The

hybrid torque has the same periodicity as the tooth geometry in the motor. This we will call the fundamental periodicity. The second term in expression (2.24), the reluctance torque, contains the excitation m.m.f. squared and has the double angular periodicity. The reluctance torque in the motor is due to the fact that the series permeance of the two air gaps is a function of the rotor angle with the double angular periodicity. The magnetic energy produced by the coil is therefore also a function of the rotor angle with the double angular periodicity which leads to a torque with a double angular periodicity.
If the excitation coil is excited in the opposite direction, the torque becomes

$$T = \frac{n}{2} P U_{pm} F_c \sin(n\theta) + \frac{n}{4} \frac{P^2}{P_0} F_c^2 \sin(2n\theta). \qquad (2.25)$$

The hybrid torque depends on the current direction whereas the reluctance torque is independent of the current direction. The reluctance torque has the double angular periodicity and therefore the total torque angle curve has the same shape for both directions of excitation. This is demonstrated in fig. 2.4 where the hybrid and reluctance torques are shown for some arbitrary values, and in fig. 2.5 where

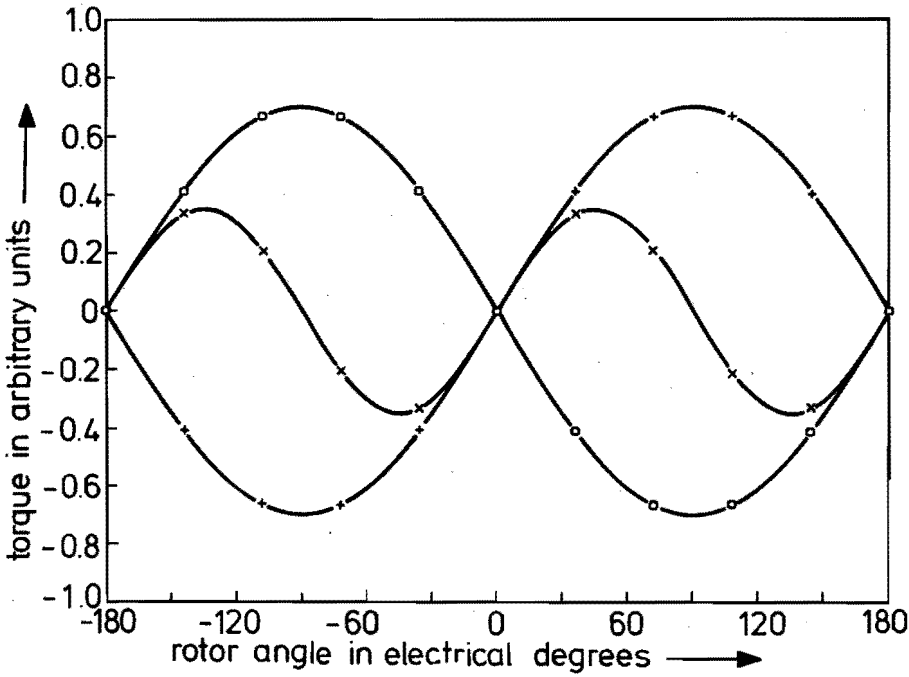

Fig. 2.4 – Hybrid torques and reluctance torque for some arbitrary values

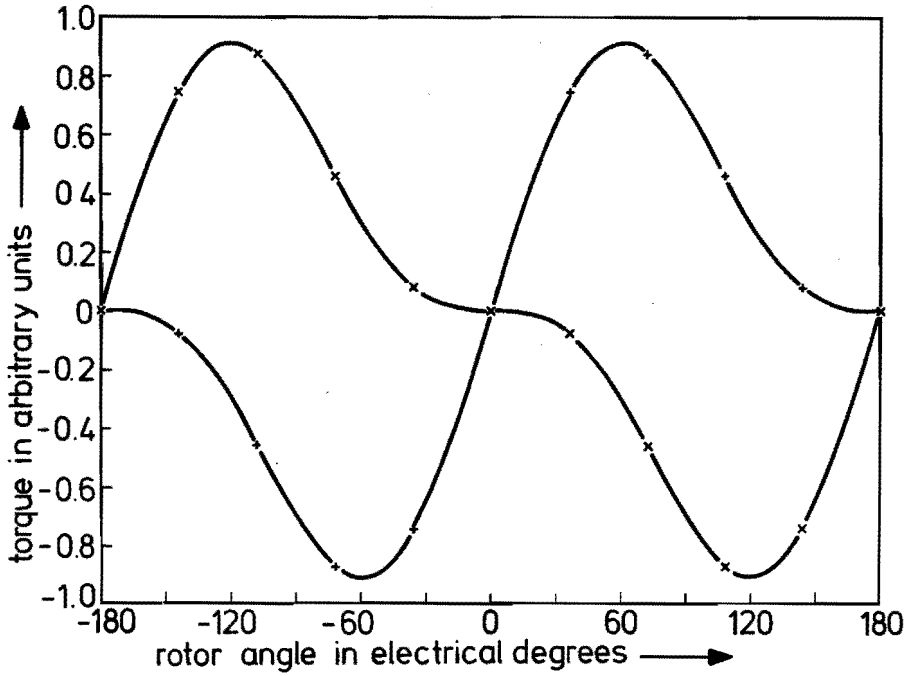

Fig. 2.5 – Sum of the reluctance and hybrid torques from fig. 2.4

the sum of the reluctance and hybrid torques is shown. The only difference between the torque angle curves for the two directions of excitation is the requisite shift by 180 electrical degrees. The arbitrarily chosen values are only taken to show the effect of the torque on the periodicity. The ratio between the hybrid and reluctance torque can be strongly varied, depending on the design parameters.

2.1. Effect of the coupling between the two stator parts

In the foregoing it was assumed that no flux generated by the excitation coil was linked with both stator parts. This is only possible if the permeance of the permanent magnet is negligibly small. In this section we will investigate the effect of the coupling between the two stator parts. We therefore retain the assumptions as done in the previous section with the exception of the decoupling of the stator parts.

The permeance between the stator parts is formed by the space in which the permanent magnet is situated and the permeability of the permanent magnet. This permeance is denoted by P_s. Fig. 2.6 gives an analogon in which all the permeances are indicated that are needed to calculate the m.m.f. distribution due to the coil excitation.

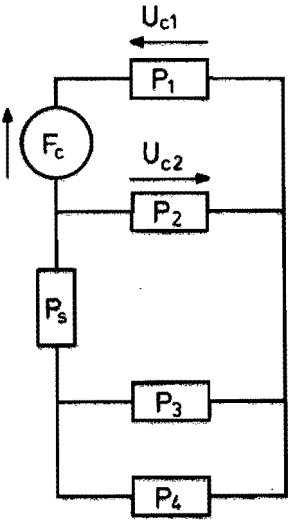

Fig. 2.6 – Analogon of the magnetic circuit needed to calculate the m.m.f. distribution due to the coil excitation

The permeances P_3 and P_4 of respectively disks 3 and 4 are in parallel and together constitute the permeance $2P_0$. The permeance $2P_0$ of disks 3 and 4 acts in series with the permeance P_S, which together are in parallel with the permeance P_2 of disk 2. The series connection of P_S and $2P_0$ yields

$$\frac{2P_0\,P_S}{P_S + 2P_0} \tag{2.26}$$

Parallel arrangement of P_2 with this permeance leads to

$$P_2 + \frac{2P_S\,P_0}{P_S + 2P_0} = P_0 - P\cos(n\theta) + \frac{2P_S P_0}{P_S + 2P_0}\,. \tag{2.27}$$

The magnetic potential difference across the air gaps from the coil excitation follows from

$$U_{c1}\,(P_0 + P\cos(n\theta)) = U_{c2}\,(P_0 - P\cos(n\theta) + \frac{2P_S P_0}{P_S + 2P_0}) \tag{2.28}$$

and

$$F_c = U_{c1} + U_{c2}, \tag{2.29}$$

where U_{c1} is

$$U_{c1} = \left\{ \frac{P_0 - P\cos(n\theta) + \frac{2P_S P_0}{P_S + 2P_0}}{2P_0 + \frac{2P_S P_0}{P_S + 2P_0}} \right\} F_c \qquad (2.30)$$

$$= \left\{ \frac{3P_S P_0 + 2P_0^2 - P(P_S + 2P_0)\cos(n\theta)}{4P_S P_0 + 4P_0^2} \right\} F_c$$

and U_{c2} is

$$U_{c2} = \left\{ \frac{P_0 + P\cos(n\theta)}{2P_0 + \frac{2P_S P_0}{P_S + 2P_0}} \right\} F_c \qquad (2.31)$$

$$= \left\{ \frac{P_S P_0 + 2P_0^2 + P(P_S + 2P_0)\cos(n\theta)}{4P_S P_0 + 4P_0^2} \right\} F_c$$

In the consideration of the magnetic potential difference from the permanent magnet nothing alters. The magnetic potential difference from the permanent magnet remains $U_{pm}/2$ across the air gaps of each disk. The torque is generated by disks 1 and 2. The disks 3 and 4 in parallel have a constant permeance and hence produce no torque. The torque for disks 1 and 2 is

$$T_1 = \frac{1}{2} U_1^2 \frac{dP_1}{d\theta} = -\frac{n}{2} \left(\frac{U_{pm}}{2} + U_{c1}\right)^2 P \sin(n\theta). \qquad (2.32)$$

and

$$T_2 = \frac{1}{2} U_2^2 \frac{dP_2}{d\theta} = \frac{n}{2} \left(\frac{U_{pm}}{2} - U_{c2}\right)^2 P \sin(n\theta). \qquad (2.33)$$

Tot total torque delivered by the motor is

$$T = T_1 + T_2 = -\frac{n}{2} P \sin(n\theta) \left\{ \left(\frac{U_{pm}}{2} + U_{c1}\right)^2 - \left(\frac{U_{pm}}{2} - U_{c2}\right)^2 \right\} \qquad (2.34)$$

$$T = -\frac{n}{2} P \sin(n\theta) \left\{ U_{pm} (U_{c1} + U_{c2}) + U_{c1}^2 - U_{c2}^2 \right\}. \tag{2.35}$$

The torque consists of a hybrid and a reluctance term. The hybrid torque is given by

$$\begin{aligned} T_H &= -\frac{n}{2} P \sin(n\theta) U_{pm} (U_{c1} + U_{c2}) \\ &= -\frac{n}{2} P \sin(n\theta) U_{pm} F_c \end{aligned} \tag{2.36}$$

This expression of the hybrid torque is equal to that for the hybrid torque in expression (2.24). This implies that the hybrid torque is independent of the coupling between the two stator parts.

The reluctance torque is equal to

$$T_R = -\frac{n}{2} P \sin(n\theta) (U_{c1}^2 - U_{c2}^2) \tag{2.37}$$

$$T_R = -\frac{n}{2} P \sin(n\theta) F_c^2 \left\{ \frac{P_S P_0}{2(P_S P_0 + P_0^2)} - \frac{P(P_S + 2P_0)}{2(P_S P_0 + P_0^2)} \cos(n\theta) \right\} \tag{2.38}$$

$$T_R = -\frac{n}{4} \frac{P_S P}{(P_S + P_0)} F_c^2 \sin(n\theta) + \frac{n}{8} \frac{P^2 (P_S + 2P_0)}{(P_S P_0 + P_0^2)} F_c^2 \sin(2n\theta). \tag{2.39}$$

The reluctance torque consists now of a part with the fundamental angular periodicity and a part with twice the angular periodicity. As already noted, the part with twice the angular periodicity does not affect the torque symmetry for the different steps. The part with the fundamental angular periodicity has the same direction irrespective of the direction of the excitation current. Hence the coupling between the two stator parts results in the reluctance torque which, depending on the current direction, decreases or increases the hybrid torque. Hence the coupling between the two stator parts causes torque asymmetry. In fig. 2.7 the hybrid and both parts of the reluctance torque are drawn for some arbitrary values to demonstrate the effect of the reluctance torque on the total torque of the motor. The total torque clearly shows the asymmetry due to the reluctance torque.

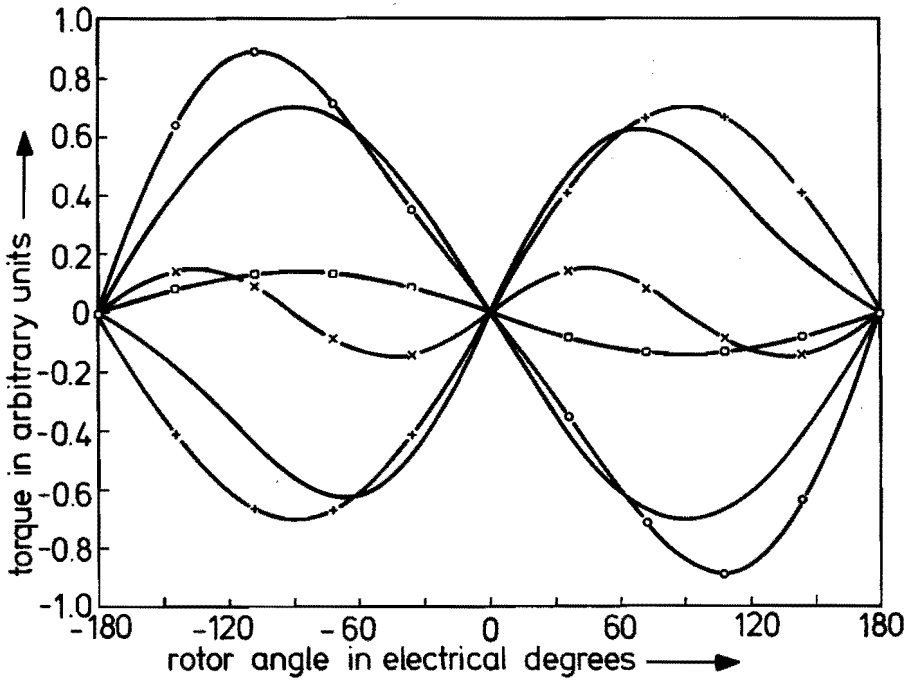

Fig. 2.7 – Asymmetry due to the reluctance torque with the fundamental periodicity of the motor torque

2.2. Effect of butt joints on torque formation

Butt joints arise between the disks and the magnetic conductors (see fig. 2.8). They may also occur in the rotor. Since the results of these butt joints on the torque formation are the same as in the stator, we shall only discuss the influence of stator butt joints. As viewed from the permanent magnet, the butt joints are arranged in series with the first or fourth disk. Since the butt joints are not arranged in series with the second and third disk the construction will be asymmetric. The butt joints decrease the permeance of the magnetic path which the flux follows if it flows through the outer disks. In principle, then, saturation of the magnetic circuit has in this case the same effect as the butt joints. To gain an insight into the effect of the decreased permeance we will only investigate the influence of the butt joints. The effect of saturation is more complicated due to the non-linear behaviour of the permeability of the iron. In the present section we will therefore make the same assumption as in section 2. with the exception of the occurrence of butt joints. The permeance of the butt joints, denoted by P_b, is assumed to be the same for both stator parts. In the case of more than one butt joint, P_b is the total permeance caused by these butt joints. Their permeance is in series with P_1 or P_4.

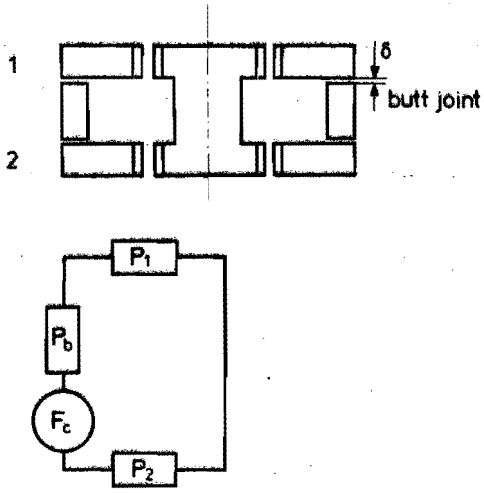

Fig. 2.8 – Butt joints in the magnetic circuit of the stator parts

The series permeance is

$$P_1' = \frac{P_b\,(P_0 + P\cos(n\theta))}{P_b + P_0 + P\cos(n\theta)} \tag{2.40}$$

$$P_4' = \frac{P_b\,(P_0 + P\sin(n\theta))}{P_b + P_0 + P\sin(n\theta)} \tag{2.41}$$

The magnetic potential difference from the permanent magnet is distributed over the two stator parts as:

$$U_{pm1} = \frac{P_3 + P_4'}{P_1' + P_2 + P_3 + P_4'}\,U_{pm} \tag{2.42}$$

$$U_{pm2} = \frac{P_1' + P_2}{P_1' + P_2 + P_3 + P_4'}\,U_{pm}. \tag{2.43}$$

Owing to the butt joints, the magnetic potential difference U_{pm} of the permanent magnet outside the permanent magnet depends on the rotor position. The total permeance of the magnet circuit as viewed from the permanent magnet is the permeance of both stator parts in series. This permeance is

$$P_t = \frac{(P_1' + P_2)\,(P_4' + P_3)}{P_1' + P_2 + P_3 + P_4'}. \tag{2.44}$$

Fully elaborated the permeance P_t is

$$P_t = \frac{\dfrac{2P_0P_b + P_0^2 - P^2\cos^2(n\theta)}{P_b + P_0 + P\cos(n\theta)} \cdot \dfrac{2P_0P_b + P_0^2 - P^2\sin^2(n\theta)}{P_b + P_0 + P\sin(n\theta)}}{\dfrac{2P_0P_b + P_0^2 - P^2\cos^2(n\theta)}{P_b + P_0 + P\cos(n\theta)} + \dfrac{2P_0P_b + P_0^2 - P^2\sin^2(n\theta)}{P_b + P_0 + P\sin(n\theta)}}. \tag{2.45}$$

In practice P_b will be much bigger than P. If we therefore treat P as negligible compared with P_b, and because $P_0 > P$, the expression (2.45) becomes

$$P_t \cong \frac{2P_0P_b + P_0^2}{2(P_b + P_0)}. \tag{2.46}$$

The expression (2.46) is independent of the rotor position. In further calculations we will therefore assume U_{pm} to be independent of the rotor position.
The m.m.f. of the coil is distributed over disks 1 and 2 as

$$U_{c1} = \frac{P_2}{P_1' + P_2} F_c, \tag{2.47}$$

$$U_{c2} = \frac{P_1'}{P_1' + P_2} F_c. \tag{2.48}$$

The torque of each disk becomes

$$T_1 = \frac{1}{2} U_1^2 \frac{dP_1'}{d\theta} = \frac{1}{2} (U_{pm1} + U_{c1})^2 \frac{dP_1'}{d\theta} \tag{2.49}$$

$$T_2 = \frac{1}{2} U_2^2 \frac{dP_2}{d\theta} = \frac{1}{2} (U_{pm1} - U_{c2})^2 \frac{dP_2}{d\theta} \tag{2.50}$$

$$T_3 = \frac{1}{2} U_3^2 \frac{dP_3}{d\theta} = \frac{1}{2} U_{pm2}^2 \frac{dP_3}{d\theta} \tag{2.51}$$

$$T_4 = \frac{1}{2} U_4^2 \frac{dP_4'}{d\theta} = \frac{1}{2} U_{pm2}^2 \frac{dP_4'}{d\theta}. \tag{2.52}$$

Elaboration of eqs. (2.49)-(2.52) leads to

$$T_1 = -\frac{1}{2}\left\{\left(\frac{P_3 + P_4'}{P_1' + P_2 + P_3 + P_4'}\right)^2 U_{pm}^2 + \frac{2\,(P_3 + P_4')}{(P_1' + P_2 + P_3 + P_4')}\,\frac{P_2}{(P_1' + P_2)}\cdot\right.$$
$$\left.\cdot\, U_{pm}\, F_c + \left(\frac{P_2}{P_1' + P_2}\right)^2 F_c^2\right\}\,\frac{n\,P_b^2\,P\,\sin(n\theta)}{(P_b + P_o + P\cos(n\theta))^2} \qquad (2.53)$$

$$T_2 = \frac{1}{2}\left\{\left(\frac{P_3 + P_4'}{P_1' + P_2 + P_3 + P_4'}\right)^2 U_{pm}^2 - \frac{2\,(P_3 + P_4')}{(P_1' + P_2 + P_3 + P_4')}\,\frac{P_1'}{(P_1' + P_2)}\cdot\right.$$
$$\left.\cdot\, U_{pm}\, F_c + \left(\frac{P_1'}{P_1' + P_2}\right)^2 F_c^2\right\}\, n\,P\sin(n\theta). \qquad (2.54)$$

$$T_3 = -\frac{n}{2}\,P\cos(n\theta)\left(\frac{P_1' + P_2}{P_1' + P_2 + P_3 + P_4'}\right)^2 U_{pm}^2 \qquad (2.55)$$

$$T_4 = \frac{n}{2}\,\frac{P_b^2\,P\cos(n\theta)}{(P_b + P_o + P\sin(n\theta))^2}\left(\frac{P_1' + P_2}{P_1' + P_2 + P_3 + P_4'}\right)^2 U_{pm}^2. \qquad (2.56)$$

Expressions (2.53)-(2.56) contain the following three types of torque terms:

1. Detent torque formed from the terms containing U_{pm}^2. The occurence of these terms is independent of the excitation current.

2. Hybrid torque formed from the product terms $U_{pm}\,F_c$ yielding a torque varying as a function of the excitation current. The direction of the torque is governed by the direction of the excitation current. The fundamental harmonic component of this term constitutes the requisite torque.

3. Reluctance torque formed from the terms with F_c^2, which yield a torque that depends on the magnitude of the current. The direction of the torque is not determined by that of the current.

Detent torque

All four disks contribute to the detent torque. The total detent torque is

$$T_D = \left\{ -\frac{n}{2}\frac{P_b^2\, P\sin(n\theta)}{(P_b + P_0 + P\cos(n\theta))^2} + \frac{n}{2} P\sin(n\theta) \right\} \cdot \left(\frac{P_3 + P_4'}{P_1' + P_2 + P_3 + P_4'} \right)^2 U_{pm}^2 + \left(\frac{P_1' + P_2}{P_1' + P_2 + P_3 + P_4'} \right)^2 U_{pm}^2 \cdot \left\{ \frac{n}{2}\frac{P_b^2\, P\cos(n\theta)}{(P_b + P_0 + P\sin(n\theta))^2} - \frac{n}{2} P\cos(n\theta) \right\} \tag{2.57}$$

The permeance terms are given in

$$P_1' + P_2 = \frac{2P_0P_b + P_0^2 - P^2\cos^2(n\theta)}{P_b + P_0 + P\cos(n\theta)} \tag{2.58}$$

$$P_3 + P_4' = \frac{2P_0P_b + P_0^2 - P^2\sin^2(n\theta)}{P_b + P_0 + P\sin(n\theta)} \tag{2.59}$$

$$\frac{P_1' + P_2}{P_1' + P_2 + P_3 + P_4'} = \frac{(2P_0P_b + P_0^2 - P^2\cos^2(n\theta))\,(P_b + P_0 + P\sin(n\theta))}{\left\{(2P_0P_b + P_0^2 - P^2\cos^2(n\theta))\,(P_b + P_0 + P\sin(n\theta)) + (2P_0P_b + P_0^2 - P^2\sin^2(n\theta))\,(P_b + P_0 + P\cos(n\theta))\right\}} \tag{2.60}$$

$$\frac{P_3 + P_4'}{P_1' + P_2 + P_3 + P_4'} = \frac{(2P_0P_b + P_0^2 - P^2\sin^2(n\theta))\,(P_b + P_0 + P\cos(n\theta))}{\left\{(2P_0P_b + P_0^2 - P^2\cos^2(n\theta))\,(P_b + P_0 + P\sin(n\theta)) + (2P_0P_b + P_0^2 - P^2\sin^2(n\theta))\,(P_b + P_0 + P\cos(n\theta))\right\}} \tag{2.61}$$

Using these expressions, we find the detent torque as:

$$T_D = \frac{n}{2} P \sin(n\theta)\, U_{pm}^2 \left\{ 1 - \frac{P_b^2}{(P_b + P_0 + P\cos(n\theta))^2} \right\} \cdot$$

$$\left\{ \frac{(2P_bP_0 + P_0^2 - P^2\sin^2(n\theta))(P_b + P_0 + P\cos(n\theta))}{(2P_bP_0 + P_0^2 - P^2\sin^2(n\theta))(P_b + P_0 + P\cos(n\theta)) + (2P_bP_0 + P_0^2 - P^2\cos^2(n\theta)) \cdot \frac{}{(P_b + P_0 + P\sin(n\theta))}} \right\}^2 +$$

$$\frac{n}{2} P\cos(n\theta)\, U_{pm}^2 \left\{ \frac{P_b^2}{(P_b + P_0 + P\sin(n\theta))^2} - 1 \right\} \cdot$$

$$\left\{ \frac{(2P_0P_b + P_0^2 - P^2\cos^2(n\theta))(P_b + P_0 + P\sin(n\theta))}{(2P_0P_b + P_0^2 - P^2\sin^2(n\theta))(P_b + P_0 + P\cos(n\theta)) + (2P_0P_b + P_0^2 - P^2\cos^2(n\theta)) \cdot \frac{}{(P_b + P_0 + P\sin(n\theta))}} \right\}^2 . \qquad (2.62)$$

This tedious expression, from which it is not at once evident how the detent torque is affected by the butt joints, becomes more straightforward if the butt joints are small enough to allow us to treat P as negligible compared with P_b. Expression (2.62) then becomes:

$$T_D \cong \left\{ \frac{n}{8} P \sin(n\theta) \frac{2P_bP_0 + P_0^2}{(P_b + P_0)^2} - \frac{n}{2} P\cos(n\theta) \frac{(2P_bP_0 + P_0^2)}{(P_b + P_0)^2} \right\} U_{pm}^2$$

$$T_D \cong \frac{n}{8} P \frac{(2P_bP_0 + P_0^2)}{(P_b + P_0)^2} \sqrt{2}\sin(n\theta - 45)\, U_{pm}^2 \qquad (2.63)$$

The detent torque is a function of the rotor position with the fundamental angular periodicity. In fig. 2.9 the detent torque and the hybrid torques are drawn for some arbitrary amplitudes. The hybrid torques are shifted by 90 electrical degrees, depending on which stator part is excited and which current direction is applied. The stable position in the hybrid torque angle curve is also shifted by 90 electrical degrees. The total torque is formed by the summation of the detent torque and the hybrid torque. The sum of the detent and hybrid torques is shown in fig. 2.10. Due to the shift of 45 or 135 electrical degrees between the detent and hybrid torques, the stable position of the total torque differs from 90 electrical degrees. For stepping motors the stepping angle is defined as the angle between the stable positions. The effect of the butt joints is therefore a deviation from the required stepping angle.

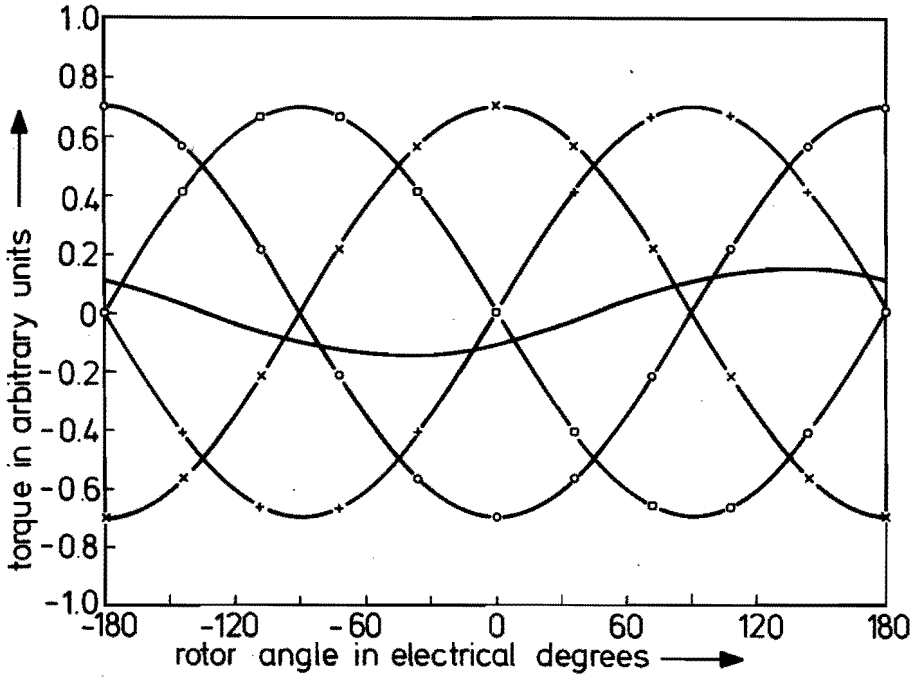

Fig. 2.9 – Detent and hybrid torques for some arbitrary values

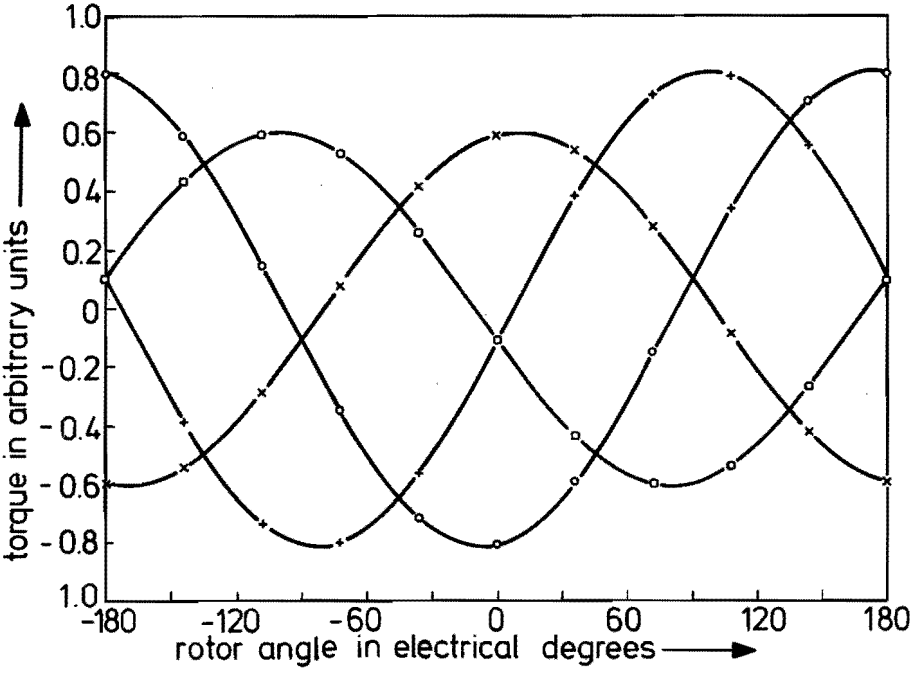

Fig. 2.10 – Sum of the detent and hybrid torques from fig. 2.9

Hybrid torque

The hybrid torque is formed by the terms containing $U_{pm}\,F_c$, which only occur in the first and second disks. The hybrid torques for these disks are

$$T_{H1} = -\frac{(P_3 + P_4')}{(P_1' + P_2 + P_3 + P_4')}\,\frac{P_2}{(P_1' + P_2)}\,U_{pm}\,\frac{F_c\,n\,P\,P_b^{\,2}\,\sin(n\theta)}{(P_b + P_0 + P\cos(n\theta))^2} \tag{2.64}$$

$$T_{H2} = -\frac{(P_3 + P_4')}{(P_1' + P_2 + P_3 + P_4')}\,\frac{P_1'}{(P_1' + P_2)}\,U_{pm}\,F_c\,n\,P\sin(n\theta). \tag{2.65}$$

The total hybrid torque of the motor is

$$T_H = T_{H1} + T_{H2} = -\frac{n\,P\sin(n\theta)\,U_{pm}\,F_c\,(P_3 + P_4')}{(P_1' + P_2)\,(P_1' + P_2 + P_3 + P_4')}\cdot \left\{\frac{P_b\,(P_0 + P\cos(n\theta))}{(P_b + P_0 + P\cos(n\theta))} + \frac{P_b^{\,2}\,(P_0 - P\cos(n\theta))}{(P_b + P_0 + P\cos(n\theta))^2}\right\} \tag{2.66}$$

Fully worked out, the expression for the hybrid torque becomes

$$T_H = -\,n\,P\sin(n\theta)\,U_{pm}\,F_c\cdot$$

$$\frac{2P_b^{\,2}P_0 + P_bP_0^{\,2} + 2P_bP_0P\cos(n\theta) + P_b\,P^2\cos^2(n\theta))}{(2P_bP_0 + P_0^{\,2} - P^2\cos^2(n\theta))\,(P_b + P_0 + P\cos(n\theta))}\cdot$$

$$\left\{\frac{(2P_bP_0 + P_0^{\,2} - P^2\sin^2(n\theta))\,(P_b + P_0 + P\cos(n\theta))}{(2P_bP_0 + P_0^{\,2} - P^2\sin^2(n\theta))\,(P_b + P_0 + P\cos(n\theta))} + \frac{}{(2P_bP_0 + P_0^{\,2} - P^2\cos^2(n\theta))\,(P_b + P_0 + P\sin(n\theta))}\right\}. \tag{2.67}$$

Neglecting the P terms in (2.67) with respect to the P_b terms, equation (2.67) becomes:

$$T_H \cong -\frac{n}{2}\,P\sin(n\theta)\,U_{pm}\,F_c\,\frac{P_b}{P_b + P_0}\,. \tag{2.68}$$

Owing to the butt joints the hybrid torque decreases. The stable positions of the hybrid torque are not effected by the butt joints.

Reluctance torque

The reluctance torque is formed by the F_c^2 terms, which only occur with the disks 1 and 2. For these disks the reluctance torque is

$$T_{R1} = -\frac{n}{2}\frac{P\sin(n\theta)\,F_c^2\,P_b^2}{(P_b + P_0 + P\cos(n\theta))^2}\left(\frac{P_2}{P_1' + P_2}\right)^2 \tag{2.69}$$

and

$$T_{R2} = \frac{n}{2}\frac{P\sin(n\theta)\,F_c^2\,P_b^2}{(P_b + P_0 + P\cos(n\theta))^2}\left(\frac{P_1}{P_1' + P_2}\right)^2. \tag{2.70}$$

The total reluctance torque is:

$$T_R = \frac{n}{2}\frac{P\sin(n\theta)\,F_c^2}{(P_1' + P_2)^2}\left\{\frac{P_b^2\,(P_0 + P\cos(n\theta))^2}{(P_b + P_0 + P\cos(n\theta))^2} - \frac{P_b^2\,(P_0 - P\cos(n\theta))^2}{(P_b + P_0 + P\cos(n\theta))^2}\right\}$$

$$T_R = 2\,n\,P\sin(n\theta)\,F_c^2\,\frac{P_0\,P\cos(n\theta)\,P_b^2}{(2P_bP_0 + P_0^2 - P^2\cos^2(n\theta))^2}. \tag{2.71}$$

When the P terms are disregarded as being negligible compared with the P_b terms, the reluctance torque becomes:

$$T_R = n\,P\sin(2n\theta)\,F_c^2\,\frac{P_0\,P\,P_b^2}{(2P_bP_0 + P_0^2)^2}. \tag{2.72}$$

The reluctance torque contains only a second harmonic component and consequently causes no asymmetry in the motor torque. The butt joints, do, however, decrease the reluctance torque.

The effects of the butt joints on the performance of the motor are therefore a reduction of the available torque and a deviation from the stepping angle.

2.3. Effect of the butt joints and the coupling of the two stator parts on the generation of the torque

The influence of the butt joints and the coupling of the two stator parts have been dealt with in sections 2.2. and 2.1. In the present section the same assumptions will

therefore be made as in section 2., except for the stator butt joints and the coupling of the two stator parts.
The butt joints and the permeances P_1 and P_4 constitute the respective permeances

$$P_1' = \frac{P_b\,(P_0 + P\cos(n\theta))}{P_b + P_0 + P\cos(n\theta)}. \tag{2.73}$$

$$P_4' = \frac{P_b\,(P_0 + P\sin(n\theta))}{P_b + P_0 + P\sin(n\theta)}. \tag{2.74}$$

The magnetic potential difference from the permanent magnet outside the magnet is distributed between the two stator parts according to

$$U_{pm1} = \frac{P_3 + P_4'}{P_1' + P_2 + P_3 + P_4'} U_{pm} \tag{2.75}$$

$$U_{pm2} = \frac{P_1' + P_2}{P_1' + P_2 + P_3 + P_4'} U_{pm} \tag{2.76}$$

The m.m.f. due to the coil excitation is distributed over disks 1 and 2 as:

$$U_{c1} = \left\{ \frac{P_2 + \dfrac{(P_3 + P_4')\,P_S}{P_3 + P_4' + P_S}}{P_1' + P_2 + \dfrac{(P_3 + P_4')\,P_S}{P_3 + P_4' + P_S}} \right\} F_c \tag{2.77}$$

$$U_{c2} = \left\{ \frac{P_1'}{P_1' + P_2 + \dfrac{(P_3 + P_4')\,P_S}{P_3 + P_4' + P_S}} \right\} F_c. \tag{2.78}$$

The directions of the magnetic potential differences are indicated in fig. 2.11.
The magnetic potential difference U_{c2} also appears across the permeance of stator parts 2 and the permeance P_S.
The magnetic potential difference across stator part 2, which is denoted as U_{c3}, follows from:

$$U_{c3} = \left(\frac{P_S}{P_3 + P_4' + P_S} \right) \left(\frac{P_1'}{P_1' + P_2 + \dfrac{(P_3 + P_4')\,P_S}{P_3 + P_4' + P_S}} \right) F_c. \tag{2.79}$$

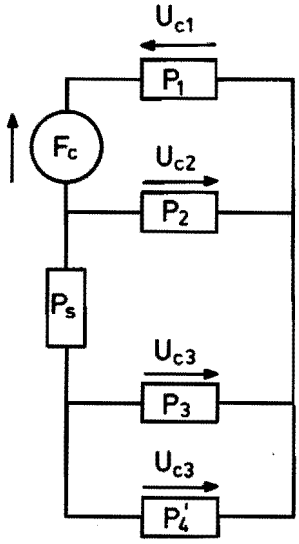

Fig. 2.11 – M.m.f. distribution

The torques delivered by the disks are

$$T_1 = \frac{U_1^2}{2} \frac{dP_1'}{d\theta} = \frac{1}{2} (U_{pm1} + U_{c1})^2 \frac{dP_1'}{d\theta} \tag{2.80}$$

$$T_2 = \frac{U_2^2}{2} \frac{dP_2}{d\theta} = \frac{1}{2} (U_{pm1} - U_{c2})^2 \frac{dP_2}{d\theta} \tag{2.81}$$

$$T_3 = \frac{U_3^2}{2} \frac{dP_3}{d\theta} = \frac{1}{2} (U_{pm2} + U_{c3})^2 \frac{dP_3}{d\theta} \tag{2.82}$$

$$T_4 = \frac{U_4^2}{2} \frac{dP_4'}{d\theta} = \frac{1}{2} (U_{pm2} + U_{c3})^2 \frac{dP_4'}{d\theta}. \tag{2.83}$$

The derivates of the disk permeances are identical with those in section 2.2. The m.m.f. from the permanent magnet is distributed over the two parts in the same manner as that referred to in section 2.2. Therefore the detent torque as calculated in section 2.2. remains unaltered. It is independent of the permeance between the stator parts and is solely produced by the butt joints.

All four disks contribute to the generation of the hybrid torque, thus:

$$T_{H1} = -\,n\,P\sin(n\theta)\,U_{pm1}\,U_{c1}\,\frac{P_b^{\,2}}{(P_b + P_0 + P\cos(n\theta))^2} \tag{2.84}$$

$$T_{H2} = -\,n\,P\sin(n\theta)\,U_{pm1}\,U_{c2} \tag{2.85}$$

$$T_{H3} = -\,n\,P\cos(n\theta)\,U_{pm2}\,U_{c3} \tag{2.86}$$

$$T_{H4} = n\,P\cos(n\theta)\,U_{pm2}\,U_{c3}\,\frac{P_b^{\,2}}{(P_b + P_0 + P\sin(n\theta))^2} \tag{2.87}$$

$T_{H1}, T_{H2}, \ldots$ being the contribution of the individual disks.

The total hybrid torque is

$$T_H = -\,n\,P\sin(n\theta)\,U_{pm}\,F_c \left\{\frac{P_3 + P_4'}{P_1' + P_2 + P_3 + P_4'}\right\} \cdot$$

$$\left\{\left(\frac{P_b^{\,2}}{(P_b + P_0 + P\cos(n\theta))^2}\right)\left(\frac{P_2 + \dfrac{(P_3 + P_4')\,P_S}{P_3 + P_4' + P_S}}{P_1' + P_2 + \dfrac{(P_3 + P_4')\,P_S}{P_3 + P_4' + P_S}}\right) + \left(\frac{P_1'}{P_1' + P_2 + \dfrac{(P_3 + P_4')\,P_S}{P_3 + P_4' + P_S}}\right)\right\} + n\,P\cos(n\theta)\,U_{pm}\,F_c \cdot$$

$$\left\{\frac{P_1' + P_2}{P_1' + P_2 + P_3 + P_4'}\right\}\left\{\frac{P_S}{P_3 + P_4' + P_S}\right\} \cdot$$

$$\left\{\frac{P_1'}{P_1' + P_2 + \dfrac{(P_3 + P_4')\,P_S}{P_3 + P_4' + P_S}}\right\}\left\{\frac{P_b^{\,2}}{(P_b + P_0 + P\sin(n\theta))^2} - 1\right\} . \tag{2.88}$$

The hybrid torque is made up of two contributions. The first is produced by stator part 1 and contains the term $\sin(n\theta)$. This contribution is similar to the hybrid

torque found in expression (2.36) but is smaller owing to the butt joints. The second contribution to the hybrid torque contains the term $\cos(n\theta)$, and is created by stator part 2. This contribution gives rise to stepping angle errors because it is shifted 90 degrees compared with the requisite hybrid torque. The amplitude of the second contribution, however, is small compared with that of the first, as follows from the following consideration. In a practical motor P_b will be much bigger than P_0 and P_s will be small compared with P_0. The second contribution contains the terms

$$\frac{P_s}{P_3 + P_4' + P_s} \tag{2.89}$$

and

$$\frac{P_b^2}{(P_b + P_0 + P\sin(n\theta))^2} - 1. \tag{2.90}$$

Both terms will be small in a practical motor.
The ratio of the amplitudes of the first and second contributions is mainly governed by the product of the terms from expressions (2.89) and (2.90).

The reluctance torque is produced by all four disks:

$$T_{R1} = -\frac{U_{c1}^2}{2} n P \sin(n\theta) \frac{P_b^2}{(P_b + P_0 + P\cos(n\theta))^2} \tag{2.91}$$

$$T_{R2} = \frac{U_{c2}^2}{2} n P \sin(n\theta) \tag{2.92}$$

$$T_{R3} = -\frac{U_{c3}^2}{2} n P \cos(n\theta) \tag{2.93}$$

$$T_{R4} = \frac{U_{c3}^2}{2} n P \cos(n\theta) \frac{P_b^2}{(P_b + P_0 + P\sin(n\theta))^2}. \tag{2.94}$$

The total reluctance torque is:

$$T_R = -\frac{n}{2} P \sin(n\theta) F_c^2 \left\{ \frac{P_b^2}{(P_b + P_0 + P\cos(n\theta))^2} \right\} \cdot$$

$$\left\{ \left(\frac{P_2 + \frac{(P_3 + P_4')P_S}{P_3 + P_4' + P_S}}{P_1' + P_2 + \frac{(P_3 + P_4')P_S}{P_3 + P_4' + P_S}} \right)^2 - \left(\frac{P_1}{P_1' + P_2 + \frac{(P_3 + P_4')P_S}{P_3 + P_4' + P_S}} \right)^2 \right\}$$

$$+ \frac{n}{2} P \cos(n\theta) F_c^2 \left\{ \frac{P_b^2}{(P_b + P_0 + P\sin(n\theta))^2} - 1 \right\} \cdot$$

$$\left(\frac{P_1'}{P_1' + P_2 + \frac{(P_3 + P_4')P_S}{P_3 + P_4' + P_S}} \right)^2 \left(\frac{P_S}{P_S + P_3 + P_4'} \right)^2 . \qquad (2.95)$$

The reluctance torque consists of two contributions. The first, containing the term $\sin(n\theta)$, is similar to the reluctance torque found in section 2.2. The other contribution to the reluctance torque, containing the term $\cos(n\theta)$, is due to the butt joints and the coupling between the two stator parts combined. The second term contains the terms from expressions (2.89) - (2.90) and will therefore be small compared with the first term. The second contribution, however, contains a term which has the fundamental periodicity and is shifted by 90 degrees from the requisite hybrid torque. This contribution therefore gives rise to stepping angle errors.

The interaction between the butt joints and the coupling causes inaccuracy in the equilibrium position. The asymmetry in the holding torque, as discussed in section 2.1, can be reduced by decreasing the butt joints permeances. This however gives rise to terms in the torque equation which produce a detent torque and which adversely affect the stepping angle accuracy. Consequently, for a practical design, this is not an appropriate method of reducing the asymmetry.

2.4. Effect of the shaft permeance on the motor torque

In the previous sections it was assumed that the rotor was a perfect magnetic conductor. It is however possible to deliberately introduce a magnetic resistance in the rotor between disks 2 and 3 (see fig. 2.12). The permeance in the rotor will be denoted by the shaft permeance P_{sh}. This shaft resistance can arise when reducing the rotor diameter between disks 2 and 3, with the result that saturation occurs.

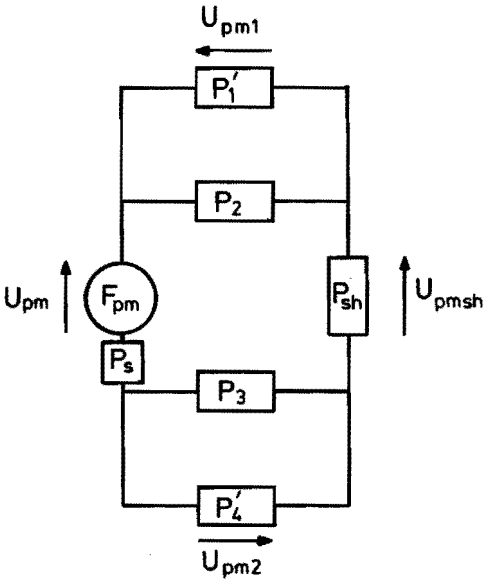

Fig. 2.12 – Magnetic resistance in the shaft

The flux through the shaft is almost independent of the rotor angle and the coil excitation. The shaft permeance therefore is almost constant. In the present section allowance is made for a constant permeance. The magnetic potential difference from the permanent magnet divides into the following parts:

$$U_{pm} = U_{pm1} + U_{pm2} + U_{pmsh}. \tag{2.96}$$

The total flux from the permanent magnet is:

$$U_{pm1}\,(P_1' + P_2) = U_{pm2}\,(P_3 + P_4') = U_{pmsh}\,P_{sh}. \tag{2.97}$$

The magnetic potential difference across the stator parts and the shaft permeances (see fig. 2.12) are:

$$U_{pm1} = \frac{P_{sh}\,(P_3 + P_4')}{P_{sh}\,(P_1' + P_2 + P_3 + P_4') + (P_1' + P_2)\,(P_3 + P_4')}\,U_{pm} \tag{2.98}$$

$$U_{pm2} = \frac{P_{sh}\,(P_1' + P_2)}{P_{sh}\,(P_1' + P_2 + P_3 + P_4') + (P_1' + P_2)\,(P_3 + P_4')}\,U_{pm} \tag{2.99}$$

$$U_{pmsh} = \frac{(P_3 + P_4')\,(P_1' + P_2)}{P_{sh}\,(P_1' + P_2 + P_3 + P_4') + (P_1' + P_2)\,(P_3 + P_4')}\,U_{pm}. \tag{2.100}$$

The detent torque is created by all four disks in a similar way to that described in section 2.3. The permeance functions remain unaltered. The magnetic potential difference from the permanent magnet across the air gaps is reduced by the shaft permeance. As a result the detent torque decreases with the square of the reduced magnetic potential difference across the air gaps. When a bigger permanent magnet is used to compensate for the loss of magnetic potential difference across the air gap, the detent torque does not change.

We can calculate the hybrid torque in a way similar to that referred to in section 2.3. The permeances P_s and P_{sh}, which are arranged in series and are both independent of the angular position, together form the permeance

$$P_s' = \frac{P_s P_{sh}}{P_s + P_{sh}} \tag{2.101}$$

Taking the permeance P_s' instead of P_s in equations (2.77, 78, 79) in section 2.3., we find the m.m.f. distribution in the motor with shaft resistance. The hybrid torque found from (2.88) is reduced by the decrease of the magnetic potential difference from the permanent magnet across stator parts 1 and 2. If the permanent magnet is made larger to such an extent that the hybrid torque retains its original value, the result will be that the shaft resistance lowers the torque with the $\cos(n\theta)$ term as follows from equation (2.89), so that a higher motor precision is obtained. The shaft permeance decreases the first harmonic reluctance torque. The magnitude of the reluctance torque is found by replacing the permeance P_s in equation (2.95) by P_s'.

When the dimensions of the permanent magnet are appropriately modified, the shaft permeance will have a favourable effect on the torque asymmetry and improve the stepping angle accuracy.

2.5. Double-phase excitation

In the previous sections we have at all times assumed that only the coil of stator part 1 is excited. The torque produced during the excitation of stator part 2 follows from the expressions found by substituting the angle $\theta + 90^\circ$ for θ.

In practice, double-phase excitation is often applied, which results in an increase of the torque.

The detent torque then remains unaltered because this is independent of excitation.

Thy hybrid torque is found by superimposing the two single-phase hybrid torques.

The reluctance torque does not vary linearly with the excitation current. Superimposing the reluctance torques is only allowed if there is no linkage between the two stator parts.

In the following the shaft resistance is assumed to be zero. The shaft resistance can easily be taken into account by substituting P_S' for P_S, as discussed in the previous section.

To shorten the equations we introduce

$$P_{12S} = \frac{(P_1' + P_2)\,P_S}{P_1' + P_2 + P_S} \tag{2.102}$$

$$P_{34S} = \frac{(P_4' + P_3)\,P_S}{P_4' + P_3 + P_S} \tag{2.103}$$

If we let the subscripts α and β denote respectively the stator coils 1 and 2 we can write

$$U_{c1\alpha} = \frac{P_2 + P_{34S}}{P_1' + P_2 + P_{34S}} F_{c\alpha} \tag{2.104}$$

$$U_{c2\alpha} = \frac{P_1'}{P_1' + P_2 + P_{34S}} F_{c\alpha} \tag{2.105}$$

$$U_{c3\alpha} = U_{c4\alpha} = \frac{P_S}{P_3 + P_4' + P_S} \quad \frac{P_1'}{P_1' + P_2 + P_{34S}} F_{c\alpha} \tag{2.106}$$

$$U_{c4\beta} = \frac{P_3 + P_{12S}}{P_3 + P_4' + P_{12S}} F_{c\beta} \tag{2.107}$$

$$U_{c3\beta} = \frac{P_4'}{P_3 + P_4' + P_{12S}} F_{c\beta} \tag{2.108}$$

$$U_{c1\beta} = U_{c2\beta} = \frac{P_S}{P_1' + P_2 + P_S} \quad \frac{P_4'}{P_3 + P_4' + P_{12S}} F_{c\beta}\,. \tag{2.109}$$

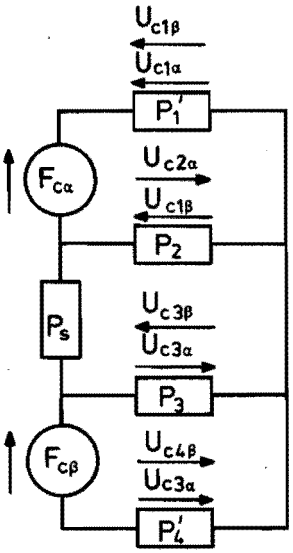

Fig. 2.13 – M.m.f. distribution with both phases excited

In fig. 2.13 the directions of the magnetic potential differences are indicated. The reluctance torque for the various disks, which are simular to those found in expressions (2.91) to (2.94), are:

$$T_{R1} = -\frac{n}{2} P \sin(n\theta) (U_{c1\alpha} + U_{c1\beta})^2 \frac{P_b^2}{(P_b + P_o + P\cos(n\theta))^2} \tag{2.110}$$

$$T_{R2} = \frac{n}{2} P \sin(n\theta) (U_{c2\alpha} - U_{c2\beta})^2 \tag{2.111}$$

$$T_{R3} = -\frac{n}{2} P \cos(n\theta) (U_{c3\beta} - U_{c3\alpha})^2 \tag{2.112}$$

$$T_{R4} = \frac{n}{2} P \cos(n\theta) (U_{c4\beta} + U_{c4\alpha})^2 \frac{P_b^2}{(P_b + P_o + P\sin(n\theta))^2} . \tag{2.113}$$

The total reluctance torque is

$$T_R = \frac{n}{2} P \sin(n\theta) \left\{ (U_{c2\alpha} - U_{c2\beta})^2 - \frac{P_b^2 (U_{c1\alpha} + U_{c1\beta})^2}{(P_b + P_o + P\cos(n\theta))^2} \right\} + \frac{n}{2} P \cos(n\theta) \left\{ \frac{P_b^2 (U_{c4\beta} + U_{c4\alpha})^2}{(P_b + P_o + P\sin(n\theta))^2} - (U_{c3\beta} - U_{c3\alpha})^2 \right\} . \tag{2.114}$$

Double-phase excitation gives rise to a relutance torque that contains an additional term as compared with the torque found by superimposing the single-phase torques. The extra torque is equal to

$$T_{Rex} = -\frac{n}{2} p \sin(n\theta) \left\{ 2\, U_{c2\alpha}\, U_{c2\beta} + \frac{2\, U_{c1\alpha}\, U_{c1\beta}\, P_b^2}{(P_b + P_o + P\cos(n\theta))^2} \right\}$$

$$+\frac{n}{2} P \cos(n\theta) \left\{ 2\, U_{c3\alpha}\, U_{c3\beta} + \frac{2\, U_{c4\alpha}\, U_{c4\beta}\, P_b^2}{(P_b + P_o + P\sin(n\theta))^2} \right\}. \qquad (2.115)$$

This extra reluctance torque, when the two phases are excited in the same direction, is in phase with the reluctance torque found earlier (equation 2.95) and in antiphase with the detent torque, with the result that a torque is created whose asymmetry is larger than in the case of single-phase excitation.

With the same direction of excitation, the reluctance torque and the detent torque are in phase or in antiphase with the hybrid torque so that no step-angle errors will be incurred.

With the opposite direction of excitation, the extra reluctance torque is in antiphase with, and larger than, the earlier calculated reluctance torque (eq. 2.114). In the case of double-phase excitation in the opposite direction, both the detent torque and the reluctance torque with the fundamental periodicity are shifted in phase by 90° with respect to the hybrid torque, and this gives rise to a stepping angle error. The stepping angle is affected in a similar way as described in section 2.2. and demonstrated in figs. 2.9 and 2.10.

3. CALCULATION OF THE TORQUE IN THE SATURATED MOTOR

In the preceding chapter we calculated the torque for an idealized motor. Fig. 3.1. shows a plot of the holding torque as a function of the excitation current, both for the measured and for the calculated torques. These holding torques are found to occur in a motor as described in Appendix 1. Both the measurements and the calculations give the holding torque of the motor with two phases excited. The ampere turns delivered by the two phases are equal. The variation of the torque as a function of the rotor angle for the four excitation states is represented in fig. 3.2. The holding torque is not the same for these four states: the one shown in fig. 3.1. is the lowest. The discrepancy between the measured and the calculated torques is substantial as a result of the assumptions made for the idealized model. In later calculations this dicrepancy will disappear when the saturation is taken into account.

As compared with the torques occuring in the existing commercially available hybrid stepping motors the measured torques at high excitation levels are very large

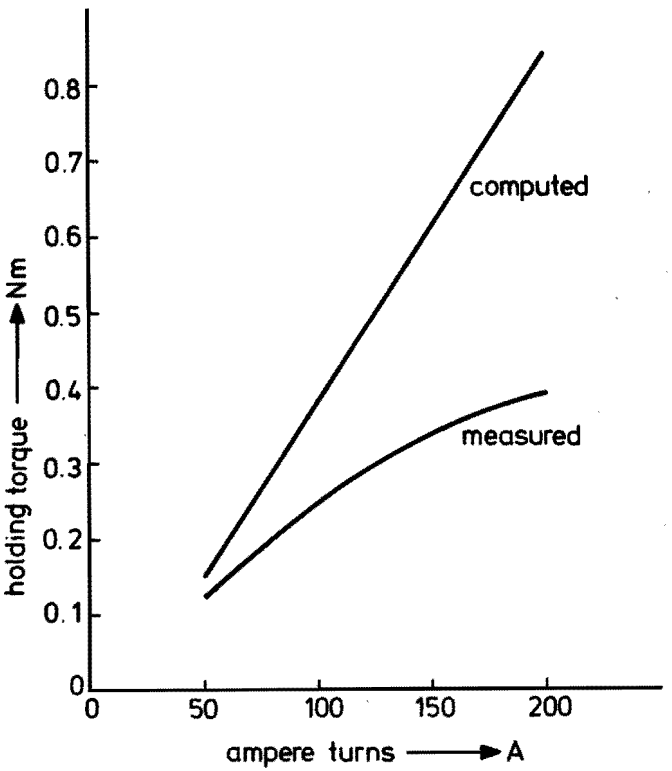

Fig. 3.1 – Holding torque as a function of excitation current

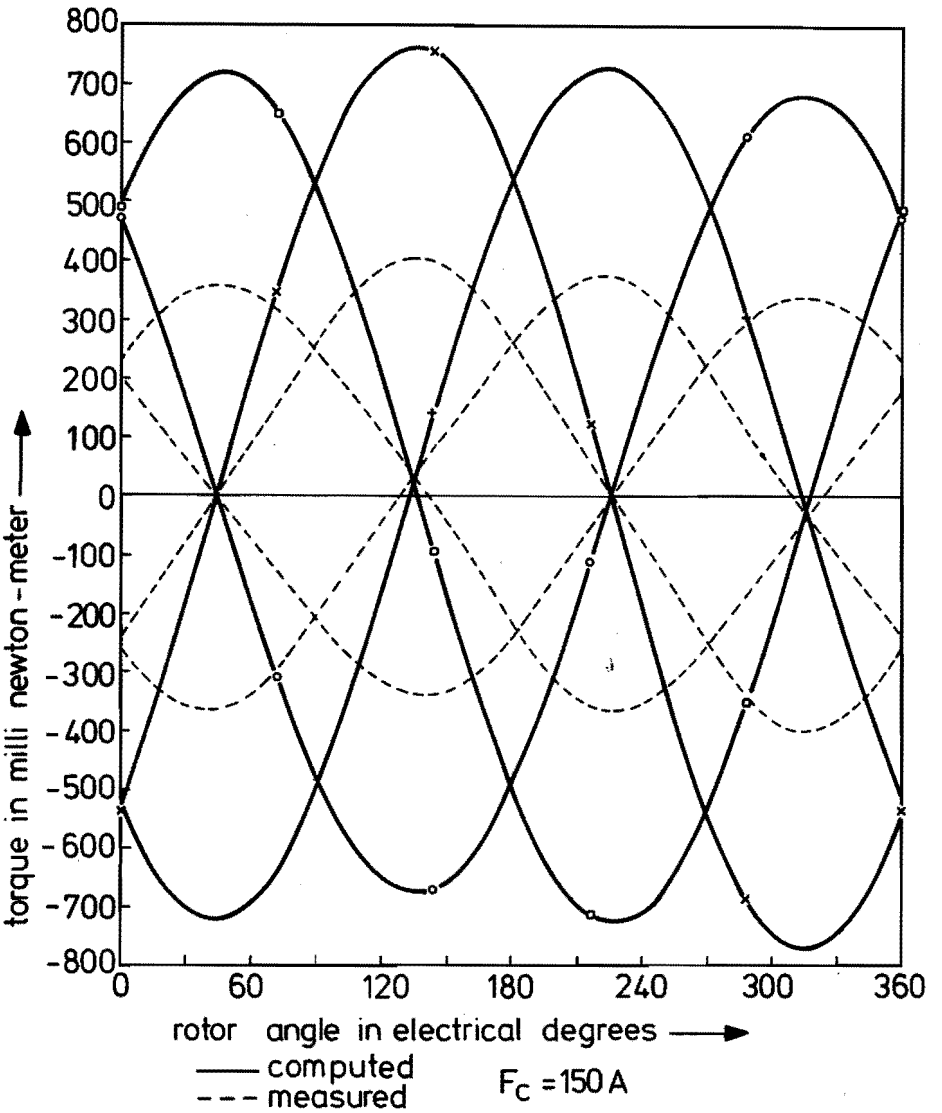

Fig. 3.2 – Torque as a function of the rotor angle

for the rotor volume used. The measured torques are promising for a high torque to volume ratio because the use of a single pole pair per phase allows much higher excitation levels than permissible in the case of the conventional hybrid motors where at all times more than one pole pair per phase is employed. This high volume to torque ratio is not obtained in this model because it was designed to make many measurements possible.

In stepping motors the accuracy of the stepping angle is a major quantity. If the torque angle characteristic for the four excitation states is known, the actual stepping angle will be known too.

We can distinguish between two stepping angle errors, namely the absolute and the relative stepping angle error (ref. 10). The relative stepping angle error is the rotor angle excursion over one step with respect to the nominal stepping angle, expressed in percents of this angle. The absolute stepping angle error is the error incurred by the motor relative to a chosen reference over an arbitrary number of steps, which is also expressed in a percentage of the nominal stepping angle.

The relative stepping angle error is used as the criterion for the stepping angle accuracy of the motor. A standard amount of stepping angle variation permitted is an error of 5%. However, for high precision applications the error is often required to be not more than 3%.

Since stepping motors are mainly energized in a two-phased mode, we will henceforth refer to the two-phase energized state when we are discussing stepping angle errors.

Both measurements and calculations reveal that stepping angle errors can far exceed the permissible error. The discrepancy between the measured and the calculated stepping angle error however is substantial. The curves in fig. 3.3. show the measured and calculated stepping angle errors. The stepping angle error has been calculated for two values of P_b corresponding with a butt joint of 10 and 20 micron respectively.

Adequate operation of a stepping motor requires the stepping angle error to be below the specified limit. The discrepancy between the measured and calculated stepping angle error increases with higher excitation levels. To gain a deeper insight into the torque mechanism it is therefore necessary to take the saturation into account.

3.1. Asymmetries in the hybrid stepping motor with ring coils

It is found from measurements and linear calculations that the torque and the stepping angle are asymmetric depending on the direction of the excitation current, which is inherent in the motor design. Apart from these inherent asymmetries, torque and stepping angle asymmetries too can be introduced by mechanical deviations. Sincer certain tolerances always have to be specified for manufacturing the motor, one ought to know the effect of a particular mechanical deviation on the torque and stepping angle accuracy.

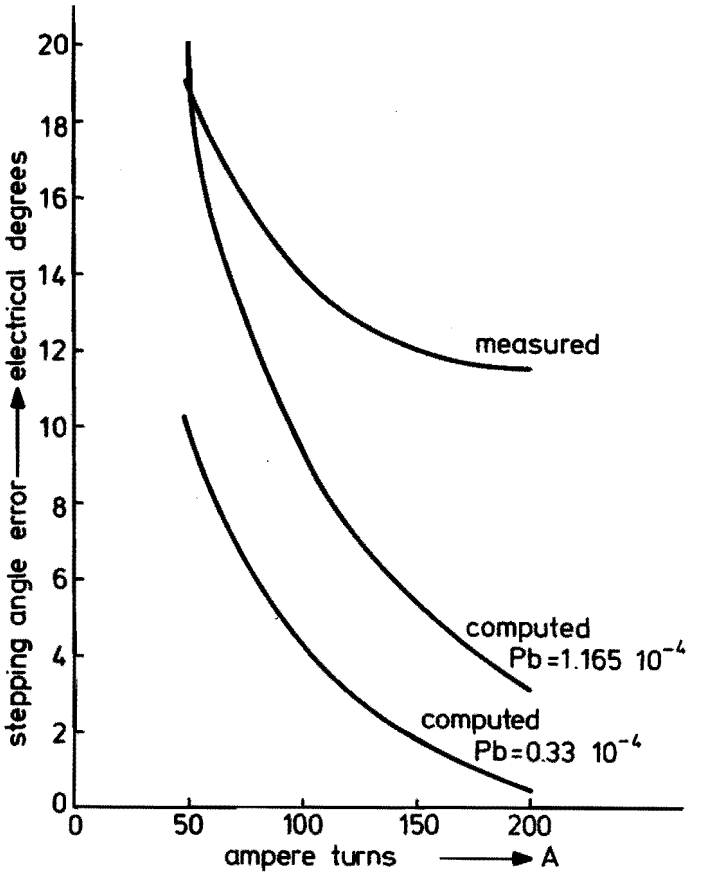

Fig. 3.3 – Stepping angle as a function of the excitation current

The motor asymmetries can be classified into the following three categories:

- asymmetry caused by coupling of the stator parts.
- asymmetry due to a difference in magnetic circuits parameters for the different excitation states.
- asymmetry resulting from mechanical deviations in the alignment of the disks, in disk height and in the air gap length, which vary from disk to disk.

Asymmetry caused by the coupling of the two stator parts is due to the permeance of the permanent magnet. As a result, the coil excitation will give rise to flux which flows consecutively through the outer disk, the rotor shaft, the other stator part and the permanent magnet. This flux produces a reluctance torque, which depends on the permeance function of the relevant outer disk as a function of the rotor angle and which is independent of the direction of the current.

The coupling of the two stator parts can be decreased by reducing the diameter of the central part of the rotor shaft and also by increasing the height of the permanent magnet. A sufficiently large reduction of the rotor shaft diameter causes the shaft to be saturated, which gives it a small differential permeance.

Asymmetries in the magnetic circuit for the various excitation states are caused by the asymmetric motor design. The inner disks are close to the permanent magnet, while the magnetic path of the outer disks is longer and contains extra butt joints. As a consequence the flux from the permanent magnet is larger for the inner disks than for the outer disks, which gives rise to a detent torque, torque asymmetry and stepping angle errors.

The effect of the stator butt joints depends directly on the dimensions of the butt joints, and the resultant extra permeance can be calculated in a straightforward manner. The influence of the extra iron path length is more difficult to assess owing to the saturation of the iron.

There are many mechanical aberrations that can give rise to torque asymmetry and stepping angle errors. It is particularly the production department that is interested in which of these aberrations lead to what stepping angle error and torque asymmetry, to enable the manufacturing tolerances of a certain electric motor to be specified, for the production costs of the motor rise as these tolerances become closer. The most frequently occurring errors are deviations in the alignment of the disks relative to one another and variations in the air gap length and in the height of the disks.

3.2. Permeance and torque of the disks

In the motor the air gap permeance of the disk varies with the rotor angle. A properly designed motor will be saturated first of all in the immediate environment of the teeth. Therefore it is essential in motor calculations to know the permeance of the air gap transition and the tooth zone that is saturated as a function of the rotor angle and the magnetic potential across this air gap region. In determining this permeance we assume the existence of two cylindrical equipotential planes at sufficient distance from the teeth, both in the stator and in the rotor. We now define the permeance between these equipotential planes as functions of the rotor angle, and the magnetic potential across the planes. In what follows we shall refer to this permeance as "disk permeance".

The disk height is many times larger than the air gap length. Therefore the air gap field contains hardly any axial components. Leaving these out of account allows a two-dimensional calculation of the air gap field using a field-computation program. The available program using vector potentials, however, was unable to do this owing

to the homopolar flux (Appendix 2). Besides it is necessary to perform the field calculations as a function of the magnetic potential across the air gap region and as a function of the rotor angle. This requires a huge number of calculations, which is an expensive matter, while the results are merely applicable to a single specific tooth geometry. We therefore preferred an experimental method in which the permeance function of the disk is determined as a function of the angle and the excitation, using a special measuring model which in addition is used to measure the torque as a function of the rotor angle and the excitation. The results are specific for the chosen geometry but are much cheaper and faster to obtain.

3.3. Measuring set-up

Fig. 3.4. presents a diagram of the measuring model. The measuring model was intended to provide the permeance function of the air gap region as a function of the rotor angle and the applied magnetic potential difference across the air gap.

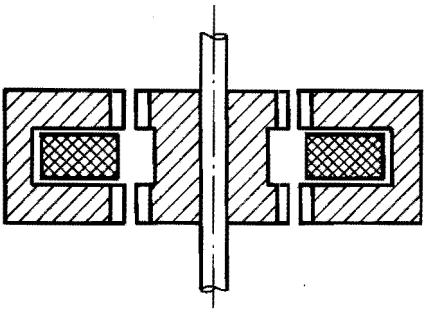

Fig. 3.4 – The measuring model

We therefore aimed at making a model without any mechanical aberrations. Since the stator butt joints are difficult to measure, we omitted them. The model is made up from two semi-cylinders, in which the coil space is milled out.
The two semi-cylindres are mounted in a cylindrical housing, after which the teeth are made by spark erosion. The spark erosion tool is shown in fig. 3.5. As the disks are linked by a solid connection, the teeth thus obtained will be excellently aligned. Fig. 3.6. shows a photograph of a half stator part. The rotor is made from a solid piece of material in which the teeth are milled parallel to the shaft. Here teeth alignment deviations hardly never occur. The model thus obtained contains two disks very accurately in line and has no stator butt joints.

The coil is a bifilar winding. One wire is used as the excitation winding, and another wire is employed as measuring coil.

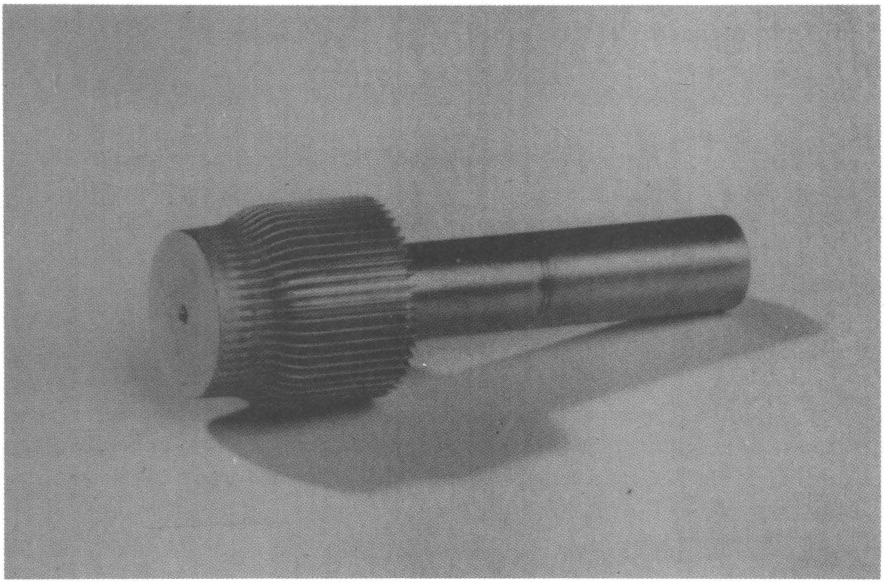

Fig. 3.5 – Spark erosion tool

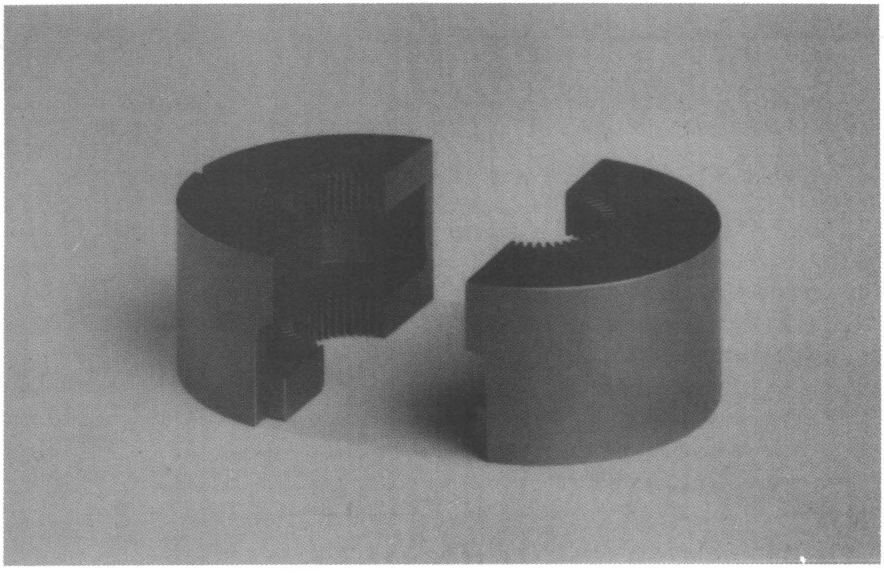

Fig. 3.6 – Both half stator parts of the measuring model

To determine the permeance of the measuring model the flux is measured with an electronic integrator as a function of the angle and the excitation, where this angle and the current through the coil are set by external means. At the same time the torque is measured as a function of the angle and the excitation. The methods used to measure the torque, the rotor angle and the flux are described in Appendix 3.

To calculate the stepping angle it is necessary to know the disk permeance and the disk torque for a large number of angular positions and excitation values. Owing to the non-linearity of the permeance functions the calculations can only be performed with the aid of a computer, which is also capable of processing a multiple of measured values. The angle, the torque and the flux of the very slowly driven rotor for 15 different current settings were measured and were registered by an analog recorder which was fed with the relevant signals for further processing. This done, several analog-to-digital converters supplied these analog signals to a mini-computer, which was programmed in such a way that the flux, the torque, the angle and the current were recorded on tape as paired numbers at a great many instants. These paired numbers were subsequently fed into the computer to be used in further calculations.

Fig. 3.7. shows a flow chart of the measured values and fig. 3.8. presents a block diagram of the measurement.

Fig. 3.7 – Flow chart of the processing of the measured values

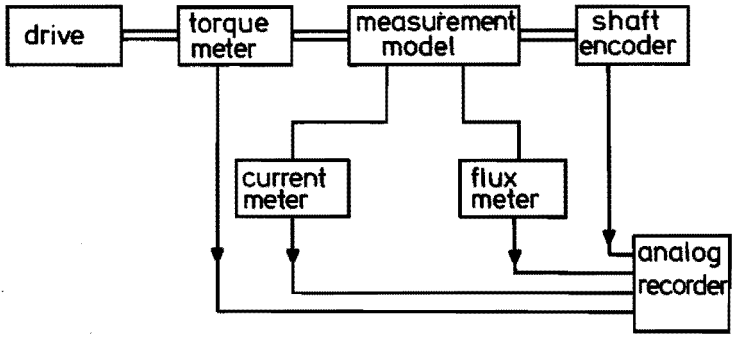

Fig. 3.8 – Block diagram of the measuring method

3.4. Results of the measurements

Using the method just described we measured the torque, the flux, the angle and the excitation current. Fig. 3.9. shows the torque and fig. 3.10. the flux as functions of the current and the angle. From the flux as a function of the angle and

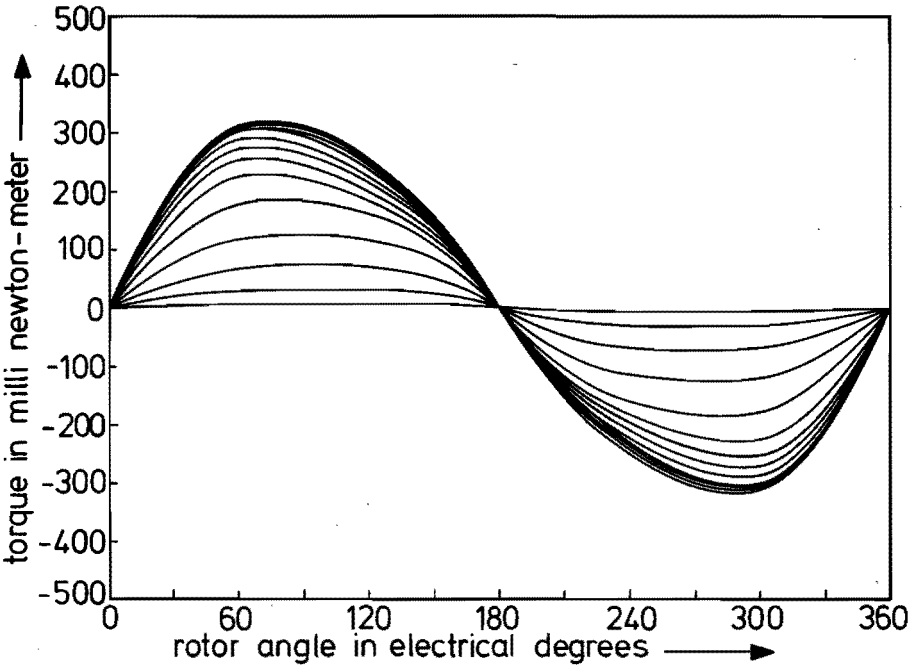

Fig. 3.9 – Torque of the measuring model

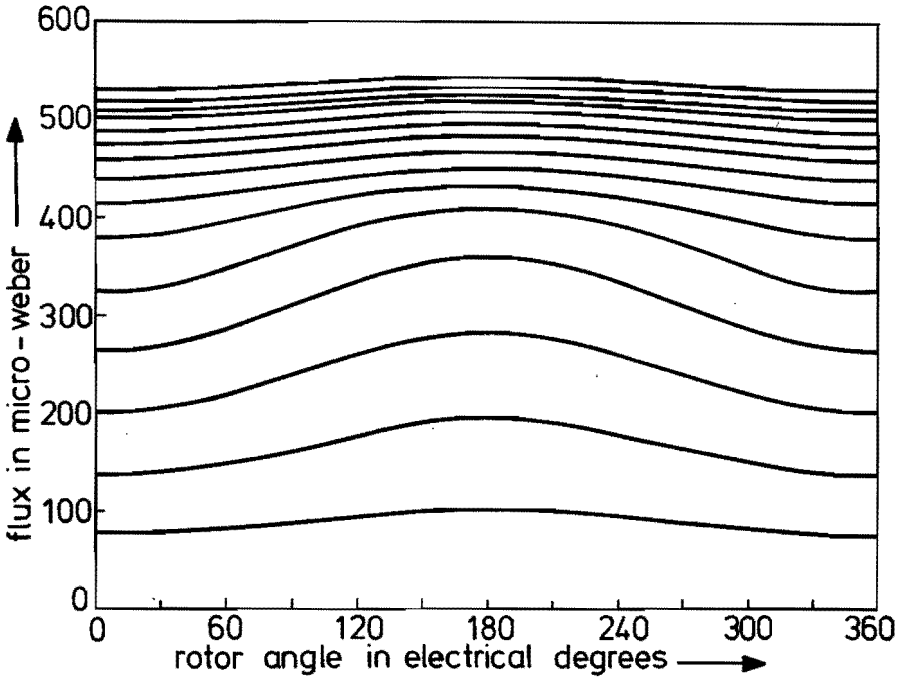

Fig. 3.10 – Flux of the measuring model

the current the permeance of the whole circuit can be derived. This is made up of twice the permeance of the air gap and the tooth zone and the permeance of the iron circuit. If the iron circuit permeance is assumed to be large compared with that of the tooth zone – in later calculations this assumption will be abandoned – it is valid to state that the tooth zone permeance is the disk permeance which, as stated before, is denoted by P_i,

$$P_i(\theta, U) = \frac{2\,\Phi(\theta, F_c)}{F_c} \tag{3.1}$$

where P_i : disk permeance
Φ : measured flux
F_c : m.m.f. of the coil
U : magnetic potential across the disk permeance which is equal to $F_c/2$.

Fig. 3.11. shows the disk permeance of the aligned teeth (maximum permeance) and the (minimum) permeance of the teeth out of line, plotted against the magnetic potential across the disk permeance.

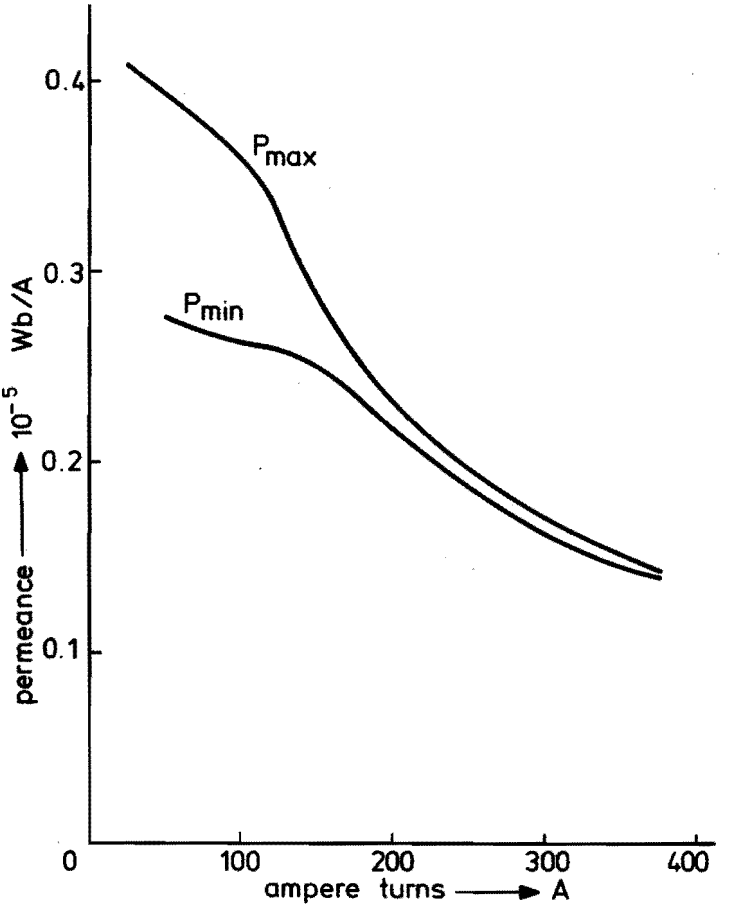

Fig. 3.11 – Disk permeance in the in- and the out- of line-position

The disk torque is related to the measured torque as:

$$T_d(\theta, U) = \frac{T_m(\theta, F_c)}{2} \tag{3.2}$$

where $T_d(\theta, U)$ is the disk torque and
$T_m(\theta, F_c)$ the measured torque.

In fig. 3.12. the maximum torque of the disk is plotted as a function of the magnetic potential difference across the disk permeance.

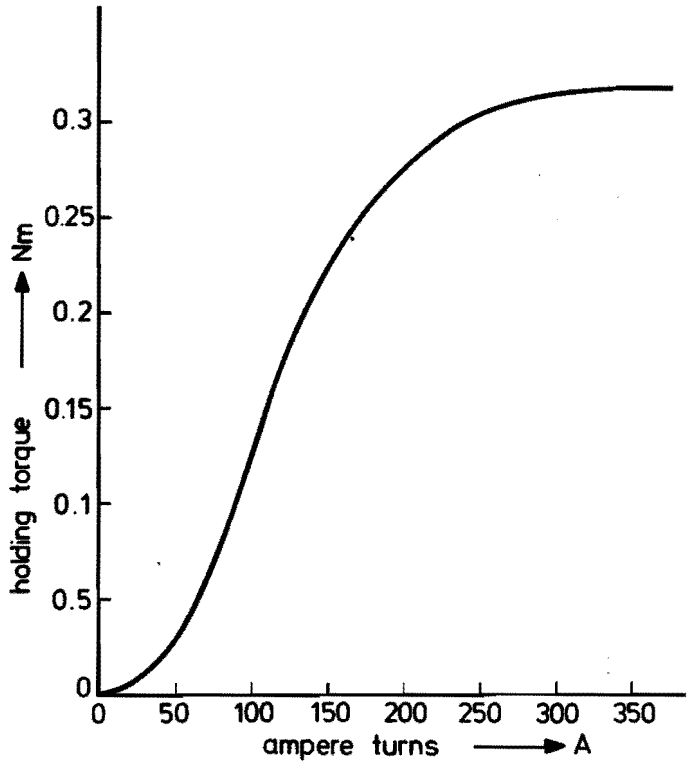

Fig. 3.12 – Holding torque as a function of the excitation current of one disk

3.5. Calculation of the magnetic potential distribution over the four disks

In the calculations the assumption has been made that it is only the tooth zones of the disks that are saturated. All other permeances in the motor behave linearly. The permeances in the equivalent circuit (fig. 3.13) used for the calculations are:

P_i : $P(\theta_i, U_i)$ permeance of disk i
P_{b1} : permeance of stator butt joints in stator part 1
P_{b2} : permeance of stator butt joints in stator part 2
P_s : permeance of permanent magnet
P_{sh} : permeance of the rotor shaft between the two stator parts
θ_i : angle in electrical degrees between the rotor and stator teeth of disk i
F_{pm} : m.m.f. of the permanent magnet
U_i : magnetic potential difference across the disk permeance of disk i.

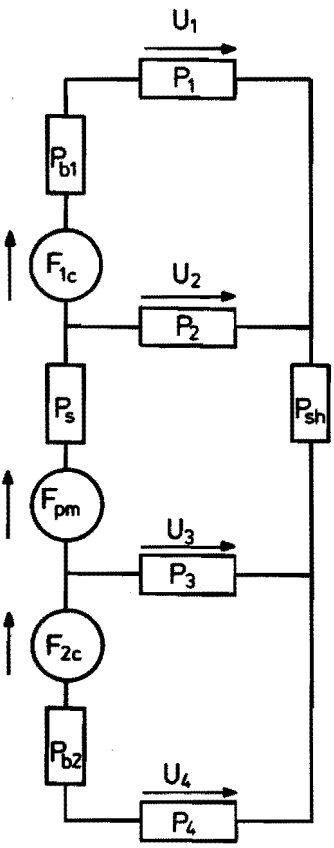

Fig. 3.13 – Electrical analogon of the motor

For the permeances P_1 and P_{b1}, which are arranged in series and are similar for the permeances P_4 and P_{b2}, we introduce

$$P_1' = \frac{P_{b1}\, P_1}{P_{b1} + P_1} \tag{3.3}$$

$$P_4' = \frac{P_{b2}\, P_4}{P_{b2} + P_4}. \tag{3.4}$$

For the permeances P_s and P_{sh}, which are also arranged in series, we introduce:

$$P_{pm} = \frac{P_s\, P_{sh}}{P_s + P_{sh}}. \tag{3.5}$$

On introducing these series permeances, the equivalent circuit of fig. 3.13. becomes as shown in fig. 3.14.

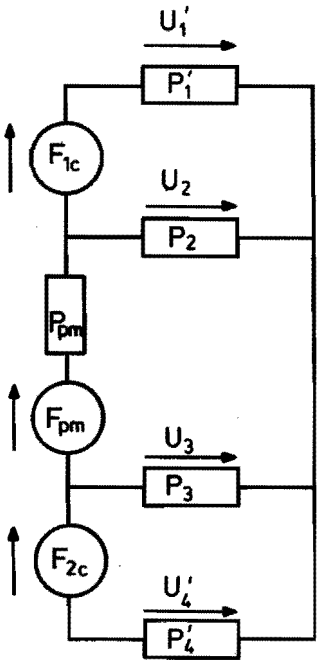

Fig. 3.14 – Simplified electrical analogon of the motor

For the magnetic potential, we may write:

$$F_{1c} = U_2 - U_1' \tag{3.6}$$

$$F_{2c} = U_4' - U_3 \tag{3.7}$$

$$F_{pm} = U_3 - U_2 - \frac{U_1' P_1'}{P_{pm}} - \frac{U_2 P_2}{P_{pm}} \tag{3.8}$$

$$U_1' P_1' + U_2 P_2 + U_3 P_3 + U_4' P_4' = 0. \tag{3.9}$$

Here U_1' is the magnetic potential difference across the permeance P_1' and U_4' and the magnetic potential difference across the permeance P_4'. Elimination of U_1' and U_3 in equations (3.8) and (3.9) by means of (3.6) and (3.7) leads to:

$$U_2 (P_1' + P_2) + U_4' (P_3 + P_4') - F_{1c} P_1' - F_{2c} P_3 = 0 \tag{3.10}$$

$$F_{pm} + U_2 \left(1 + \frac{P_1' + P_2}{P_{pm}}\right) - U_4' + F_{2c} - F_{1c} \frac{P_1'}{P_{pm}} = 0. \tag{3.11}$$

All permeances in these equations either are direct or indirect functions of U_2 and U_4' or are independent constant permeances.

These two non-linear equations of the variables U_2 and U_4' can be solved simultaneously by a numerical iteration method. The set of equations is thus solved afresh for each angular position to yield U_2 and U_4' as functions of the angle for given excitations F_{1c}, F_{2c} and F_{pm}. The numerical method chosen here is known as Newton's method, which is described in much detail by Ortega and Rheinboldt (ref.11).

$$-f_1 (U_2, U_4') = \frac{\partial f_1}{\partial U_2} dU_2 + \frac{\partial f_1}{\partial U_4'} dU_4' \tag{3.12}$$

$$-f_2 (U_2, U_4') = \frac{\partial f_2}{\partial U_2} dU_2 + \frac{\partial f_2}{\partial U_4'} dU_4' \tag{3.13}$$

with

$$f_1 (U_2, U_4') = U_2 (P_1' + P_2) + U_4' (P_3 + P_4') - F_{1c} P_1' - F_{2c} P_3 \tag{3.14}$$

$$f_2 (U_2, U_4') = F_{pm} + U_2 \left(1 + \frac{P_1' + P_2}{P_{pm}}\right) - U_4' + F_{2c} - F_{1c} \frac{P_1'}{P_{pm}}. \tag{3.15}$$

The partial derivatives are defined with a Taylor first-order expansion. Thc two non-linear equations are solved iteratively.

The solution is used to caculate all the magnetic disk potentials with the equations:

$$U_1 = (U_2 - F_{1c}) \frac{P_{b1}}{P_{b1} + P_1} \tag{3.17}$$

$$U_2 = U_2 \tag{3.18}$$

$$U_3 = U_4' - F_{2c} \tag{3.19}$$

$$U_4 = U_4' \frac{P_{b2}}{P_{b2} + P_4}. \tag{3.20}$$

The torque on each disk is measured as a function of the rotor angle and the applied magnetic potential difference across the disk by means of the measurement model. The calculated magnetic potentials at the angle for which the calculations are done therefore lead straightforwardly to the torque of each disk. The total motor torque is the sum of the disk torques. In this way the motor torque can be computed for a large number of rotor angles.

The motor torque is zero in the stable and in the unstable position. In the stable position the rotor will be driven back to this position if a small excursion from the stable position is made. However, the rotor will be driven from the unstable position if a small excursion from this position has been made. The stable position is found by determining the angle at which the torque is zero and which position is intermediate between the inline positions of the two disks, i.e. where the magnetic potential difference is at a maximum. The stepping angles of the motor follow from the stable positions at the various exitation polarities.

Fig. 3.15. represents the flow chart of the computational program.

3.6. Application of the computational method

Using the expressions found in the preceding section a computer program has been written for calculating the torque of the double-phase excited motor as a function of the rotor angle. The stepping angle can be assessed by performing the calculations for the four different excitation states and determining the stable-equilibrium points.
In the calculations use was made of the results obtained from a measuring model as described in section 3.3. in which the air gap geometry is identical with that of the motor as described in Appendix 1. The stator butt joints in the motor are unknown in this case and therefore we made the calculations for several different practical stator butt joints, which were to be of the order of 10 μm but were expected to be even smaller. In our calculation we took the butt joints size as 10 and 20 μm. The latter is large, so that it is appropriate for demonstrating the effect of the butt joint on the torque angle curve. The permeance of the two butt joints arranged in series is

$$P_b = \frac{\mu_0 A}{2 l} \tag{3.21}$$

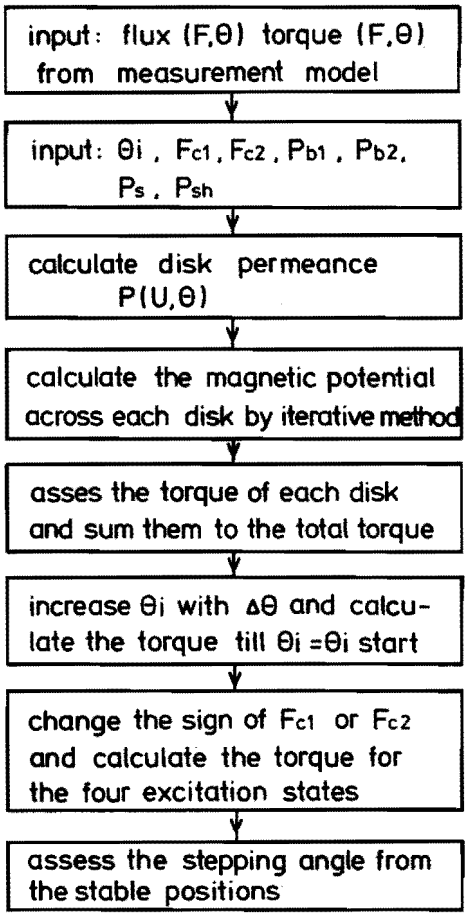

Fig. 3.15 – Flow chart of the computation program

where A is the surface area of the butt joint and *l* its length. For 10 and 20 μm the butt joint permeance is 0.33×10^{-4} and 0.165×10^{-4} Wb/a, respectively.

The torque angle characteristic was calculated for four values of the current excitation. The excitation of 150 At is equal to the nominal excitation. At the nominal excitation the thermally determined limit of the motor is just not exceeded.

Fig. 3.16. shows how the holding torque depends on excitation. This graph also presents the measured holding torque, which is invariably the lowest holding torque of the four obtained from the different excitation states.
The graph reveals that, at a stator butt joint between zero and 10 μm, the calculated

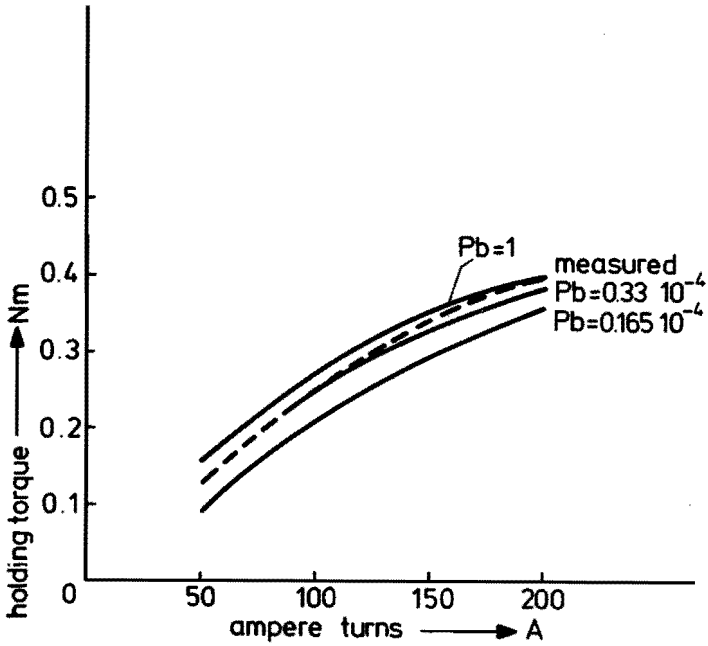

Fig. 3.16 – Holding torque as a function of the excitation current

holding torque is in excellent agreement with the measured one. The stator butt joint only sligthly affects the holding torque, because for a butt joint of 20 μm the calculated and measured holding torque still agree well. The stepping angle error, which, due to the symmetry in the configuration of the motor, is the same for all steps, is plotted against the excitation current in fig. 3.17. If the butt joint is zero the stepping angle error vanishes. The measured stepping-angle error is also represented in this figure.
Between the measured and calculated stepping-angle error there is a marked difference which increases with excitation current. Higher currents require the use of a much larger stator butt joint so as to arrive in the calculation at a stepping-angle error equal to the measured stepping-angle error. This indicates that the magnetic circuit is saturated outside the tooth zone, because the effect of the saturated teeth has already been taken into account.

Fig. 3.18. shows the behaviour of the motor torque as a function of rotor angle for measured and calculated values, at an excitation of 150 At. The agreement between the measured and calculated torque is sufficient.

The torque angle curve is hardly affected by varying the shaft permeance, as follows from calculations.

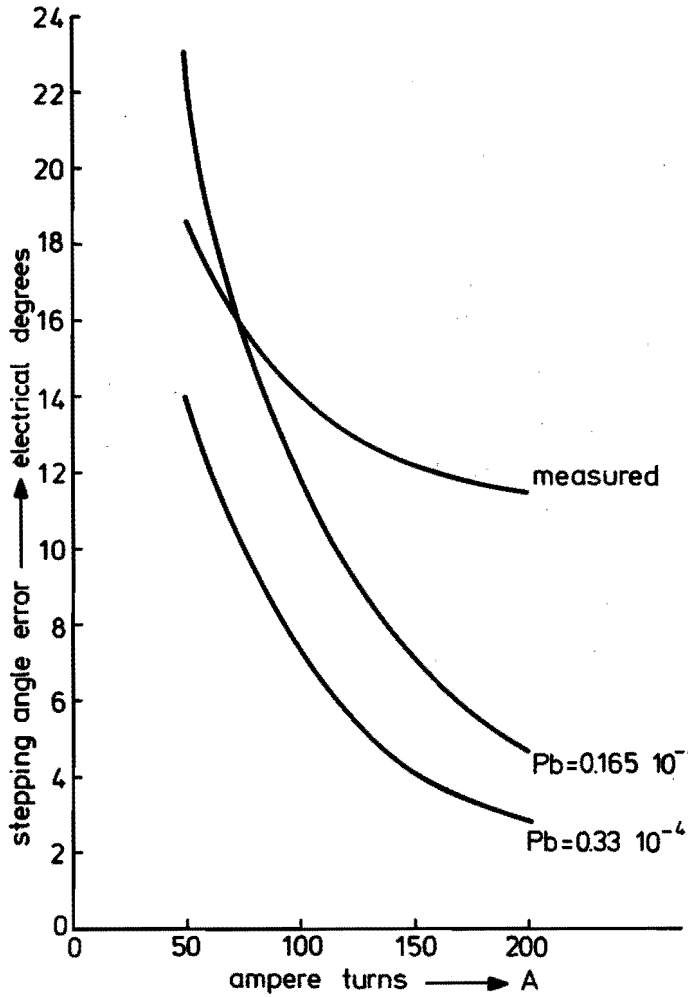

Fig. 3.17 – Stepping angle error as a function of the excitation currents

The latter is connected in series with the permeance of the permanent magnet. which, owing to the large height of the permanent magnet and a low permeability, is much smaller than the shaft permeance.

In fig. 3.19. the measured and calculated detent torques are exhibited for a 10 μm butt joint. Comparison of the calculated and measured detent torques shows the discrepancy between them to be large; this may be due to several different causes. With these low torques measuring errors are comparatively large, saturation of the magnetic circuit may occur and errors may arise in the mechancial construction of the measured motor.

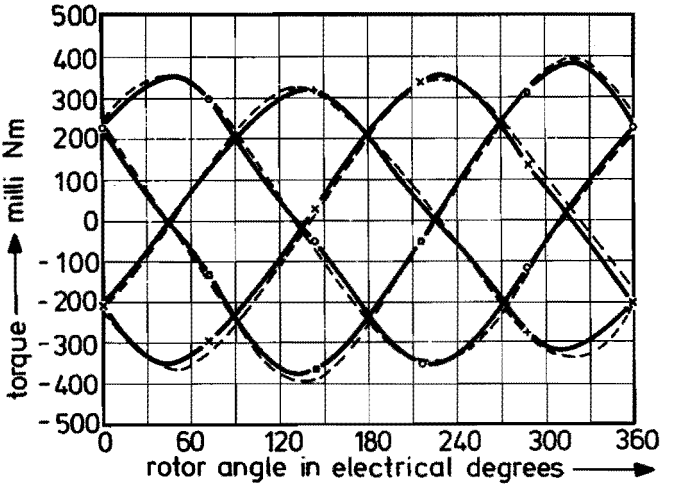

Fig. 3.18 – Torque as a function of the rotor angle

3.7. Effect of the iron saturation on the stepping-angle error

In the preceding section we stated that the stepping-angle error might be caused by saturation of the iron circuit between the two disks of one stator part. This iron-path saturation cannot be determined by means of the results from the measuring model referred to in 3.3. The permeance of the iron outside the tooth zones can however be predicted from a special measuring model.

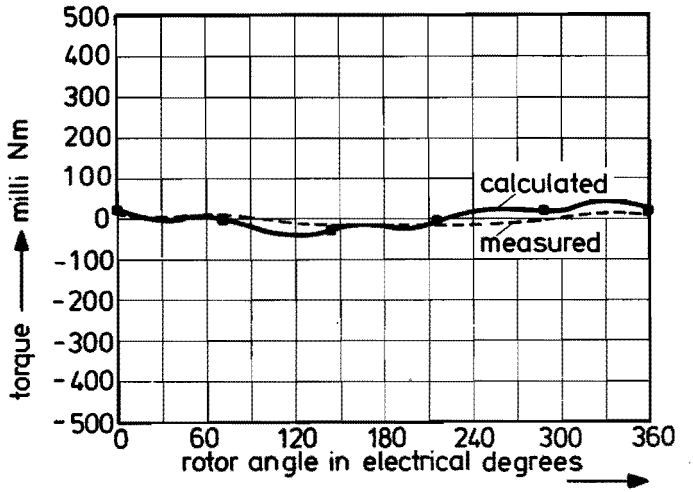

Fig. 3.19 – Detent torque if $P_b = 0.33\ 10^{-4}$ Wb/A

For this purpose we take a model of the same size as that of a stator part with rotor, but without slots. In this model we measure the variation of the flux as a function of excitation, which is independent of the rotor angle. Now if we assume that the whole flux passes straight through the air gap and that the end effects are negligible – which is permissible because in the measuring model the length of the air gap is smaller by a factor of 100 than the disk height, – then the air gap permeance P_a can be written as:

$$P_a = \frac{\mu_0 A_g}{l_g} \tag{3.22}$$

where A_g is the surface area of the disk in the air gap and l_g the air gap length. The total permeance of the measuring model follows from the measuring results:

$$P_{tm} = \frac{\Phi}{F} \tag{3.23}$$

Here Φ is the measured flux and F the excitation m.m.f.

The total permeance P_{tm} of the measuring model consists of the permeance of the two air gaps and the permeance of the iron circuit, and is given by

$$P_{tm} = \frac{P_y \frac{P_a}{2}}{P_y + \frac{P_a}{2}} \tag{3.24}$$

where P_y is the permeance of the iron circuit. Since P_{tm} is a function of the flux, P_y is a function of the flux as well. As the tooth zones contain only a minimum fraction of the iron circuit it is valid to state that the permeance of the measuring model as described in 3.3 is made up of the series permeance P_y of the iron circuit and P_{tz} of the tooth zone, so that for the measured permeance P_m as a function of flux Φ we can write:

$$P_m(\Phi) = \frac{P_y(\Phi) \frac{P_{tz}(\Phi)}{2}}{P_y(\Phi) + \frac{P_{tz}(\Phi)}{2}}. \tag{3.25}$$

Thus the two measuring models enable use to define the permeance both in the iron circuit and in the tooth zone.

In addition to the method just referred to a field-computation program is also used for calculating the iron circuit permeance. Such a program is for instance the one established by Maggy, with which static two-dimensional magnetic fields can be calculated (ref. 18). Fig. 3.20. is a plot of the iron circuit in cylindrical coordinates. The problem is rotational-symmetric in nature and hence a cross-section for φ constant provides the complete information required. The dimensions of the area are those of the motor as given in Appendix 1, i.e. with no slots. We solved the problem by performing the calculations for different applied excitations. The solution of the field in the whole area allows the line integral of the magnetic field strength to be calculated. The flux linked with the turns is not uniform for all these turns, but the flux that is not linked with all the turns is extremely small. Accordingly, in further calculations we assumed that the whole flux is linked with all the turns so that there is no flux in the space of the coil itself. The permeance of the iron circuit outside the air gaps can be expressed by

$$P_y = \frac{\Phi}{U_y} \tag{3.26}$$

where U_y is the loss of the number of ampere turns over the iron circuit. A deeper analysis of the line integral of the magnetic field strength reveals that the number of ampere turns over the disks is small compared with the number over the rest of the circuit.

From the calculation of the magnetic field with the above-mentioned program it follows that the number of ampere turns over one disk is about 20% of the total loss of ampere turns over the iron circuit. The greater part of the permeance of this circuit is connected in series with the outer disk, only part of the inner disk permeance being in series with the permeance P_{tz} of the inner disk. Assuming in further calculations that the total iron permeance is in series only with the tooth zone permeance P_{tz} of the outer disk we will introduce a small error. In calculating the magnetic potential distribution over the four disks, we utilize the analogon from fig. 3.21. Here the iron circuit permeance takes the same place in the equations as the stator butt joints permenace P_b used in section 3.5.

The disk permeance can now be written:

$$P_i = \frac{2\,\Phi}{F - U_y} \tag{3.27}$$

where P_i is the disk permeance, Φ is the measured flux, F the applied excitation and U_y the loss of ampere turns across the iron circuit at the flux Φ, as calculated above.

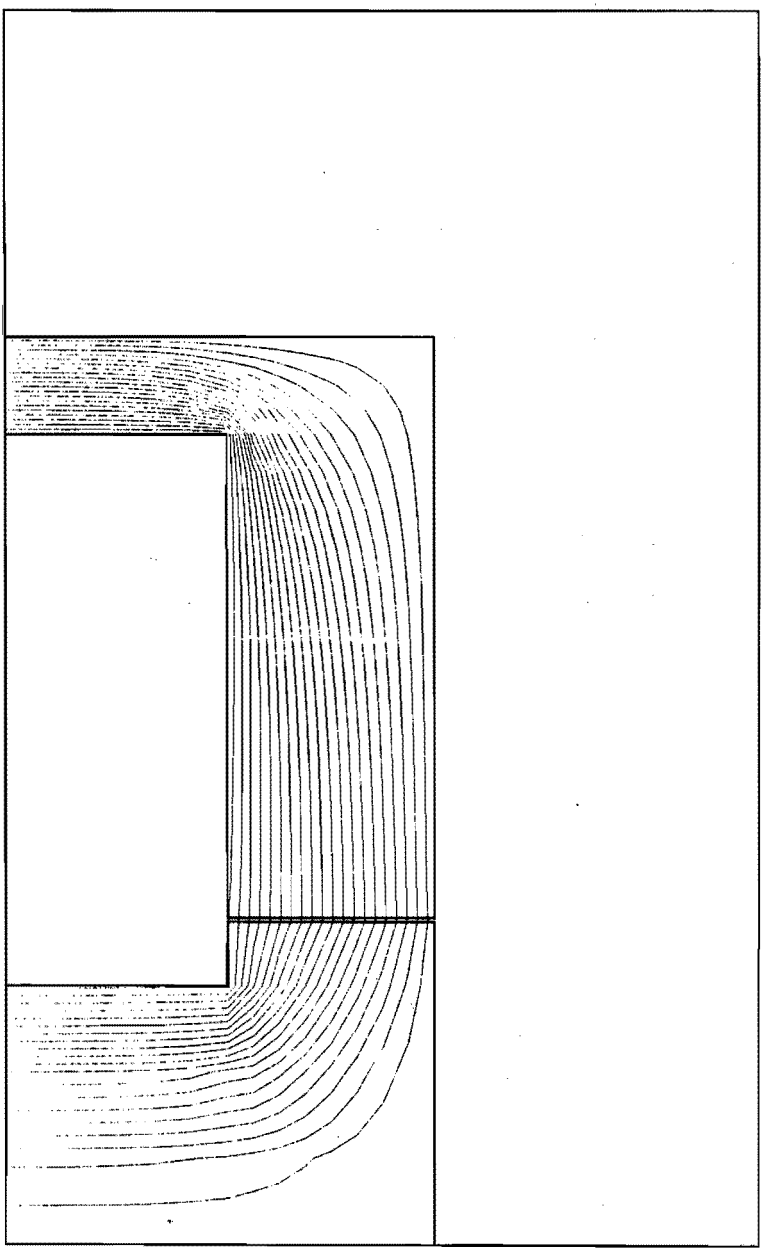

Fig. 3.20 – Magnetic field lines in the measuring model

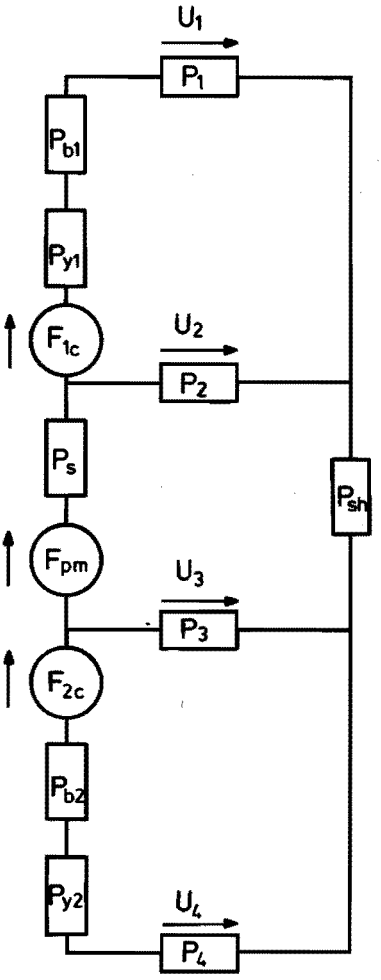

Fig. 3.21 – Analogon of the motor

The disk permeance is now a function of (F-U_y) and θ. The torque measured at the excitation applied also varies with (F-U_y).

Fig. 3.22 exhibits the variation of flux as a function of U_y.

The shaft permeance has so far been assumed to be a constant. In further calculations the shaft saturation will be taken into account. The shaft permeance can be found as

$$P_{sh} = \frac{\mu_y \, A_{sh}}{l_{sh}} \tag{3.28}$$

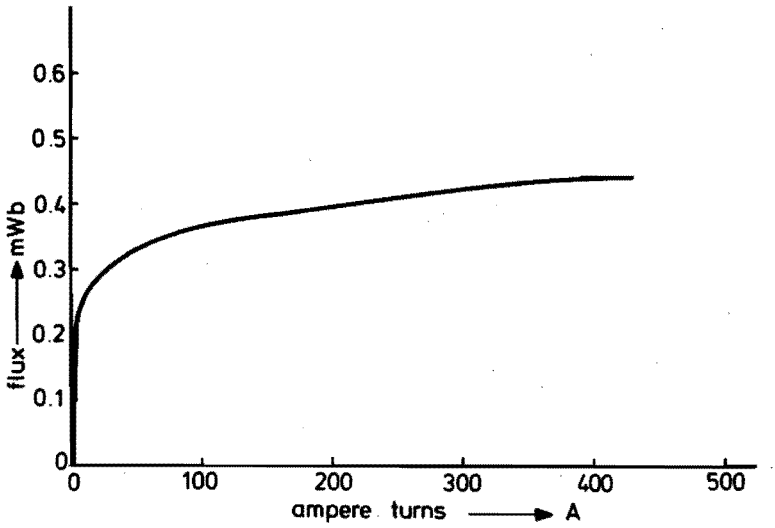

Fig. 3.22 – Flux as a function of the loss of ampere turns U_y across the iron circuit

P_{sh} being the shaft permeance, A_{sh} the cross-sectional area of the shaft, l_{sh} the length of the shaft and μ_y the iron permeability.

Fig. 3.23. shows the B-H curve of the iron, from which the iron permeability can be deduced.

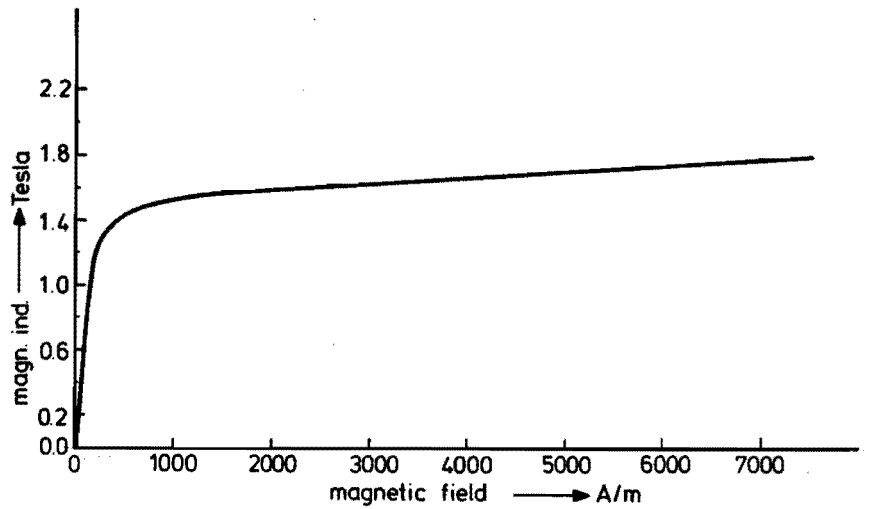

Fig. 3.23 – B.H. Curve of the iron

In calculating the potential distributions use is made of the following equations:

$$P_{by1} = \frac{P_{b1}\, P_y(\Phi_1)}{P_{b1} + P_y(\Phi_1)} \tag{3.29}$$

$$P_{by2} = \frac{P_{b2}\, P_y(\Phi_4)}{P_{b2} + P_y(\Phi_4)} \tag{3.30}$$

$$P_1' = \frac{P_1(\Phi_1)\, P_{by1}(\Phi_1)}{P_1(\Phi_1) + P_{by1}(\Phi_1)} \tag{3.31}$$

$$P_4' = \frac{P_4(\Phi_4)\, P_{by2}(\Phi_4)}{P_4(\Phi_4) + P_{by2}(\Phi_4)} \tag{3.32}$$

$$P_{pm} = \frac{P_s\, P_{sh}(\Phi_{sh})}{P_s + P_{sh}(\Phi_{sh})} \tag{3.33}$$

$$\Phi_{sh} = \Phi_1 + \Phi_2 \tag{3.34}$$

$$U_1' = \frac{\Phi_1}{P_1(\Phi_1)} + \frac{\Phi_1}{P_{b1}} + \frac{\Phi_1}{P_y(\Phi_1)} \tag{3.35}$$

$$U_4' = \frac{\Phi_4}{P_4(\Phi_4)} + \frac{\Phi_4}{P_{b2}} + \frac{\Phi_4}{P_y(\Phi_4)} \tag{3.36}$$

$$F_{1c} = U_2 - U_1' \tag{3.37}$$

$$F_{2c} = U_4' - U_3 \tag{3.38}$$

$$F_{pm} = U_3 - U_2 - \frac{U_1' P_1'}{P_{pm}} - \frac{U_2 P_2}{P_{pm}} \tag{3.39}$$

$$U_1' P_1' + U_2 P_2 + U_3 P_3 + U_4' P_4' = 0. \tag{3.40}$$

Elimination of U_1' and U_3 in (3.39) and (3.40) by (3.37) and (3.38) leads to:

$$U_2 (P_2 + P_1') + U_4' (P_3 + P_4') - F_{1c} P_1' - F_{2c} P_3 = 0 \tag{3.41}$$

and

$$F_{pm} + U_2 \left(1 + \frac{P_1' + P_2}{P_{pm}}\right) - U_4' + F_{2c} - F_{1c} \frac{P_1'}{P_{pm}} = 0. \tag{3.42}$$

Eqs. (3.41) and (3.42) are two non-linear equations for U_2 and U_4' in which all the permeances are direct or indirect functions of U_2 or U_4', which can be solved by an iterative method as indicated in sec. 3.5. From the solution of U_2 and U_4' and by the use of (3.37) and (3.38) we can obtain the magnetic potential differences U_1 and U_3. The torque delivered by the motor is found by calculating the disk magnetic potential differences as:

$$U_1 = U_1' - \frac{\Phi_1}{P_{b1}} - \frac{\Phi_1}{P_y(\Phi_1)} \tag{3.43}$$

$$U_4 = U_4' - \frac{\Phi_4}{P_{b2}} - \frac{\Phi_4}{P_y(\Phi_4)} \tag{3.44}$$

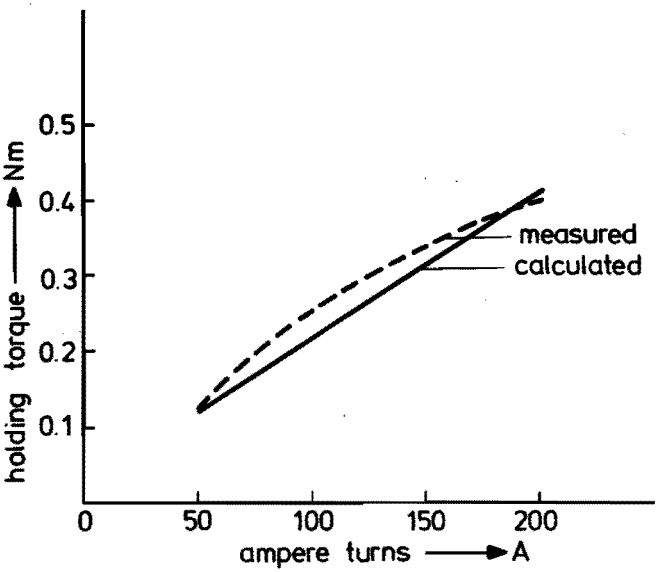

Fig. 3.24 – Torque as a function of the excitation current

where Φ_1 and Φ_4 follow from:

$$\Phi_1 = P_1' U_1' \tag{3.45}$$

$$\Phi_4 = P_1' U_4' \tag{3.46}$$

The torque of each disk can be calculated by finding them back at the angle for which the calculations have been done and the potential across the disk permeance. The total torque can be derived by summing the four disk torques.

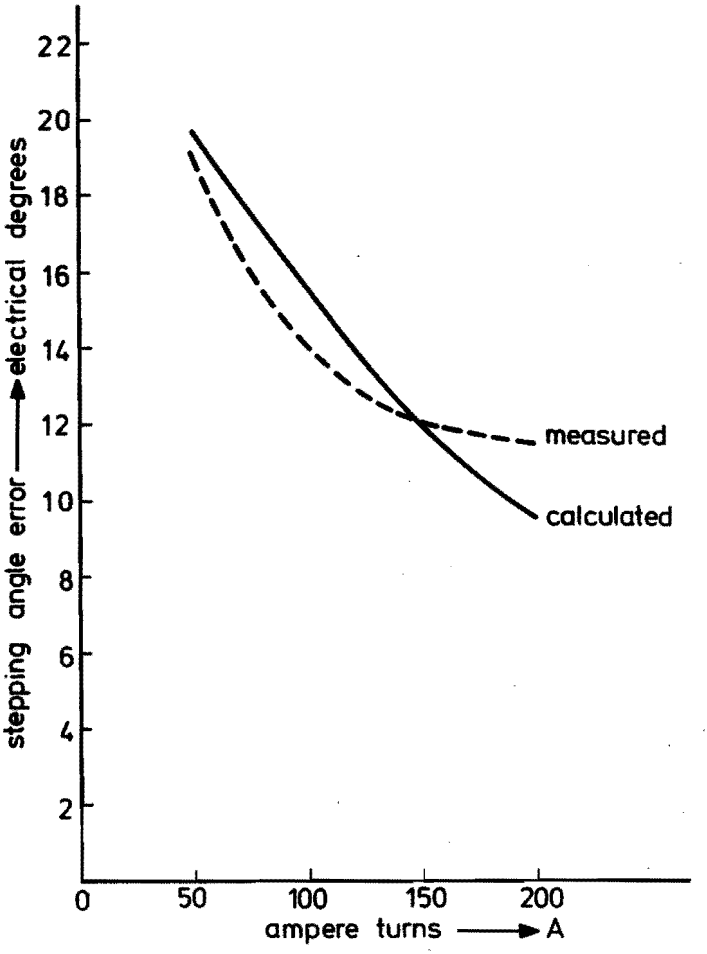

Fig. 3.25 – Stepping angle error as a function of the excitation current

Using the above expressions we designed a computer program with which we calculated the torque and the stepping angle of the motor described in Appendix 1. Fig. 3.24. shows a plot of the measured and the calculated holding torque. There is a reasonable agreement between these two torques.

Fig. 3.25. presents the calculated and measured stepping angle error for a stator butt joint of 10 μm. As can be seen, there is now a satisfactory agreement between the measured and calculated stepping angle errors.

Fig. 3.26. represents the measured and calculated torque rotor angle characteristics of the motor excited by 150 ampere turns. When the saturation outside the tooth zones is taken into account the agreement between the calculated and measured value is sufficient to need no further sophistication of the computational method used.

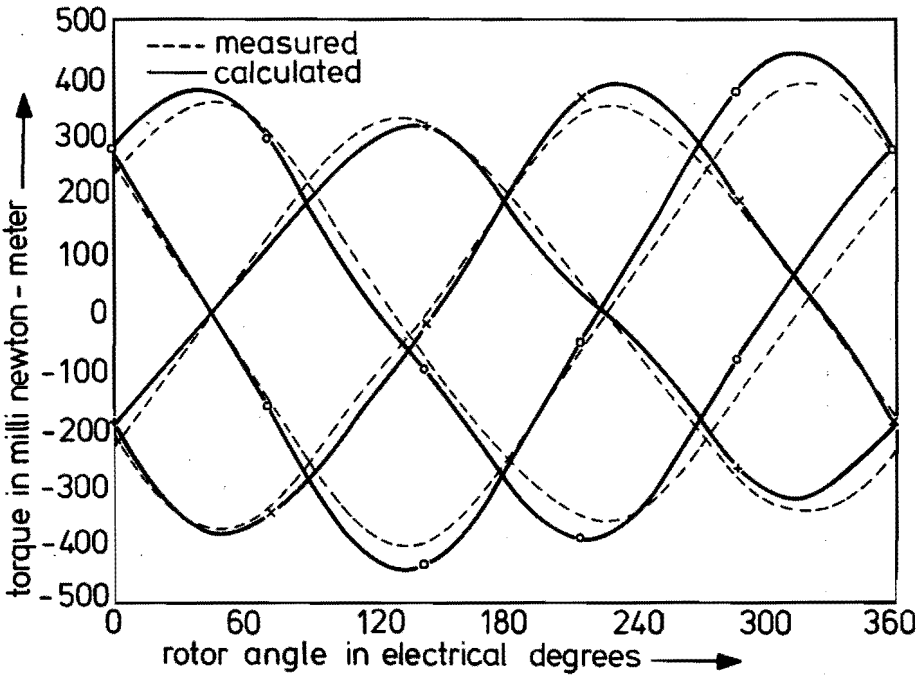

Fig. 3.26 – Torque as a function of the rotor angle

4. IMPROVEMENTS ON THE BASIC DESIGN

In the previous chapter we have given calculations of the torque and the stepping angle error of the motor. The motor torque suffices to obtain a satisfactory stepping motor. The stepping angle error of the motor is unduly large. The stepping angle error of such a motor is required to be less than 5%, and that of accurate motors even less than 3%. In the production of the motor, the stepping angle error, owing to mechanical deviations, will be even larger than the calculated inherent stepping angle error. The production cost of the motor is lower if the tolerances are larger. One should therefore modify the motor in such a way that the inherent stepping angle error is eliminated. Most stepping motors are driven in double phase, so that elimination of the stepping angle errors will suffice for a motor with a nominal double-phase excitation.

The stepping angle error in the motor is due to the magnetic circuit being asymmetric. This error can be removed by making the motor symmetric. The inherent stepping angle error then disappears both for single- and double-phase excitation. In section 4.1. we shall be dealing with a method by which such a symmetric motor can be made.

It is also possible to compensate for the stepping angle error by providing for an additional asymmetry of the motor, with the result that, for a nominal double-phase excitation, the motor does not suffer from a stepping angle error (ref. 12, 13). In the case of an excitation deviation, however, a stepping angle error will indeed arise. In section 4.2. it is shown and calculated which asymmetries are capable of compensating for the inherent stepping angle error of the motor. Compensation of the stepping angle error by introducing new asymmetries is preferable because it does not lead to a more complex motor design.

4.1. Motor segmentation

The asymmetries in the basic design of the motor as described in the preceding chapter may lead to inherent errors, which are removed if the motor is made symmetric. this is the case when the torque-creating mechanism in the motor is identical for the different directions of the excitation currents.

Making the motor symmetric requires the introduction of thorough modifications. This can be achieved, e.g. by dividing the motor into four segments, each segment retaining the properties of the motor described in the preceding chapters. The segments, however, are chosen in such a way that, on excitation, the flux through the inner disks in two segments, and that through the outer disks in the two other segments, are at all times enhanced.

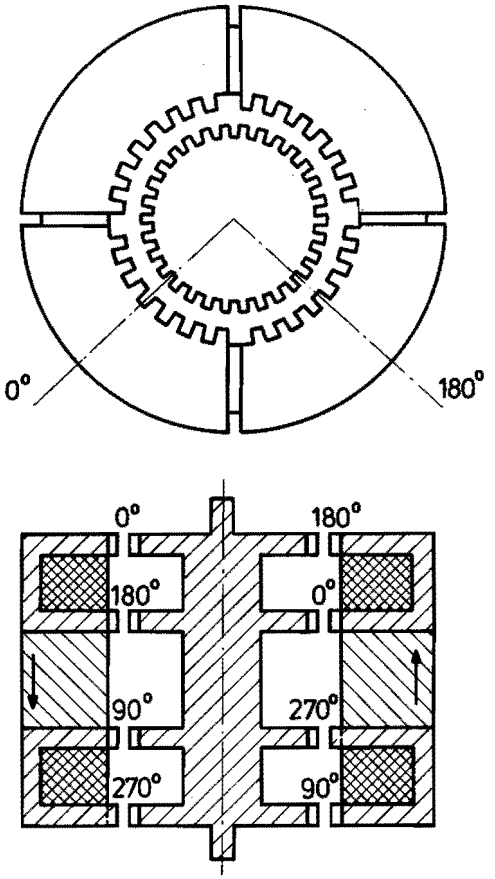

Fig. 4.1 – Segmented motor

We have constructed a motor according to this principle of segmentation (fig. 4.1.). The excitation coils remained unaltered, so that there is still one pole pair per phase. We also did not modify the permanent magnet. The magnetization of the permanent magnet, however, was changed so as to obtain opposite flux directions in two adjacent segments.

Excitation of the stator part causes the flux of the excitation coil to have the same direction in all the segments. The direction of the flux from the permanent magnet will be opposite for two adjacent segments, so that this flux when excited by the coil is enhanced in two segments in the inner disk as well as in the two other segments in the outer disk.

The teeth of the segments are chosen in such a way that, when the rotor teeth for a

disk are in line with the teeth of one segment, they will be out of line with the teeth of the adjacent segments.

The motor torque is the sum of the torques produced by the four segments. Independent of the direction of the excitation current there are always two segments per stator part where the flux in the inner disk is enhanced and two segments where the flux in the outer disk is enhanced. Accordingly, the torque mechanism has become independent of the direction of the excitation current.

It is possible in principle to split up the motor into two parts. This however gives rise to radial forces loading the bearings. We opted for a division into four segments, thus avoiding radial forces acting on the bearings.

The segments of each stator part should be magnetically insulated, otherwise the flux from the permanent magnet will be short-circuited via the segments of a stator part. However, complete magnetic insulation is not feasible, and therefore some permanent magnet flux always flows from one segment to the other without reaching the rotor. This means that the excitation by the permanent magnet is not particularly effective, which results in torque losses. Besides, segmentation is only possible if the number of stator teeth per disk is smaller than the number of rotor teeth. This implies that segmentation of the motor reduces the number of active rotor teeth and decreases both the torque per volume ratio and the ratio between the torque and the moment of inertia.

We have built a motor according to this principle, making use of axial U-shaped lamination sheets. One such sheet is shown in fig. 4.2. The lamination sheets are mounted on a coil former provided with slots into which the lamination sheets are fitted. The slots determine the position of the lamination sheets, which are bent to reduce the volume. Fig. 4.3. shows how this has been done. The shift by 180

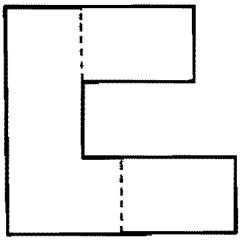

Fig. 4.2 – U-shaped lamination

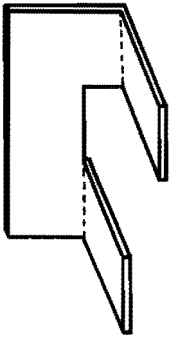

Fig. 4.3 – U-shaped lamination after bending

electrical degrees for the two "disks" has been achieved by bending the lamination sheets about the dashed lines. Axial lamination has the advantage that there are no butt joints between the two disks of a stator part.

Fig. 4.4. shows a photograph of a stator part with axial lamination. The sheet thickness with axial lamination is equal to the tooth width when only a single sheet per tooth is used. Fig. 4.5. shows the torque angle curve of a motor exhibiting an asymmetry of the holding torque owing to deviations in the mechanical construction and unbalance in the permanent magnet excitation for the different segments.

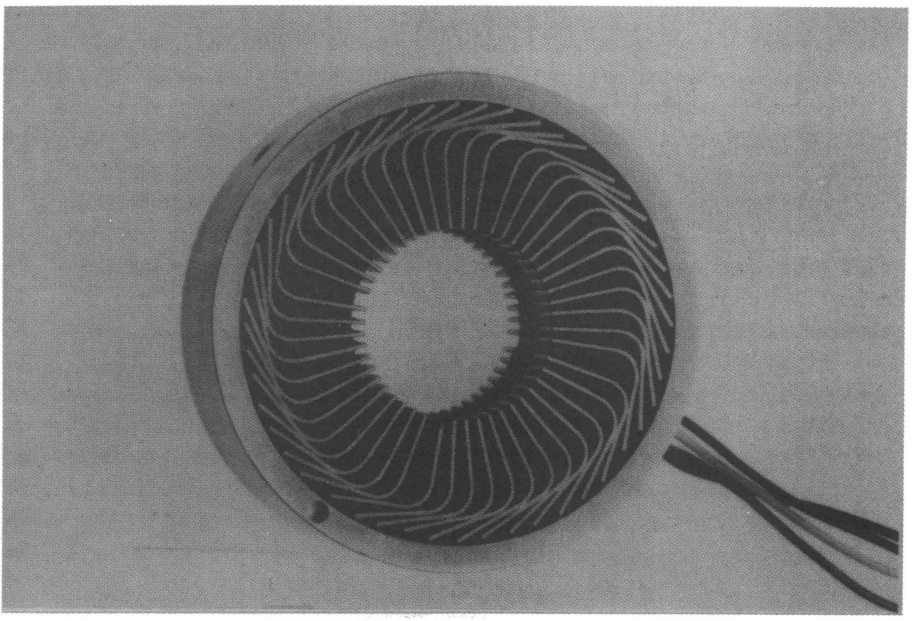

Fig. 4.4 – Axial laminated stator part

The stepping angle error of the motor, which is less than 3%, is also caused by departures from the mechanical design and is smaller than the stepping angle tolerance. The detent torque of the motor represented in fig. 4.6. is made up of two torques, one with the fundamental and the other with a fourth-harmonic periodicity. The fourth harmonic arises because the permeance function of the air gap possesses not only the fundamental periodicity but also a fourth harmonic. The torques produced by the fourth harmonic are in phase for all the segments and consequently emerge in the detent torque, which due to mechanical errors in the motor construction has also a fundamental periodicity. The amplitude of the detent torque, however, is low compared with that of the holding torque.

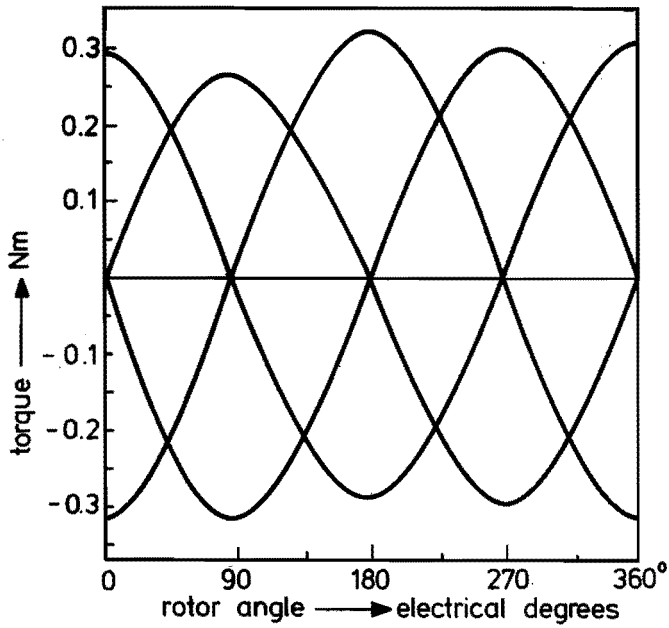

Fig. 4.5 – Torque angle curve of the segmented motor

A comparison between the torque of the segmented motor and that of the motor described in Appendix 1 is not relevant because in the latter case different magnetic materials are employed.

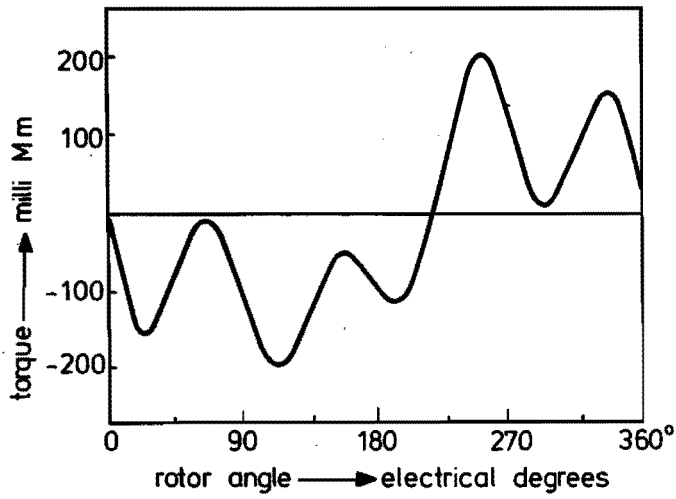

Fig. 4.6 – Torque-angle curve of the original motor with axial lamination

The torque angle curves in fig. 4.7 refer to a motor of the original construction in which axial lamanation is again applied but which is not segmented. The detent torque of this motor, which is substantially higher, is also shown in fig. 4.7. The detent torque of the motor built according to the basic design is larger by a factor of about 2 or 3 than that of the segmented motor and is practically solely governed by the term with the fundamental periodicity. The stepping angle error of the non-segmented motor is 12% and hence impermissibly large.

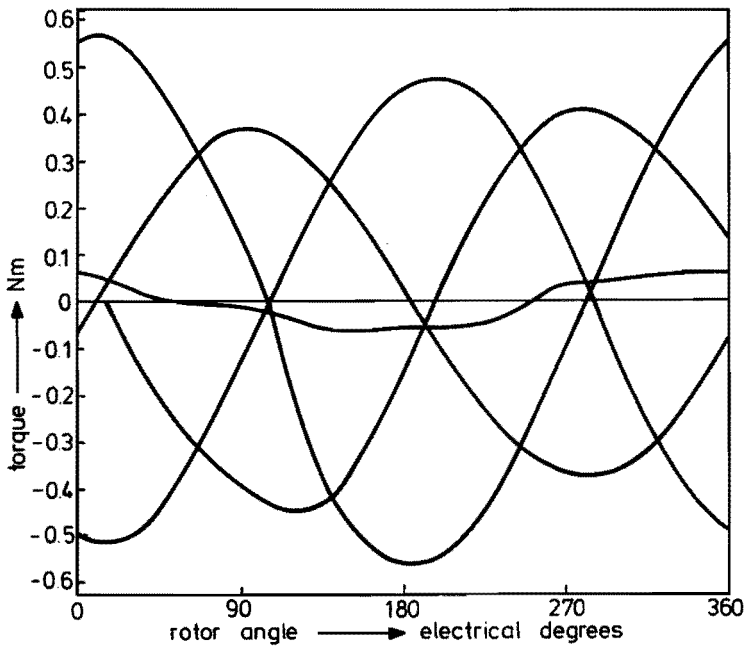

Fig. 4.7 – Torque-angle curve of the original motor with axial lamination

The ratio between the minimum holding torques reveals that segmentation decreases the holding torque by about 30%. This decrease is likely to be larger than is necessary because in the segmented motors sheets of two segments are touching, so that the leakage of the permanent-magnet flux is higher than is necessary. The measurements on the motors with axial lamination demonstrate that the motor can be made symmetric by segmentation, which results in an acceptable stepping angle error. However, segmentation has the drawback of decreasing the holding torque.

4.2. Methods of compensating for the asymmetries in the motor

Segmentation, discussed in the previous section, makes the motor symmetric and its stepping angle error will be small. However, this gives rise to a loss in torque and the

motor construction becomes in addition more intricate which renders it more expensive and increases the probability of deviations caused by mechanical tolerances. In the present section we will study the feasibility of changing the motor, by applying new asymmetries in the magnetic circuit, in such a way as to remove inherent stepping angle errors at a rated double-phase excitation. In doing so, the motor must not become more intricate and its torque must not be more than slightly affected.

The asymmetries in the magnetic circuit are caused by a difference in magnetic path that the flux from the permanent magnet sees for the various disks. The permeance of the magnet circuit via the inner disks is larger than that via the outer disks.

The coupling between the two stator parts causes reluctance torques that adversely affect the motor performance. This coupling is governed by the permeances of the permanent magnet and the rotor between the inner disks. The coupling between the two stator parts can be substantially reduced by turning off the rotor between the inner disks to such an extent that the remaining portion of the rotor core becomes saturated owing to the flux generated by the permanent magnet. The permeance in the magnetic circuit of the flux produced by the coils is then reduced, thus decreasing the effect of the coupling. The effect of the coupling on the stepping angle error of the motor is slight compared with the effect caused by the difference in path length between the various disks. Turning off the rotor between the inner disks is therefore only useful to reduce the asymmetry in the holding torques.

The stepping angle error in the motor can be changed by introducing the following new asymmetries in the magnetic circuit.

1. The permeances of the air gap transitions at the inner and outer disks are made to be different, which can be done by varying:
   - the height of the disks in axial direction,
   - the length of the air gap in radial direction,
   - the shape of the teeth.

2. An additional magnetic resistance is connected in series with the air gap permeance at the inner or outer disks. This can be achieved for instance by providing an extra air gap in the iron circuit, which is arranged in series with the inner disk permeance.

3. The teeth of the disks are not aligned at the normal angles of 0, 180, 270 and 90 electrical degrees but are shifted with respect to the normal alignment.

The above measures hardly affect the cost of the motor because the design is not altered. The measures referred to in items 1 and 2 have the effect of matching the permeances of the magnetic paths to one another in such a way that the stepping

angle error is eliminated in the case of a rated double-phase excitation. There are many ways in which this can be done. For practical reasons we only examined the effect of the disk height on the motor performance. This has the advantage that no drastic changes need to be introduced into the experiments and into the calculations. The variation in disk height is achieved experimentally by turning off the rotor disks. In the computations of the motor torque the disk permeance varies with the changed disk height in a linear fashion. It is therefore possible, without drastically changing the existing programs, to calculate the effect of the disk height on the motor performance.

The last-mentioned measure, in which the disks are aligned in a different way, is directly accessible to calculation using the program described in chapter 3, but the effect of the shift cannot be determined experimentally using the motor dealt with in Appendix 1. This can, however, be done using the motor described in chapter 5. Hence the two compensation methods can only be compared with the aid of the computational results.

4.3. Effect of the variation in permeance

The permeances P_2 and P_3 are linear functions of the tooth height. In view of the symmetry between the two stator parts, we consistently assume that the variation in disk height is equal for the two stator parts, so that the disk height is the same for the inner disks and for the outer disks. In the calculations, the height of the two outer disks is assumed to remain unaltered, and a constant factor K by which the permeance P_2 and P_3 are multiplied is written in the program:

$$K = \frac{t_{h1}}{t_{h2}} \tag{4.1}$$

where t_{h1} is the disk height of disk 1 and t_{h2} is the disk height of disk 2. The torque on the disk as well as the permeance are linear functions of the tooth height at a specific m.m.f. across the disk. The torque is at all times calculated as a function of the rotor angle for the four different states of excitation. The results of the calculations are plotted as a function of the excitation current with the disk height as parameter. Fig. 4.8. represents the stepping angle error as a function of the excitation current for a number of disk heights. Fig. 4.9. shows the holding torque plotted against the excitation current for several different disk heights.

The holding torques represented in fig. 4.9. are minimum ones. The effect of the disk height on the minimum holding torque is slight, because then the flux in the inner disks is reduced. Its effect on the maximum holding torque, however, is larger, because then the flux in the inner disks is enhanced. So as to be able to study this effect, we introduce the factor.

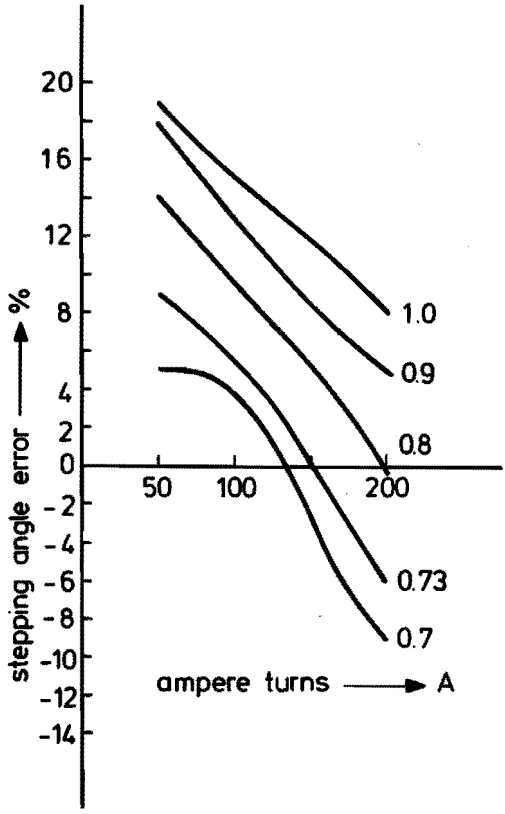

Fig. 4.8 – Stepping angle error as a function of the excitation

$$\gamma = \frac{T_{H\,min}}{T_{H\,max}} \tag{4.2}$$

where $T_{H\,min}$ is the minimum and $T_{H\,max}$ is the maximum holding torque.

The factor γ refers to the asymmetry in the holding torques.

The curve in fig. 4.10. shows the factor γ related to the excitation current with the disk height as parameter.

Fig. 4.11. is the torque-angle characteristic of the motor for the disk height at which the stepping angle error is 0% and the excitation 150 ampere turns, i.e. the rated excitation. The factor K is then 0.73.

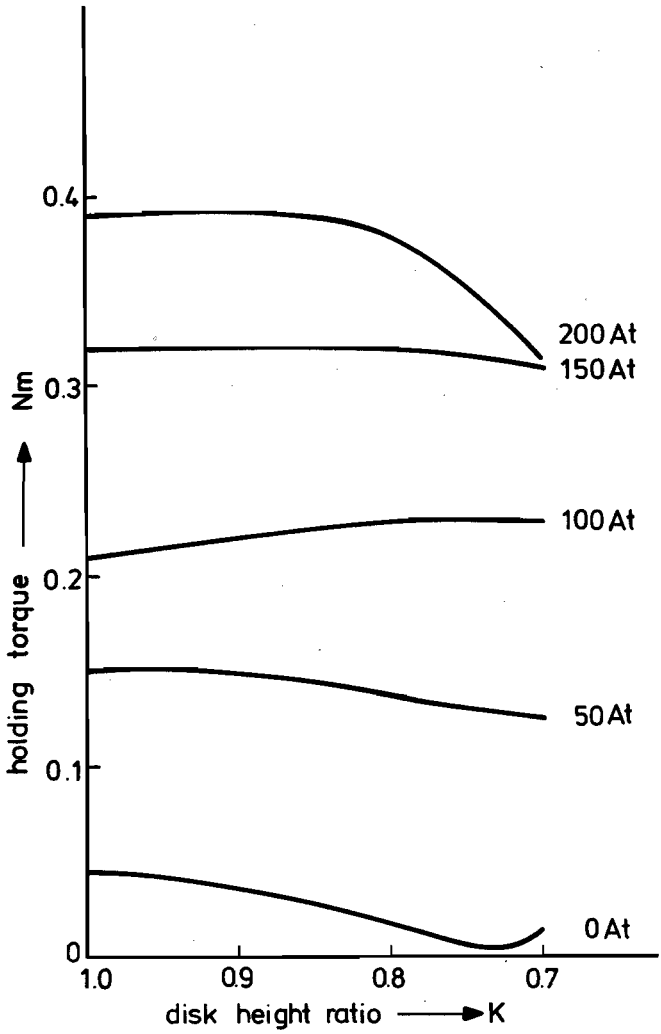

Fig. 4.9 – Holding torque as a function of the disk-height ratio

Fig. 4.12 is a plot of the measured torque angle curve of the motor excited with 150 ampere turns at a disk height ration of K = 0.79 in which the stepping angle error is at a minimum.

In Fig. 4.13 the stepping angle error is plotted in terms of the disk height ratio K at an excitation of 150 ampere turns. In the same figure the measured stepping angle is also plotted. The measured and calculated stepping angle errors show good agreement.

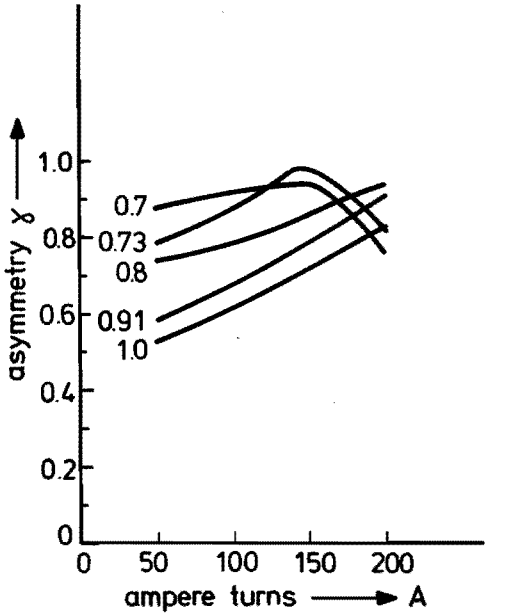

Fig. 4.10 – Asymmetry as a function of the excitation current

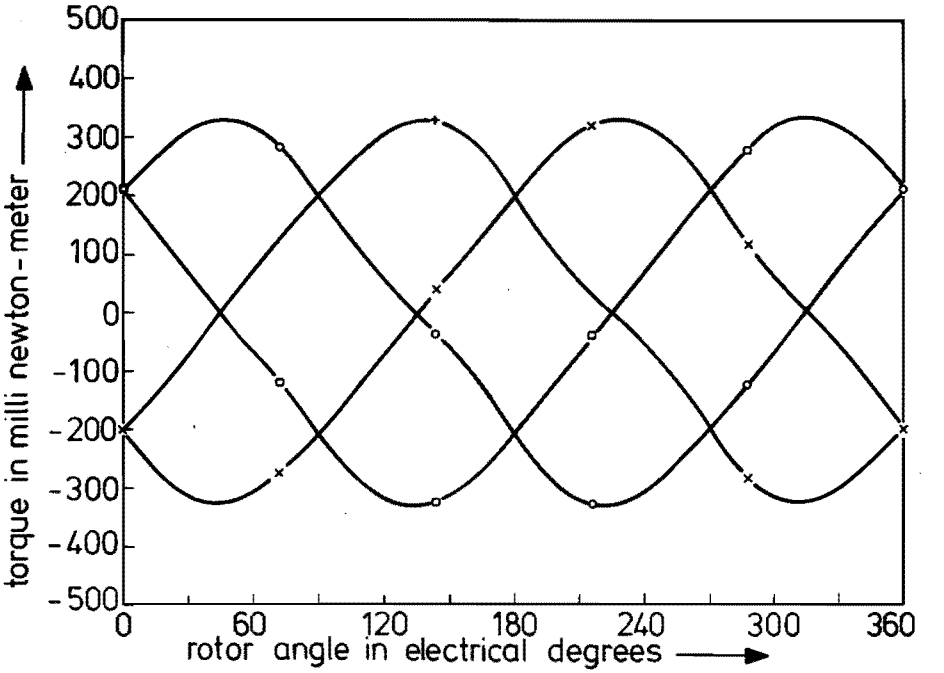

Fig. 4.11 – Calculated torque angle curve for K = 0.73

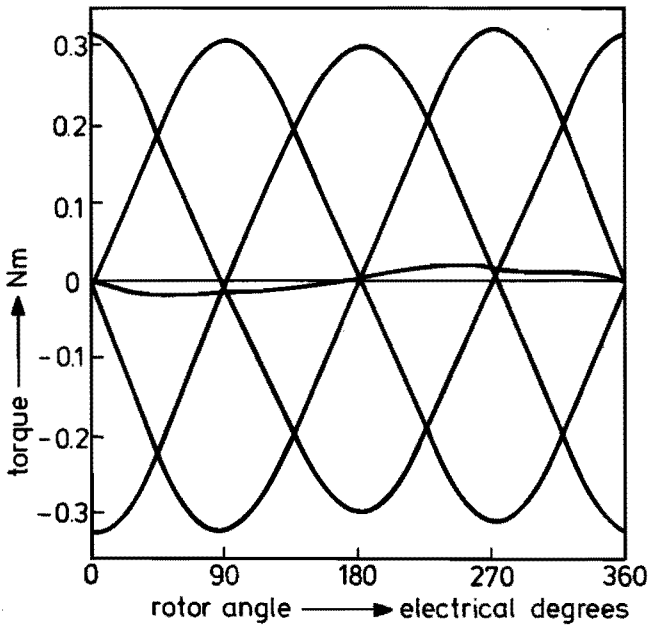

Fig. 4.12 – Measured torque angle curve for K = 0.79

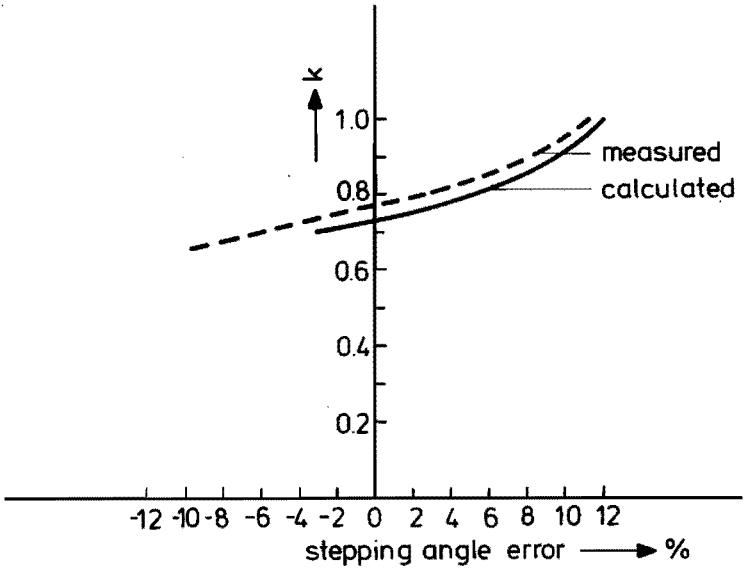

Fig. 4.13 – Stepping angle error as a function of the disk height ratio

The results of the calculation and the measurements reveal that the stepping angle error can be entirely compensated by taking the disk height of the inner disks to be smaller than that of the outer disks, where the disk height ratio K is determined by the applied excitation. This correction decreases the asymmetry in the holding torque, whereas it hardly reduces the minimal holding torque.

We have already indicated that by varying the air gap length or the shape of the teeth the permeance function of the disks can be varied as well.

These methods differ sligthly from the method described above in which the disk height is varied. A calculation on a motor with a fluctuating air gap or with a different tooth shape is however much more complex because the permeance function of the disk does not vary linearly with the relevant parameters such as air gap length or tooth width (see ref. 8). An exact calculation would require the air gap permeance to be measured for every variation, after which the values found could be used in the calculations of the torque. This would be time-consuming and expensive, and is unlikely to provide essentially new insights.

It has been demonstrated by measurements and calculations that the stepping angle error can be compensated by varying the height of the inner disk with respect to that of the outer disks. This method has the great advantage that the holding torque hardly decreases and that it entails no additional manufacturing costs.

4.4. Effect of disk shifting

When the angles of the disks are shifted relative to the normal alignment positions then the torque-angle curve will be changed and consequently the stepping angle error will be altered also. The motor described in appendix 1 does not allow mutual adjustment of the disk angles. In the calculations, however, this can be done in a straight-forward manner, because the angles of the disks are then computed for each point of the torque-angle curve. On account of the symmetry in the motor, due to the two stator parts being identical, we only made allowance for symmetric angular shifts. Fig. 4.14. shows an arrow diagram in which the axes indicate the directions of the normally aligned disks. The arrows indicate the equilibrium positions as they should be in the ideal case. A similar arrow diagram is presented in fig. 4.15. where the arrows indicate the actual equilibrium positions. The ideal holding positions are given by dashed lines. In the case that the two coils are excited in the same direction the actual and ideal equilibrium positions are equal. In the case that the two coils are excited in a different direction a stepping angle error occurs.

Angular shifts in the motor are represented in the diagram by rotating the axis, the angle of rotation with respect to the axis of symmetry of the two inner disks or the two outer disks being assumed to be equal at all times.

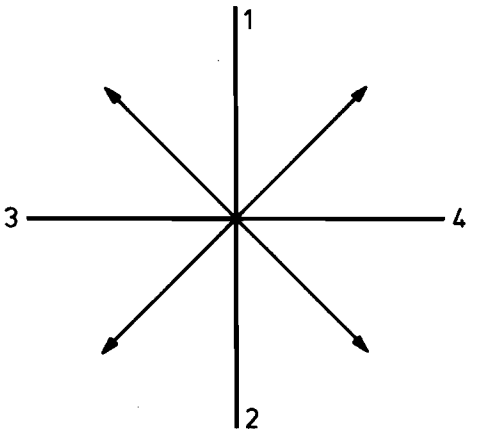

Fig. 4.14 – Diagram indicating the disks alignment

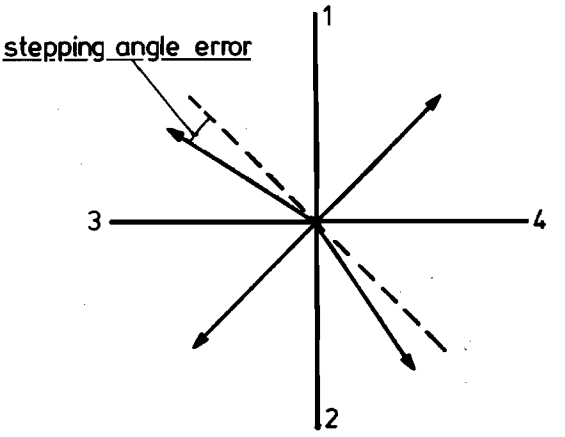

Fig. 4.15 – Actual equilibrium positons

Fig. 4.16. presents an arrow diagram in which the inner disks are turned through such an angle as to increase the electric angle between the inner disks, which is normally 90°.
We first calculated the variation of the stepping angle as a function of the angular shift of the inner disks. Fig. 4.17. shows a plot of the stepping angle error versus the angle between the inner disks for several different states of excitation. Fig. 4.18. gives the holding torque as a function of the angular shift for the same states of excitation as represented in fig. 4.17.

Fig. 4.19. exhibits the asymmetry in the holding torque.

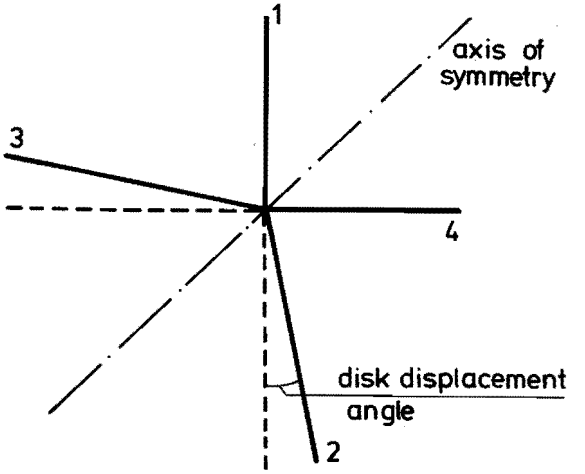

Fig. 4.16 – Displacement of the inner disks

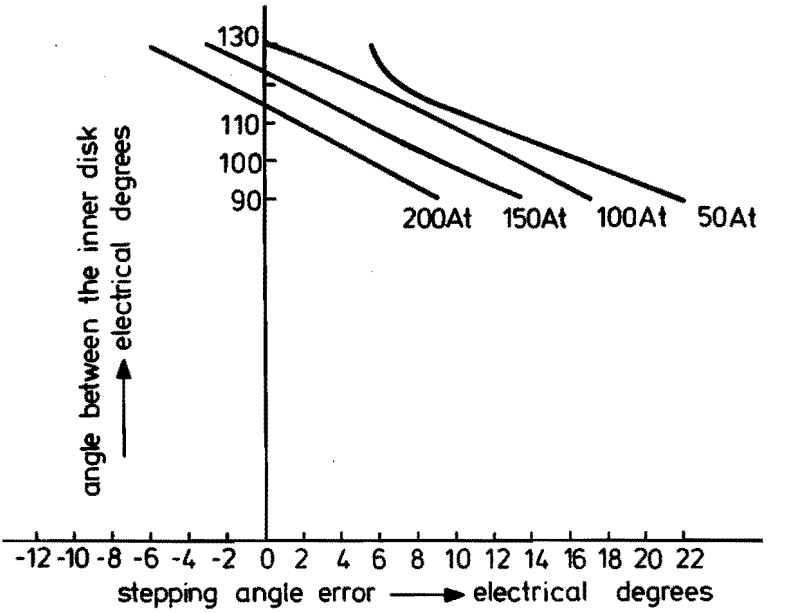

Fig. 4.17 – Stepping angle error as a function of the angle between the inner disks

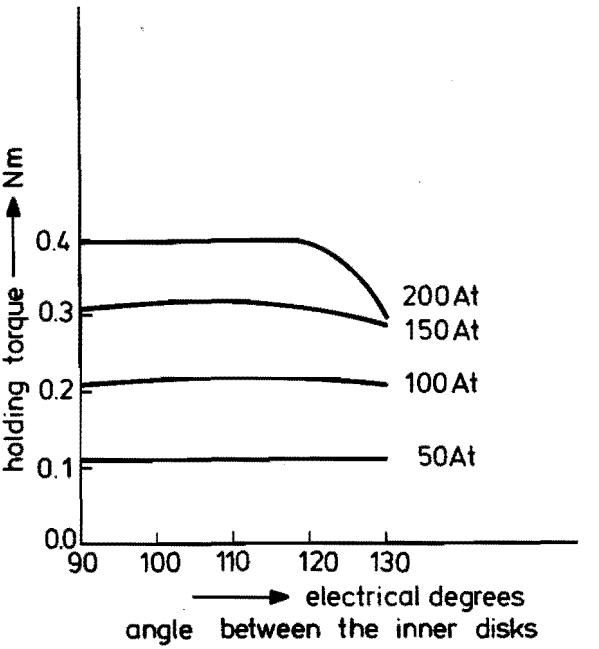

Fig. 4.18 – Holding torques as a function of the angle between the inner disks

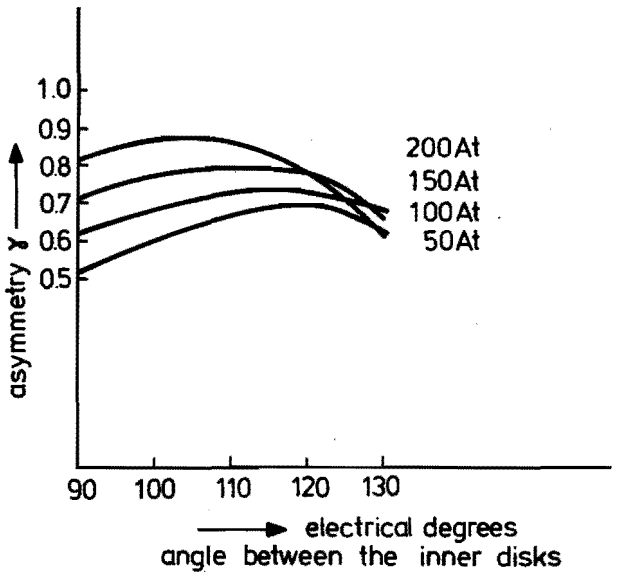

Fig. 4.19 – Asymmetry of the holding torques as a function of the angle between the inner disks

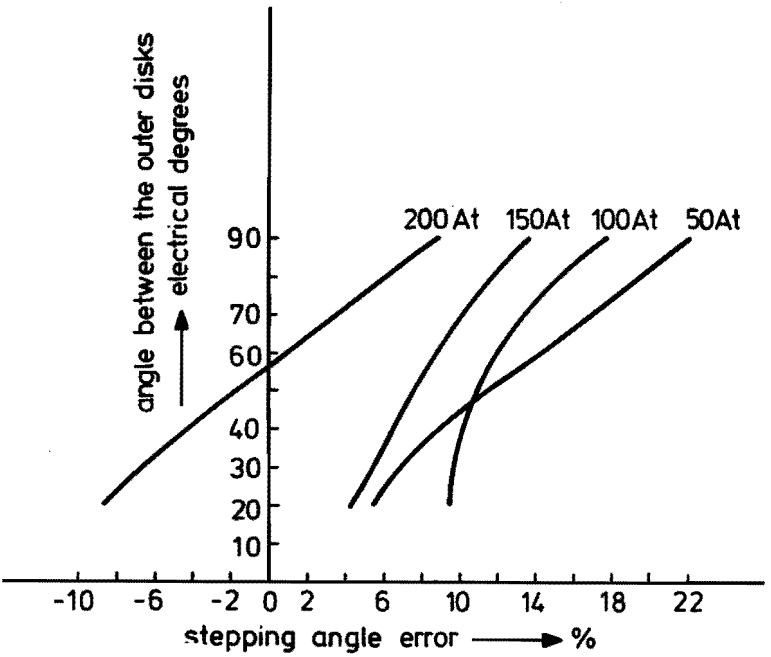

Fig. 4.20 – Stepping angle error as a function of the angle between the outer disks

Figs. 4.20. - 4.22. are similar to figs. 4.17. - 4.19.; in the latter, however, the angle between the two outer disks has been varied.

The calculations reveal that the stepping angle error in the motor can be eliminated by rotating both the inner and the outer disks, but that this has different effects on the holding torque.

By rotating both the inner and outer disks we are able to calculate a torque-angle curve for which the stepping angle error is 0% and the asymmetry in the holding torques has vanished. The minimum holding torque is now, however, about 10% larger than that of the normally aligned motor. Fig. 4.23. shows the torque-angle curve of the motor in which the angle between the inner disks is 116° and between the outer disks 72°. Here the asymmetry in the holding torque has almost been eliminated and the stepping angle error is reduced to 1%.

The conclusion is that adjustment of the disk alignment is a powerful means of removing the stepping angle error at rated excitation, which increases the holding torque without additional costs.

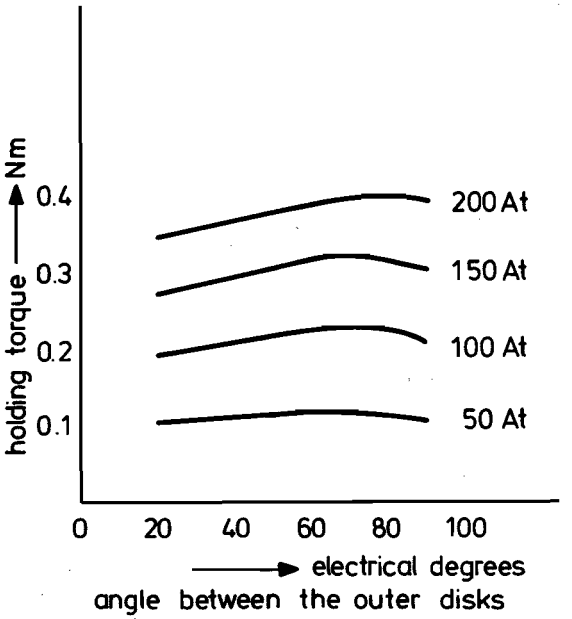

Fig. 4.21 – Holding torque as a function of the angle between the outer disks

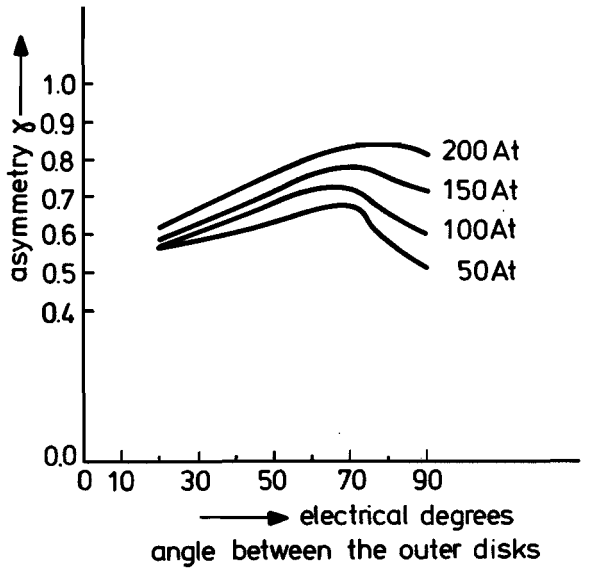

Fig. 4.22 – Asymmetry of the holding torques as a function of the angle between the outer disks

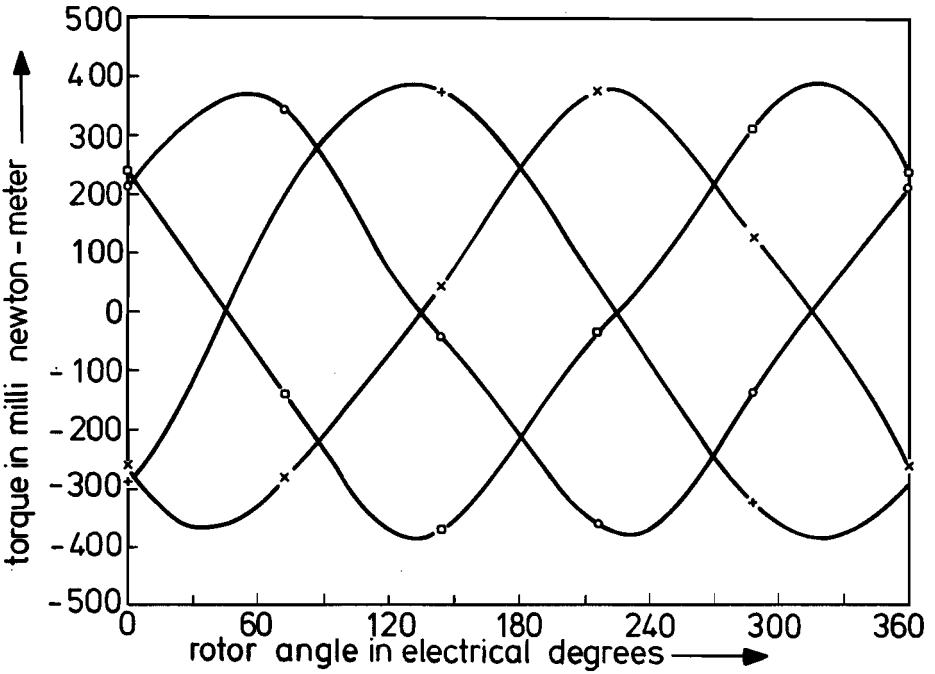

Fig. 4.23 – Torque angle curve of the motor with eliminated stepping angle and no asymmetry in the holding torques

5. MOTOR WITH ROTOR WITH HELICAL TEETH

In the preceding chapter we found that our calculations enabled us a motor to be designed which no longer has any stepping angle errors, by applying corrections for the disk alignment in the case of nominal double-phase excitation.

In the motor as described in Appendix 1 it proved impossible to realize the required angular shifts, Mechanically adjustable alignment of the disks is exceedingly difficult on account of the high precision required for small stepping angles. For a 1.8° stepping motor an error in stepping angle of 1% corresponds to a "mechanical" angle of about one minute. Moreover in a motor whose alignment can be adjusted it is in addition difficult to keep the stator butt joints small and reproducible.

To enable adjustable alignment experiments to be undertaken we adopted a different approach (ref. 14). The stator was fabricated with high precision in a single operation. The teeth of all the stator disks are in line. The high precision of stator alignment is achieved by making the disk teeth by wire spark erosion, the stator being mounted in a housing. The teeth are then exactly in line. Disk alignment is effected by means of the rotor disks.

The rotor disks are aligned by means of a helical tooth arrangement (skewing) (see fig. 5.1.). The helical tooth arrangement is realized by gear hobbing, which is a

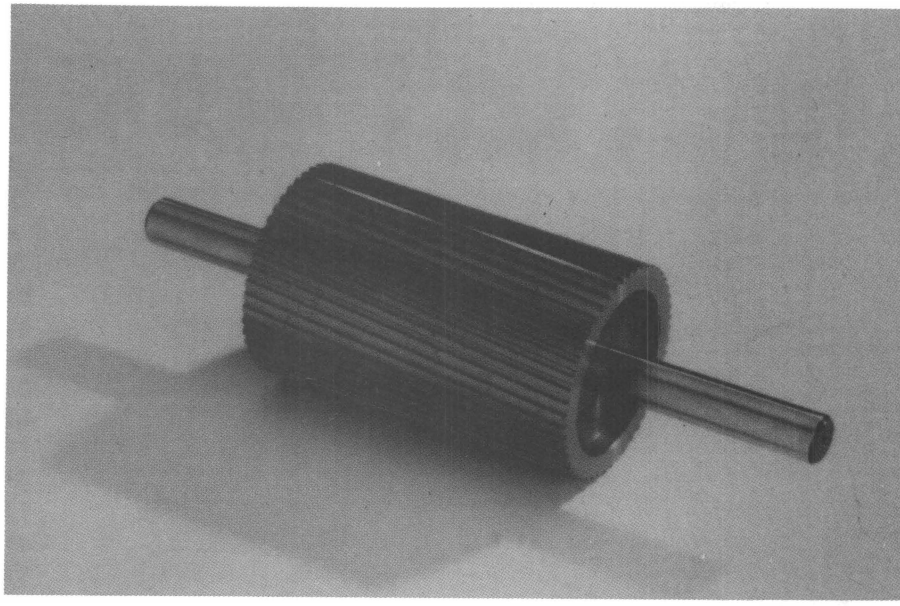

Fig. 5.1 – Rotor with helical teeth

well-known technique in the manufacture of gear wheels and which has reached a high degree of perfection. The rotor disks are obtained by partially turning off the rotor (see fig. 5.2.). The height of the rotor disks is made smaller than that of the stator disks. Hence every rotor disk surface is completely covered by the companion stator disk.

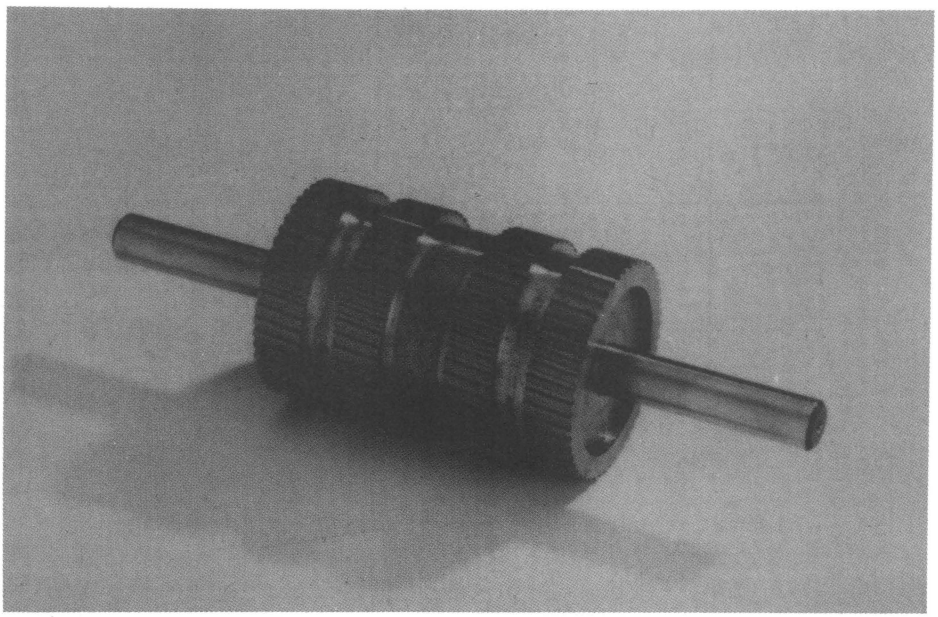

Fig. 5.2 – Rotor with disks with helical teeth

The angular alignment is now fully determined by the machining of the rotor. The centre distance between the rotor disks determines the angle through which the disks are to be displaced relative to each other (see fig. 5.3.). In the original arrangement the angles between the rotor disks are chosen such that the electrical angle between the inner and outer disks of each stator part is 180°, whereas the electrical angle between the two inner disks is 270°. Hence the centre distance between the two inner rotor disks is larger by a factor of 1.5 than that between the inner and outer disks of a single stator part.

The angular alignment can be realized by varying the centre distance between the disks. A high alignment accuracy can be attained because the alignment is determined by only a single workpiece.

In the motor made by this method the helix on the rotor was taken so as to obtain an electrical angular shift of 1.83° for a variation of 0.1 mm in the centre distance. The stator disks are higher by 2 mm than the rotor disks, with the result that each

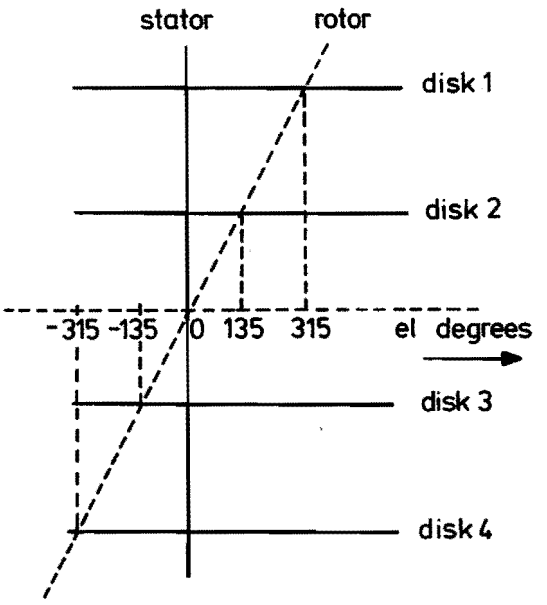

Fig. 5.3 – Disk alignment by means of a helical rotor

disk can be shifted in both directions by an electrical angle of 18° with respect to the nominal alignment.

The helical-teeth method has the drawback that the rotor teeth never fully overlap the stator teeth (fig. 5.4.), which influences the permeance function of the disks in such away that the torque decreases. The effect of the angular adjustment on the torque depends on the disk height. For the disk height that we have chosen the measured torque loss in 12%.

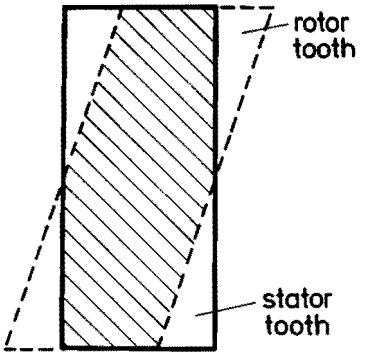

Fig. 5.4 – Partial overlap of rotor and stator teeth

The helical teeth method allows us to do very accurate measurements. The loss of torque limits however its use. The helical teeth method therefore will only be applied when the alignment of the disk is not possible by other methods as for example may be the case in very small stepping motors.

5.1. Measurements on the motor with helical rotor

In the new model the rotor radius is taken to be 13 mm instead of the 10 mm radius of the motor described in appendix 1. As a result the measurement torques are higher than those found from the previous measurements. The motor is fitted with bifilar windings. If a single wire of the bifilar winding is used, a power of 5W per phase is dissipated at the nominal current of 700 mA. During this heat dissipation in the windings the thermally permissible limit is not exceeded. When two wires are used in parallel the total current at which the motor is still not thermally overloaded amounts to 1A.

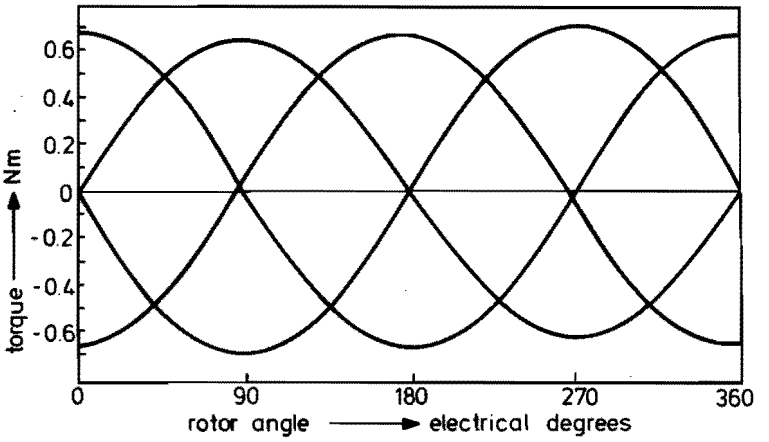

Fig. 5.5 – Torque angle curve with a nominal disk alignment

Fig. 5.5. shows the torque-angle curve of the motor for an excitation current of 700 mA per phase. The alignment is nominal, i.e. the disks are electrically shifted relative to the first disk by angles of 180, 90 and 270 degrees. The stepping angle error of the motor is smaller than 5.6%. This stepping angle error is smaller for the uncompensated motor than for the motor dealt with in Appendix 1, because outside the tooth zones the magnetic circuit in the motor with helical rotor is less saturated. The number of rotors with which it is possible to perform experiments is too limited to measure the complete curve. We therefore attempted to correct only the motor in such a way as to remove the stepping angle error at a nominal excitation current of 700 mA. This can be achieved by either increasing the angle

between the inner disks or by decreasing the angle between the outer disks or by changing the permeance functions of the various disks. In the first method the stepping angle error is eliminated at an electrical angle between the inner disks of 99.8°. The holding torque of the motor is then 0.59 Nm and the asymmetry in the holding torques 0.79. In the second method at an electrical angle between the outer disks of 80.2° the stepping angle error also vanishes. The minimum holding torque is now 0.63 Nm and its asymmetry 0.85. Therefore, for this motor, it is recommended to use the outer disks for effecting the angular rotation needed to compensate for the stepping angle error.

Fig. 5.6. presents the effect of the disk height on the holding torque of the motor, with the mentioned correction for the outer disks, for several different values of the excitation currents.

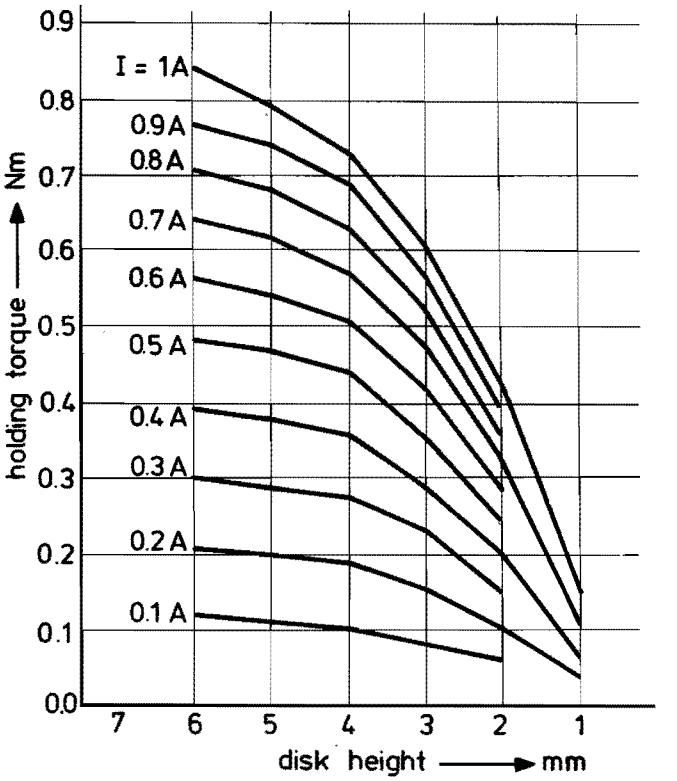

Fig. 5.6 – Effect of the disk height on the holding torque

In this experiment the heights of all the disks are taken to be equal. It is striking that a disk height above 4 mm the torque increases very little; this is caused by the permanent magnet generating a constant flux, resulting in a decrease of the

potential difference across the air gap with rising disk height. In addition, the helical teeth have an increasingly negative effect on the permeance function the greater the disk heights are.

At an excitation current of 1A, i.e. the nominal value when two coil wires are used, the holding torque of the motor is 0.85 Nm. The motor volume is 127 cm^3. The torque-to-volume ratio of the motor is 6693 Nm/m^3. Harris et al. (ref. 15) have compiled the torque-to-volume ratio of a large number of commercially available motors. Comparison of their measuring results with the torque-to-volume ratio of the motor with helical rotor shows that the latter is roughly 25% higher and is even higher if a rotor with straigth teeth is used. Experiments reveal that the torque is then 13.5% higher.

A motor with helical rotor also allows its stepping angle error to be compensated if the height of its inner disks is reduced. Fig. 5.7. shows the stepping angle error as a function of the excitation current for several different values of the disk-height ratio K. The height of the outer disks is at all times 6 mm. The disk alignment is

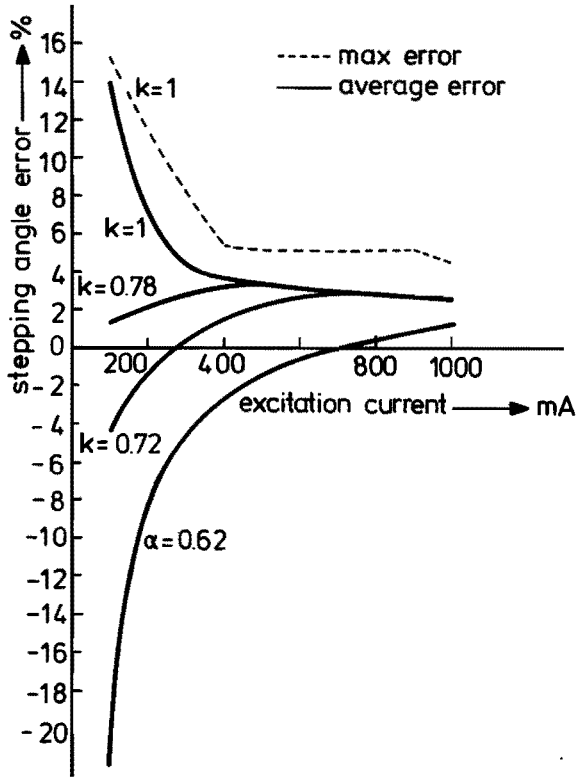

Fig. 5.7 – Stepping angle error as a function of excitation current

nominal. The graph reveals that small variations from the nominal value in the ratio K have little effect on the stepping angle error. At larger currents, the slight effect at larger disk heights is in agreement with the variation of the holding torque, which was represented in fig. 5.6. The dashed curve in fig. 5.7. refers to the maximum stepping angle error at K = 1 and the other curves relate to the average stepping angle error. The discrepancy between the two curves is due to the fact that the stepping angle error caused by mechanical deviations is not constant throughout 200 steps.

At lower excitation currents the effect of the disk-height ratio on the stepping angle error is strongest, because the detent torque is then comparatively large compared with the hybrid torque. Fig. 5.8. presents the detent torque as a function of the disk height ratio K. This torque is at a minimum for a disk height-ratio about 0.75. At this ratio the stepping angle error is also a minimum at lower excitation currents.

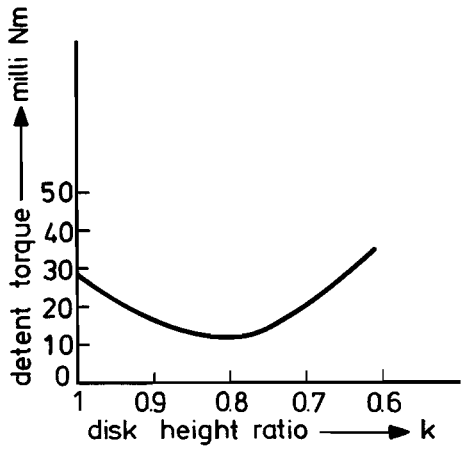

Fig. 5.8 – Detent torque as a function of the disk height ratio

At a disk height ratio of 0.62 the stepping angle error disappears if the excitation current is 700 mA. In this case the motor holding torque is 0.53 Nm and its asymmetry 0.79.

A comparison between the two methods of compensation reveals that compensation by additional angular shift of the disks results in a holding torque that is about 20% larger than that obtained by a compensation method in which the disk height ratio is varied.

Accordingly, it is advisable to compensate the motor by additional angular shifts of the disks.

5.2. Dynamic behaviour of the motor

The dynamic behaviour of a stepping motor is determined by the motor performance and the properties of the motor control.

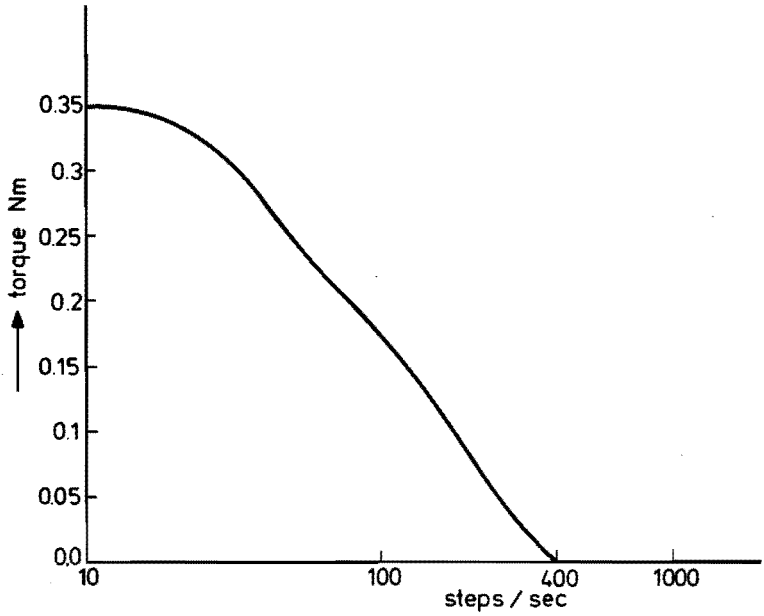

Fig. 5.9 – Pull-out curve

Fig. 5.9. shows the pull out torque-speed characteristic of the motor with helical rotor. Here use is made of a voltage drive producing a voltage that supplies a current of 700 mA to each phase when the motor stands still. Fig. 5.10. gives the step response of the motor for a double phase excitation of 700 mA. The single step response of the motor demonstrates an overcritical damped response on which an oscillation is superimposed.
This type of single step response occurs in the electro-magnetic damped motor (ref. 17, 18). In the motor solid iron is used. On exciting the motor eddy currents will flow in the solid iron, which gives the described type of electromagnetic damping.

The torque-speed curve of the motor reveals that, even at low speeds, the motor torque loss is substantial owing to the high self-inductance of the motor and the large eddy current losses. The motor is made up from solid iron in which extremely high eddy currents are induced. The alternating flux through the rotor causes an annular eddy current in the solid iron disks. The dynamic behaviour of the motor appears to be improved by using the lamination described in sec. 4.1.

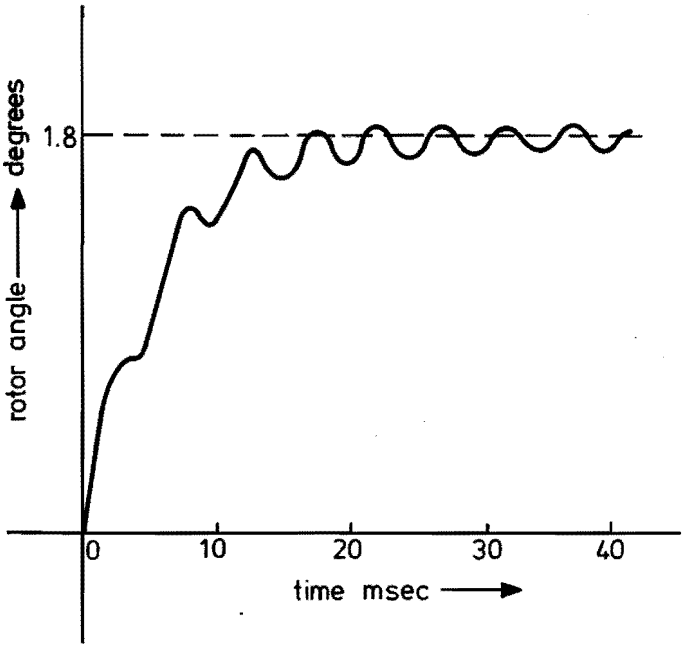

Fig. 5.10 – Single step response

The motor lends itself particularly well for incorporation of a Lanchester damper in the rotor. It is well known from the literatur that a Lanchester damper favourably affects the pull out rate of the motor (ref. 16). By using an external Lanchester damper an additional moment of inertia is introduced into the motor, which determines the pull in rate. The rotor of the motor described here can be used as a Lanchester damper by hollowing out the rotor and filling the recess thus obtained with a viscously coupled iron mass (fig. 5.11.). Thus an air gap is created in the magnetic circuit of the rotor. Experiments have revealed that this air gap only slightly affects the static behaviour of the motor. This rotor assembly enables the pull out rate to be raised to 1500 steps per second using the same drive.

Improvement of the dynamic behaviour of the motor requires additional research, which is beyond the scope of this dissertation.

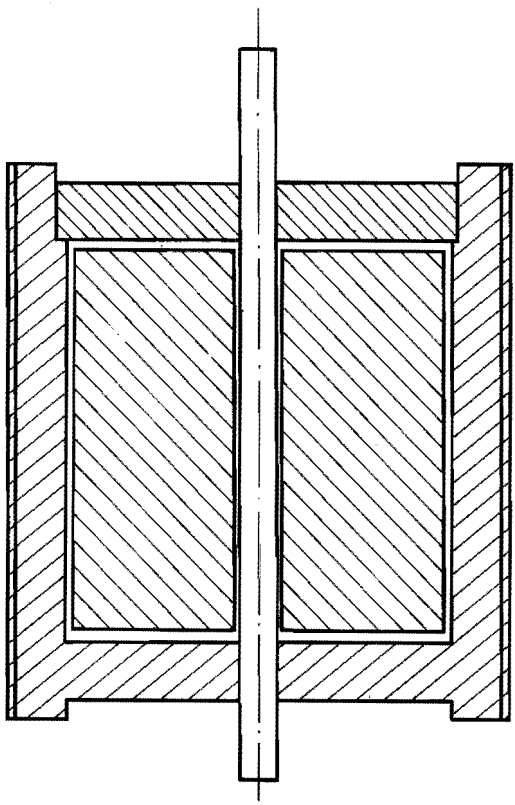

Fig. 5.11 – Lanchester damper

6. CONCLUSION

Owing to the asymmetric design of the hybrid stepping motor with ring coils the motor exhibits annoying features of asymmetry in the holding torque and stepping angle errors. Calculations on the motor with idealized iron provide an insight into the effects caused by the coupling of the two stator parts and by the differences in magnetic paths for the disk fluxes generated by the permanent magnet.

A special model used for measuring the properties of the air gap region enables the effect of the non-idealized iron on the motor performance to be described. The motor torque calculated on the basis of these measuring results as a function of rotor angle is in good agreement with experiments.

The inherent stepping angle error and asymmetry in the holding torque can be corrected in different ways.

By segmentation the motor is made symmetric and consequently exhibits no inherent stepping angle error either for single or for double-phase excitation. However, the segmentation of the motor results in a lower torque, and also increases the production costs.

Elimination of the stepping angle error by introducing new asymmetries in the magnetic circuits leads to satisfactory results. When this is done the holding torque of the motor remains unaltered. The cost of producing the compensated motor is not greater than that for the original motor. Compensation by new assymmetries has the drawback, however, that the requisite accuracy is only obtained at double-phase excitation.

The torque-to-volume ratio of the motor is very high because only one pole pair per phase is used.

The static performance of the compensated motor is better than that of comparable, commercially available types. The dynamic behaviour of the present prototype is inferior to that of the existing types, mainly due to the use of solid iron in the magnetic circuit. It is particularly the dynamic behaviour of the motor which is recommended for further investigation.

The knowledge gained in the previous chapters makes it possible to design an accurately operating stepping motor, which delivers an very high torque-per-volume ratio and which can be made in a cheap mass production process.

REFERENCES

(1) **Snowdon**, A.E. and E.W. **Madsen**
CHARACTERISTICS OF A SYNCHRONOUS INDUCTOR MOTOR.
AIEE Trans. Part II, Vol. 81 (1962), p. 1-5 = Appl. and Industry, No. 59 (March 1962), p. 1-5.

(2) **Bakhuizen**, A.J.C.
A CONTRIBUTION TO THE DEVELOPMENT OF STEPPING MOTORS.
Doctoral Diss. Eindhoven University of Technology, 1973.

(3) **Goddijn**, B.H.A.
Patent application No. 7607381.
The Hague: Netherlands Patent Office, 1976.

(4) **Goddijn**, B.H.A.
A NOVEL HYBRID STEPPING MOTOR WITH RING COILS.
In: Proc. 3rd Int. Conf. on Stepping Motors and Systems, Leeds, 19-20 Sept. 1979. Ed. by A. **Hughes**. Leeds: Department of Electrical and Electronic Engineering, University of Leeds, 1979. P. 1-5.

(5) **Goddijn**, B.H.A.
EFFECT OF THE NUMBER OF POLE PAIRS AND PERMANENT-MAGNET EXCITATION ON THE PERFORMANCE OF A HYBRID STEPPING MOTOR.
In: Proc. 7th Annual Symp. Incremental Motion Control Systems and Devices, Chicago, Ill., 24-26 May 1978. Ed. by B.C. **Kuo**. Champaign, IL 61820 (P.O. Box 2772, Station A): Incremental Motion Control Society, 1978. P. 7-12.

(6) **Singh**, G.
MATHEMATICAL MODELING OF STEP MOTORS.
In: Theory and Applications of Step Motors. Ed. by B.C. **Kuo**.
St. Paul, Minnesota: West Publishing Co., 1974.
(Some papers of the 1972 and 1973 Proc. Annual Symp. Incremental Motion Control Systems and Divices). P. 33-75.

(7) **Chai**, H.D.
MAGNETIC CIRCUIT AND FORMULATION OF STATIC TORQUE FOR SINGLE-STACK PERMANENT MAGNET AND VARIABLE RELUCTANCE STEP MOTORS.
In: Theory and Applications of Step Motors. Ed. by B.C. **Kuo**.
St. Paul, Minnesota: West Publishing Co., 1974.
(Some papers of the 1972 and 1973 Proc. Annual Symp. Incremental Motion Control Systems and Devices). P. 120-140.

(8) **Mukherji, K.C. and S. Neville**
MAGNETIC PERMEANCE OF IDENTICAL DOUBLE SLOTTING: Deductions from analysis by F.W. Carter.
Proc. Inst. Electr. Eng. (London), Vol. 118 (1971), p. 1257-1268.

(9) **Woodson, H.H. and J.R. Melcher**
ELECTROMECHANICAL DYNAMICS. New York: Wiley, 1968.
Part 1: Discrete systems (chapter 3).

(10) **Singh, G., A.C. Leenhouts and M. Kaplan**
ACCURACY CONSIDERATIONS IN STEP MOTOR SYSTEMS.
In: Proc. 7th Annual Symp. Incremental Motion Control Systems and Devices, Chicago, Ill., 24-26 May 1978. Ed. by B.C. **Kuo.**
Champaign, IL 61820 (P.O. Box 2772, Station A): Incremental Motion Control Society, 1978. P. 319-327.

(11) **Ortega, J.M. and W.C. Rheinboldt**
ITERATIVE SOLUTION OF NONLINEAR EQUATIONS IN SEVERAL VARIABLES. New York: Academic Press, 1970.
Computer Science and Applied Mathematics Series
Chapter 7

(12) **Goddijn, B.H.A.**
Patent application No. 7904818.
The Hague: Netherlands Patent Office, 1979.

(13) **Goddijn, B.H.A.**
Patent application No. 7904816.
The Hague: Netherlands Patent Office, 1979.

(14) **Goddijn, B.H.A.**
Patent application No. 7904817.
The Hague: Netherlands Patent Office, 1979.

(15) **Harris, M.R. and V. Andjargholi**
LIMITATIONS ON RELUCTANCE TORQUE IN DOUBLY-SALIENT STRUCTURES.
In: Proc. 1st Int. Conf. on Stepping Motors and Systems, Leeds, 15-18 July 1974. Ed. by P.J. Lawrenson et al. Leeds: Department of Electrical and Electronic Engineering, University of Leeds, 1974. P. 158-168.

(16) **Lawrenson, P.J. and I.E. Kingham**
DESIGN OF VISCOUSLY-COUPLED INERTIAL DAMPERS.
In: Proc. 1st Inst. Conf. on Stepping Motors and Systems, Leeds, 15-18 July

1974, Ed. by P.J. **Lawrenson** et al. Leeds: Department of Electrical and Electronic Engineering, University of Leeds, 1974. P. 169-176.

(17) **Hughes**, A. and P.J. **Lawrenson**
INTRODUCTION TO ELECTROMAGNETIC DAMPING IN STEPPING MOTORS.
In: Proc. 1st Inst. Conf. on Stepping Motors and Systems, Leeds, 15-18 July 1974. Ed. by P.J. **Lawrenson** et al. Leeds: Department of Electrical and Electronic Engineering, University of Leeds, 1974. P. 135-147.

(18) **Goddijn**, B.H.A.
ANALOG ELECTRONIC DAMPING ON STEPPING MOTORS.
In: Proc. 2nd Int. Conf. on Stepping Motors and Systems, Leeds, 13-15 July 1976. Ed. by A. **Hughes**. Leeds: Department of Electrical and Electronic Engineering, University of Leeds, 1976. P. 61-67.

(19) **Polak**, S.J., A. de **Beer**, A. **Wachters** and J.S. van **Welij**
MAGGY 2, A PROGRAM PACKAGE FOR TWO-DIMENSIONAL MAGNETOSTATIC PROBLEMS.
Int. J. Numerical Methods Eng., Vo. 15 (1980). p. 113-127.

APPENDIX 1 DESCRIPTION OF THE EXPERIMENTAL MOTOR

The motor shown in fig. A1.1 is provided with 50 teeth per disk, resulting in a stepping angle of 1.8 degrees. The stator disks are aligned with key and key slots. The four stator disks are identical. Each of these disks has four key slots which are spaced by nine degrees. The disks are mounted on the key in the stator housing. The angle between the teeth of the stator disks is determined by the choice of the key slot on each disk. The rotor teeth are in line for all disks. The height of the permanent magnet is 15 mm; this is more than required but we took this value to reduce the effect of the coupling between the stator parts. The permanent magnet

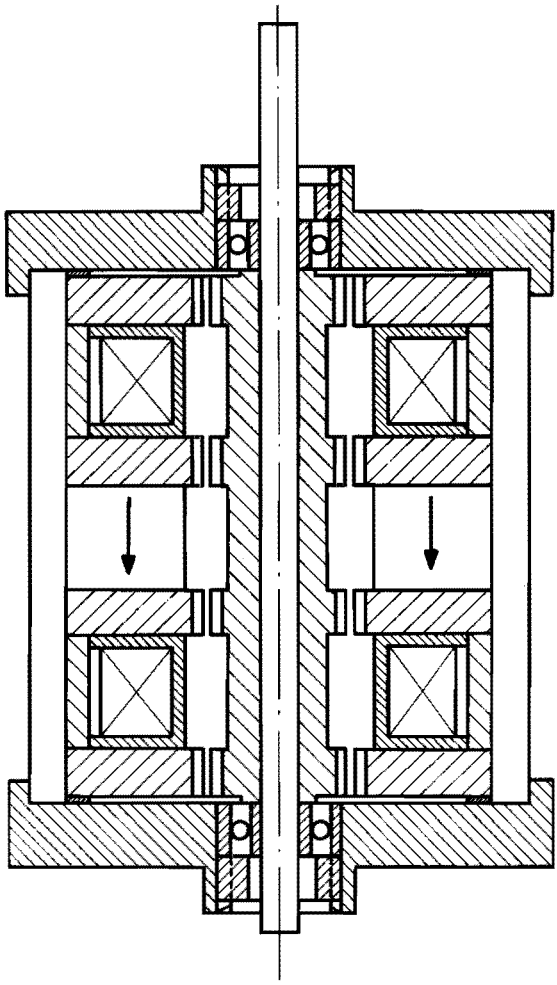

Fig. A1.1 – The experimental motor

is made of ceramic material (ferroxdure 370) and is set at a very high working point because of the large length of the magnet.

The motor housing thickness is taken to be large so as to minimize the introduction of mechanical deviations during the assembly and disassembly of the motor.

In designing the motor we did not aim at obtaining a small volume, and therefore the torque-to-volume ratio of this motor is not optimized.

APPENDIX 2 MAGNETIC FIELD CALCULATIONS

In chapter 3 the magnetic field in the tooth zone of the measuring model is assumed to have no axial components. The field therefore is two-dimensional. In fig. A2.1 the air gap region over one tooth pitch is described by the polar coordinates r and φ. At the boundaries of region, on the arcs of the circle, we may assume that the flux entering and leaving the region is uniform and has no component in the φ-direction. This assumption is permitted provided that the greater part of the magnetic potential difference is found to occur across the saturated teeth and the air gap.

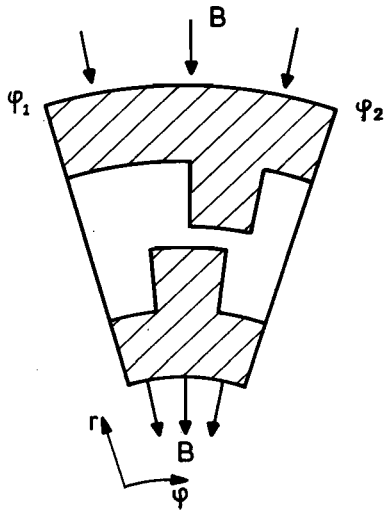

Fig. A2.1 – The air gap region over one tooth pitch

No currents are flowing in the air gap region. Therefore the field can be calculated by introducing a scalar potential and solving the problem numerically. The field can also be assessed by introducing a vector potential. Since the field in the air gap region has no component in the axial direction it is possible to describe this field in terms of the normal component of the vector potential.

The boundaries of one period of the region are made up from the arcs of the circle and the two radial lines. On the radial lines the boundary condition follows from the periodicity on these lines, i.e. the whole field pattern is repeated with respect to this boundary. The periodicity on the radial lines can be expressed by

$$\frac{\partial A_Z(\varphi_1, r)}{\partial \varphi} = \frac{\partial A_Z(\varphi_2, r)}{\partial \varphi} \qquad \text{(A2.1)}$$

where A_Z is the normal component of the vector potential.
φ_1, φ_2 the φ-coordinates of the radial lines.
The flux entering and leaving the region through the arcs of the circle is constant.
The boundary condition expressing the periodicity on the radial lines is:

$$A_Z(\varphi_1, r) = A_Z(\varphi_2, r) + C_1. \tag{A2.2}$$

C_1 follows from the flux entering the region over one period

$$C_1 = \int_{\varphi_1}^{\varphi_2} B_r \; r \; d\varphi = B_r \, r \, (\varphi_2 - \varphi_2) \tag{A2.3}$$

where B_r is the radial component of the magnetic induction. If we consider the problem not for a single tooth pitch but for the whole of the circumference, then it follows from equation (A2.3) that after a complete circumference along a circle the vector potential thus introduced is a multivalued function.

The assumption has been made that the flux entering and leaving the region through the arcs of the circle is uniform and has no component in the φ-direction. To solve the problem one of these conditions must be imposed on the boundaries. The boundary condition, which follows from the assumption B_r is homogeneous, is expressed by:

$$B_r(\varphi) = \frac{1}{r} \frac{\partial A_Z}{\partial \varphi} = c \tag{A2.4}$$

The boundary condition which follows from the assumption that the flux has no φ-component is found as:

$$B_\varphi = \frac{\partial A_Z}{\partial \varphi} = 0. \tag{A2.5}$$

The boundary condition expressed by (A2.5) is the same as occurs on a boundary defined by symmetry.
To the boundary condition imposed by (A2.4) it applies that:

$$A_Z(\varphi, r) = B_r(\varphi) \; r \; \varphi + C_2 \tag{A2.6}$$

where C_2 is an integration constant.

On one of the circle boundaries the integration constant can be taken as zero, on the other circle boundary the integration constant then follows from the field distribution in the region. Therefore it is only possible to use the boundary condition from (A2.6) for one of the circle boundaries. On the other boundary the condition (A2.5) must be chosen. The available program Maggy for calculating the magnetic field uses vector potentials. In calculating the field in the air gap region, errors were introduced by the program. These errors were caused by the way in which it implemented the periodicity boundaries. It gave points where the periodicity applies to the same vector potential, so that it cannot be used for calculations with homopolar fluxes. The above field problem has been solved by modifying the periodicity conditions in such a way that the program allows of a constant difference in vector potential at the boundaries where periodicity occurs. In fig. A2.2. an example of the field distribution over one tooth pitch is given.

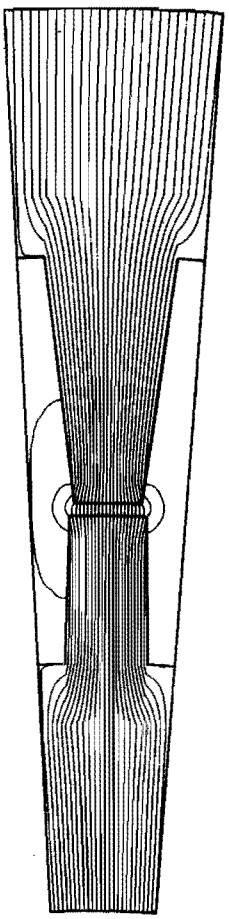

Fig. A2.2 – The calculated field distribution

This problem of a multivalued vector potential does not arise in the three-dimensional field problem if there is a homopolar flux. The vector potential at the boundaries, on the arc of the circle where the field is rotationally symmetric, will have a constant component in the φ-direction and no component in the z-direction. In the region where owing to the teeth, there is no longer any rotational symmetry, the vector potential will have components both in the φ- and in the z-direction.

APPENDIX 3 MEASURING METHODS

In chapter 3 use has been made of the results obtained from a measuring model employed for determining the torque, the flux and the angular position.

Torque measurement
The torque is determined by means of a Staiger Mohilo measuring shaft on the basis of angular rotation of a torsion shaft through which the torque is passed: the torsion of this shaft is a measure of the torque. This torsion is measured by a contactless method. The linearity error of the measurement is less than 0.3% from 5% of the maximum measured value (1 Nm).

Flux measurement
The flux linked with the coil of the measuring model is determined by means of an electronic integrator. The coil in the model is a bifilar winding. The excitation current flows through one wire, while the other wire is connected to an electronic integrator.

The voltage induced in the coil is given by

$$E = -\frac{d\Phi}{dt} \tag{A3.1}$$

and for the flux linkage we may write

$$\Phi = -\int_{t_0}^{t} E dt. \tag{A3.2}$$

If the coil is terminated by an integrator with a high internal impedance, then the terminal voltage across it is equal to the generated e.m.f. Integration of the terminal voltage yields the variation in flux. The total flux is measured when, at the time t_0, the flux is zero.

We considere the measured flux to be linked with all the windings. The flux can be found by dividing the linked flux by the number of windings.

The flux meter used was supplied by Norma.

The angular position transducer
The angular position is measured by means of an incremental shaft encoder, which has two outputs delivering sinusoidal voltages shifted by 90° as functions of the angular position. The transducer contains a grating provided with 3600 marks. The

zero transitions of the sinusoidal voltages are used as positional signals. Hence the resolution of the transducer is 14400 pulses per revolution.

The moment of inertia of the transducer is 15 gcm^2, its frictional torque is 10 gcm. These values are so low as to be ignored in the measurement.

Assuming the torque to be a sinusoidal function of the angular position, we introduce an electrical measuring error of 0.28 degrees in measuring the stepping angle error if the holding torque is 0.2 Nm. For a 1.8 degree stepping motor this amounts to an error of 0.32%. The transducer resolution for a 1.8 degree stepping motor is 72 increments per step or 1.39%. Here it is permissible to neglect the frictional torque of the angular transducer. The transducer used is a Minirod 150 of Heidenhain.

A further enhancement of the measuring accuracy by an incremental shaft encoder is not readily feasible at low torques. The commercially available transducers with a high resolution invariably had a much higher frictional torque, so that there was no point in increasing the resolution.

Dankbetuiging

Bij deze wil ik mijn dank uitspreken aan allen die in welke vorm dan ook bijgedragen hebben aan de totstandkoming van dit proefschrift, in het bijzonder aan:

De directie van het Natuurkundig Laboratorium van de N.V. Philips voor de mogelijkheid die mij geboden is dit proefschrift te schrijven en voor alle faciliteiten welke mij ter beschikking zijn gesteld om deze publikatie te verwezenlijken.

De heer H. Baron voor het realiseren van de meetmodellen en de vele metingen daaraan verricht.

Ir. R. Raes, de heer A. Christiaens en de heer F. van Huizen voor de terugkoppeling naar de realiteit van de producent waardoor het onderzoek praktisch toepasbaar werd.

Prof. dr. ir. J. Niesten en dr. ir. A. Bakhuizen voor de vele discussies welke tot de uiteindelijke tekst geleid hebben.

Ing. P. Logtenberg voor de vertaling in het engels.

Dr. ir. E. Kamerbeek en dr. ir. W. Joosen voor het kritisch doorlezen van het manuscript.

STELLINGEN

Behorende bij het proefschrift van

B.H.A. GODDIJN

I

De koppel volume verhouding in de hybride stappenmotor wordt in belangrijke mate door het aantal poolparen per fase bepaald (hoofdstuk 1).

II

In de hybride stappenmotor met ringspoelen bevinden zich geen spoelen ter hoogte van de permanente magneet. De homopolaire flux van de permanente magneet kan hierdoor maximaal zijn. Dit leidt tot een optimale koppel volume verhouding.

III

Literatuur over optimale tand gleuf verhoudingen beperkt zich tot identieke stator en rotor vertandingen. In de praktijk wordt vaak voor rotor en stator een verschillende verhouding gekozen. Het verdient onderzocht te worden in hoeverre afwijkende verhoudingen voor stator en rotor tot betere resultaten leiden.

IV

Het bestrijden van inherente staphoekfouten met behulp van extra asymmetrieen leidt tot specifieke goede resultaten (hoofdstuk 4).

V

Het compenseren van staphoekfouten door middel van de schijfuitlijning verdient de voorkeur boven het veranderen van de permeantie functies van de schijven (hoofdstuk 5).

VI

Bij het ontwerpen van motoren is het niet voldoende een goed motor ontwerp te maken wat prestatie betreft, doch is het minstens zo belangrijk een motor te ontwerpen welke eenvoudig en goedkoop construeerbaar is. Dit laatste aspect vereist kennis welke slechts zeer summier onderwezen wordt.

VII

De aandacht in de opleiding tot electrotechnisch ingenieur voor de specifieke problemen betreffende kleine motoren (< 1kW) ten opzichte van die voor grote motoren en generatoren komt niet overeen met de grotere omzet in kleine motoren t.o.v. die in grote motoren.

VIII

Het verantwoord gebruik van veldberekeningsprogramma's is slechts goed mogelijk indien de gebruiker ook zonder deze programma's reeds een voldoende fysisch inzicht heeft in het veldverloop.

IX

De veelal negatieve benadering uitgedrukt in "Japan Incorporated" houdt de erkenning in van de sterkte van een geleide ekonomie.

X

Het begrip wa is een sleutel voor het begrijpen van Japan.

XI

Reeds jaren wijzen economen en politici op de zwakke economische situatie waar in wij ons bevinden. Ieder jaar blijkt het bruto nationaal produkt evenwel een nieuw absoluut hoogtepunt te bereiken.

XII

Het beeldschrift (b.v. N.S.-indikatie, wasvoorschriften) als primitief communicatie-middel wordt door het toenemen van internationale contacten gestimuleerd.